A NEW SOFT TISSUE ARTIFACT COMPENSATION TECHNIQUE IN HUMAN MOTION ANALYSIS AND CLINICAL APPLICATIONS

By

BO GAO

A DISSERTATION PRESENTED TO THE GRADUATE SCHOOL
OF THE UNIVERSITY OF FLORIDA IN PARTIAL FULFILLMENT
OF THE REQUIREMENTS FOR THE DEGREE OF
DOCTOR OF PHILOSOPHY

UNIVERSITY OF FLORIDA

2009

To the mentors who guided me to the world of scientific reasoning and creative exploring; and to my family who provided me constant support and encouragement, making this milestone possible

ACKNOWLEDGMENTS

I thank Professor Nigel Zheng and Professor Scott Banks for their direct mentoring on my program study and research work, and Professor B.J. Fregly and Professor MaryBeth Horodyski for their guidance along my progress. I thank Bryan Conrad for his numerous help during my daily work. I thank Judith Barry, Shang Mu, Brooke Organ, Jason Bouwkamp, David Walker, Alexander Bennett, Poorya Shidfar, Bing Xiao, Hongsheng Wang for their assistance in data collection and post-processing. I thank Dr. Peter Gearen, Dr. Peter Indelicato, Dr. Michael Moser, Butch Landsiedel, Mieko Dunn for their assistance in subject recruitment, and all the research subjects who participated in my study. I also thank my parents and wife for their loving encouragement, which motivated me to where I am today.

TABLE OF CONTENTS

page

LIST OF TABLES

LIST OF FIGURES

LIST OF ABBREVIATIONS AND ACRONYMS

ACL	Anterior cruciate ligament
ACL-D	ACL-deficient
ACL-I	ACL-intact
ACL-R	ACL-reconstructed
AP	Anterior/posterior
BMI	Body mass index
CHS	Contralateral heel strike
CT	Computed tomography
CTO	Contralateral toe off
DWO	Directional weighted optimization
FE valley	Minimum knee flexion during midstance
GCS	Global coordinate system
HS	Heel strike
IRB	Institutional review board
LCS	Local coordinate system
LCS_{RT}	Local coordinate systems of the reference triad
ML	Medial/lateral
MRI	Magnetic resonance imaging
PCT	Point cluster technique
RBO	Rigid body optimization
ROM	Range of motion
RMS	Root-mean-square
SI	Superior/inferior
STA	Soft tissue artifact

STAD	STA deduction
STD/SD	Standard deviation
TKA	Total knee arthroplasty
TO	Toe off
UF	University of Florida
1st FE peak	Maximum knee flexion during the stance phase
2nd FE peak	Maximum knee flexion during the swing phase
2D	Two-dimensional
3D	Three-dimensional
α_{ankle}	Ankle plantarflexion angle
α_{hip}	Hip flexion angle
α_{knee}	Knee flexion angle
$f_{avg}(i)$	The average of a variable at *i*% gait cycle across all subjects
$f_{std}(i)$	The STD of a variable at *i*% gait cycle across all subjects
$\vec{O}_{bone}$	Position vector of the bone
$\vec{O}_{RT}$	Position vector of the reference triad in GCS
$\vec{p}_i$	The i^{th} marker's position in *GCS* at a dynamic instant
$\vec{p}_i^{\,g\_dynanic}$	The global position of a marker at a dynamic instance
$\vec{p}_i^{\,initial}$	The i^{th} marker's position in LCS_{RT} at the initial standing posture
$\vec{p}_i^{\,l\_static}$	Local position of a marker in the anatomical reference system at the static neutral posture
$[R_{bone}]$	Orientation matrix of bone
$[R_i^{RT}]$	A triad's orientation matrix in LCS_{RT}

$[R_j]$	The j^{th} triad's orientation matrix in *GCS* at a dynamic instant
$[R_{RT}]$	Orientation matrix of the reference triad in GCS
$\vec{V}_i^{RT}$	A marker's translation vector in LCS_{RT}
$\vec{V}_{STA\_shank}^{i}$	A shank marker's STA vector
$\vec{V}_{STA\_thigh}^{i}$	A thigh marker's STA vector
$(wx_i \quad wy_i \quad wz_i)$	Weight vector for marker *i*

Abstract of Dissertation Presented to the Graduate School
of the University of Florida in Partial Fulfillment of the
Requirements for the Degree of Doctor of Philosophy

A NEW SOFT TISSUE ARTIFACT COMPENSATION TECHNIQUE IN HUMAN MOTION ANALYSIS AND CLINICAL APPLICATIONS

By

Bo Gao

December 2009

Chair: Nigel Zheng
Cochair: Scott Banks
Major: Biomedical Engineering

Human motion analysis plays an important role in understanding normal function as well as pathological abnormalities of human musculoskeletal systems. Among different motion analysis techniques, skin marker-based stereophotogrammetry is the one used most widely in the biomechanical community. A major limitation of this technique is that motion-tracking markers are attached to skin surface of body segments and these markers can move relative to the underlying bone during activities. The relative movement between skin markers and the underlying bones is usually referred to as soft tissue artifact (STA) and it has been proved to be a major source of error of the technique. Much effort has been devoted by the research community to developing techniques to compensate for STA effects and improve motion analysis accuracy. However, the problem has not yet been solved satisfactorily.

In the framework of this dissertation, a new STA compensation method was developed based on *in vivo* soft tissue movements and inter-subject similarities. First, it was demonstrated that soft tissue deformation on the lower extremity has inter-subject similarities, which was a new insight contrary to the prevailing opinion. Second, a

simultaneous fluoroscopy and stereophotogrammetry study was conducted to assess STA *in vivo* on six subjects who had total knee arthroplasty (TKA), during a series of knee flexion movements and a step-up activity. Both inter-subject similarity and inter-motor-task similarity were observed on the STA results. Based on these similarities, a "universal" STA model was constructed using multilinear regression on the STA measurements obtained from multiple subjects and multiple activities. Third, from the "universal" STA model, a new STA compensation concept was implemented in two methods: an STA deduction (STAD) method and a directional weighted optimization (DWO) method. The performance of the two methods was evaluated on the *in vivo* knee joint kinematics. Both methods demonstrated improvement over the conventional rigid body optimization (RBO) method, and the STAD method exhibited the best performance. Overall, the STAD method reduced analysis errors by 37% to 75% for different kinematic variables. Finally, the newly developed STA compensation technique was applied clinically to investigate three-dimensional (3D) knee joint kinematics of patients after anterior cruciate ligament (ACL) injury and reconstructive surgery. 3D knee joint kinematics of ACL-deficient patients and ACL-reconstructed patients were investigated during level walking and compared to a group of healthy subjects who had bilateral ACL-intact knees. Significant reduction of extension was observed in the ACL-deficient knees during midstance and in the ACL-reconstructed knees during swing phase. Greater varus and internal tibial rotation were identified in the ACL-deficient knees. The kinematics of the ACL-reconstructed knees exhibited some improvement, but had not been fully restored to a normal level.

CHAPTER 1
BACKGROUND AND INTRODUCTION

Human Motion Analysis

The major function of human musculoskeletal system is to generate motion. As a quantitative tool, human motion analysis plays an important role in understanding normal function and abnormities of human musculoskeletal systems (Andriacchi and Alexander, 2000). It has been widely utilized in the areas of biomechanical research, clinical assessment, sports performance evaluation, and orthopedic prosthesis design optimizations (Banks and Hodge, 2004; Benoit et al., 2006; Dennis et al., 2005; Noyes et al., 1996). Many different techniques have been developed and used in various applications of human motion analyses. These techniques include video cameras (Rowe, 1996), electrogoniometers (Martelli, 2003), inertial motion recorder (Elble, 2005), stereophotogrammetry (Cappozzo et al., 2005), electromagnetic tracking system (Meyer et al., 2008), Roentgen stereophotogrammetric analysis (Adam et al., 2004), single plane and biplane fluoroscopy (Banks et al., 1997; Li et al., 2005), magnetic resonance imaging (MRI) (Patel et al., 2004), computed tomography (CT) (Feipel and Rooze, 1999), etc. Each of these techniques has its own strengths and limitations and is suitable for certain applications.

Skin Marker-Based Stereophotogrammetry

Among different motion analysis techniques, skin marker-based stereophotogrammetry has the features of being non-invasive, radiation-free, flexible and easy to implement, suitable for measuring high speed movement and movement occurring in large spatial volumes. Benefiting from these advantages, skin marker-based stereophotogrammetry is currently the most widely used technique in human

motion analyses. Since mid 1970s, stereophotogrammetry has been used as an analysis tool in biomechanical research for over 30 years (Andriacchi and Alexander, 2000). With the significant improvement of hardware and software performance during the past decade, modern commercial systems can usually achieve an accuracy of better than one millimeter in 3D marker tracking with hundreds of frames captured per second (Chiari et al., 2005). However, there is a major issue related to this technique and it largely limits the applications for accurate skeletal movement measurement. Since human body segments are not rigid bodies, markers attached to skin surface cannot perfectly follow the bone movement during activities. Thus when skin marker trajectories are used to determine skeletal movement, soft tissue movement will result in analysis errors.

Soft Tissue Artifact (STA)

In the biomechanical research community, the movement of skin markers with respect to the underlying bones is usually referred to as soft tissue artifact (STA). STA can be caused by a combination of muscle contraction, skin stretching and sliding, inertial effects of markers, and other experimental errors (Leardini et al., 2005). STA has been proved as a major source of error associated with skin marker-based motion analysis, and the error caused by STA is usually significantly larger than instrument errors (Leardini et al., 2005). In gait analysis, STA is especially disruptive in secondary rotational and translational components of knee kinematics, but these small kinematic components are considered of high interest in detecting gait deficiencies (Croce, 2006). As reported in one study, during level walking individual marker's STA can be up to 30 mm and the resultant peak-to-peak error in bone orientation can be up to 20° for the femur and 10° for the tibia (Cappozzo et al., 1996). Because the accuracy of skin

marker-based motion analysis is largely limited by the effects of STA, other invasive or radiation-involved techniques have to be considered when high accuracy is required (Fleming et al., 2001; Lafortune et al., 1992; You et al., 2001).

To understand the behavior of STA and to evaluate its influence on skeletal motion analysis, many studies were conducted during the past twenty years. As STA is the relative movement between skin markers and bones, the position and orientation of bones need to be measured. For this purpose, invasive devices were most commonly used. These devices including intracortical bone pins (Benoit et al., 2006; Fuller et al., 1997; Reinschmidt et al., 1997a; Reinschmidt et al., 1997b), external fixators (Cappozzo et al., 1996) and percutaneous trackers (Holden et al., 1997; Manal et al., 2000), can be rigidly fixed to bones. By tracking trajectories of markers fixed on the invasive device and markers attached to the skin surface, both bone motion and skin motion can be measured. Thus STA and its resultant errors on joint kinematic determination can be evaluated. These invasive devices provide a direct and reliable measurement of skeletal motion, but they could potentially constrain or alter the free movement of soft tissues. Pain and/or anesthesia involved in the test may also affect the normal skeletal motion pattern. To overcome these shortcomings of invasive techniques, a few studies used non-invasive radiographic techniques including two-dimensional (2D) X-ray and 3D fluoroscopy to investigate STA on the lower extremity (Sati et al., 1996; Stagni et al., 2005). These techniques made it possible to measure bone pose and unconstrained skin marker positions simultaneously. Because of the limited fluoroscopic field of view, the motor tasks that are studied usually need to be confined in a relatively small space.

Because of the diversities of techniques, motor tasks, marker placements, and subjects in the previous studies, the reported STA results had considerable variability. But some basic characteristics of STA are consistent for most studies: 1) STA for individual markers is usually in the magnitude of millimeters to centimeters; 2) the errors caused by STA are much larger than instrument errors of motion analysis systems; 3) STA is skin location specific, i.e., markers on different skin locations have different movement relative to the bone during an activity. Although joint landmarks are often selected as marker placement locations in clinical motion analysis, these locations could have larger STA than other areas on the segment; 4) STA is motor task specific, i.e., a marker on the same location may have different STA during different activities; 5) For the lower extremity, STA is usually larger on the thigh than on the shank; 6) STA imposes larger influence on those kinematic variables that have smaller range of motion (such as translations and axial rotations of the knee joint), which often leads to low reliability of the analysis on these variables; 7) STA usually has similar frequency content with skeletal movement, which reflects the inherent influence of muscle contraction and joint position on STA. This also indicates the impossibility to isolate STA effects from bone motion simply by using a frequency filtering process.

STA Compensation Techniques

Since STA is a critical issue in skeletal motion analysis, much effort has been devoted by biomechanical researchers to looking for solutions for the problem. Various STA compensation techniques have been proposed to improve the motion analysis accuracy (Alexander and Andriacchi, 2001; Andriacchi et al., 1998; Cappello et al., 1997; Cappello et al., 2005; Cheze et al., 1995; Lu and O'Connor, 1999; Soderkvist and Wedin, 1993; Spoor and Veldpaus, 1980).

In clinical gait analysis and many other applications, usually only a small number of skin markers are placed on joint landmarks to track the movement of body segments. This practice is based on the theory that three non-collinear markers are adequate to determine the 3D pose of a rigid-body segment. However, human body segments are not rigid bodies, and STA at joint landmarks is even more prominent than at other locations on the body segments (Cappozzo et al., 1996). To reduce the effect of STA on 3D bone pose determination, a reasonable approach is to employ redundant skin markers. On each body segment, more than three markers could be used and distributed on the skin surface. With more markers covering a larger area of the segment, it is expected that the marker cluster as a whole will represent a better approximation of the bony segment in pose measurement. To derive the bone pose from the position of the marker clusters, different calculation algorithms have been proposed and can be generally divided into two categories: rigid body optimization (Soderkvist and Wedin, 1993; Spoor and Veldpaus, 1980) and non-rigid body optimization (Alexander and Andriacchi, 2001; Andriacchi et al., 1998). In the first category, a segment is considered as a rigid frame plus perturbation, and each marker's local coordinates in the anatomical reference system are considered constant during the activities. Then a best-fit solid frame will be determined at each time instant to minimize the overall spatial perturbation. Typically a least squares method is used to solve this over-determined question. A similar experimental "solidification" approach often used in motion labs is to attach a rigid shell with no less than three markers to each body segment. These shells serve as a rigid representation of the bony segment but their efficacy compared with other marker sets is debated (Manal et al., 2000). In non-rigid

optimization approaches, a body segment will be allowed to deform in the models, and the local coordinates of each marker in its anatomical reference system are non-constant with time. A representative method is called “point cluster technique” (Andriacchi et al., 1998). This technique uses eigenvalues of the inertia tensor of each marker cluster to determine the non-rigid body poses, based on the fact that the eigenvalues will remain constant if the marker cluster is rigid. A virtual mass as a weight factor is assigned to each marker at each time frame, and the mass will be adjusted so that a lower mass will be assigned to a point with larger displacement relative to the segment reference frame. Although the concept of this non-rigid body optimization approach seems more realistic, their effectiveness compared to traditional rigid optimization methods remains controversial (Cereatti et al., 2006; Gao et al., 2007; Taylor et al., 2005). One major limitation of both rigid and non-rigid optimization approaches is that they can only compensate for “internal” deformation within marker clusters but do nothing on the overall shift of the marker cluster relative to the bone. All these methods have no effect if the whole marker cluster shifts relative to the bone. The anatomical structures of soft tissue and the relationship between the behaviors of soft tissue movements and skeletal positions are not taken into account in these approaches. STA is treated as a random noise, and the optimizations aim in geometrically smoothing the noise off. However, muscle and skin movement is not random in nature but related to the skeletal position and adjacent joint angles (Cappozzo et al., 1996). STA is also not geometrically uniform. It could be larger at some locations and smaller at others. Without including physiological and anatomical

information of soft tissue movement, the effectiveness of pure geometrical optimizations is limited.

To overcome the aforementioned limitations, a few other techniques have been proposed in order to include subject-specific physiological information of soft tissue movement. Cappello et al introduced a “double calibration” method which utilized two extremes of expected range of motion as reference postures and calibrated each marker’s local coordinates at these two postures (Cappello et al., 1997). The instantaneous local coordinates of each skin marker were computed by linear interpolation between the two reference instants along time. The time-varying local coordinates of markers were finally used to determine the bone pose at each instant. This method was tested on a subject with external fixator on the femur. The results showed that root-mean-square (RMS) errors of the femur orientation and position were reduced from about 5 º and 7 mm to less than 4 º and 4.5 mm. More recently, the same group applied a linear interpolation STA model with knee flexion angle to several non-ambulation activities and demonstrated its effectiveness in error reduction (Cappello et al., 2005). One of our studies also demonstrated that using multiple reference postures can reduce the STA errors during simulated level walking (Gao and Zheng, 2006). Another similar but different technique propose by Lucchetti et al is called “dynamic calibration” (Cappello et al., 1997). Rather than selecting a few discrete instants as the reference postures, a continuous relationship between the soft tissue movement on the thigh and the hip joint angles was measured. This was achieved by pre-analyzing knee-locked hip rotation trials under the assumption that STA on the shank is negligible. The relationship between STA and hip joint flexion/extension, abduction/adduction, and

internal/external rotation angles were described as an STA table which was later used in the analysis for other trials. This dynamic calibration method was tested on a patient wearing a single degree of freedom (DOF) knee prosthesis and the RMS errors of knee joint translations and rotations were reduced from 14 mm and 6º to 6 mm and 3º.

The multiple reference posture approaches (Cappello et al., 1997; Cappello et al., 2005; Gao and Zheng, 2006) and dynamic calibration approach (Lucchetti et al., 1998) achieved better STA compensation effectiveness because of the inclusion of subject anatomical information and specific motor task information into the method. This is a substantial improvement from previous geometrical optimization algorithms. Since skin and muscle movement is related to skeletal movement, the strategies of these methods are more reasonable. However, apparent limitations also exist for these methods. For the multiple reference posture approach, only a few discrete postures are calibrated and interpolation has to be used for other postures in between. Even at the calibration postures, the anatomical landmark misplacement could lead to considerable errors in determination of markers' local coordinates (Della Croce et al., 2005). The dynamic calibration method overcomes this shortcoming by obtaining a continuous relationship between markers' local coordinates and the hip angles. But a large simplification in this method is the assumption that STA on the thigh is only related to hip joint angles but not knee joint angles. STA on the thigh is dependent on both hip and knee joint angles (Cappozzo et al., 1996), but this is not reflected in the dynamic calibration method. In addition, both dynamic calibration and multiple calibration methods require extra trials during the test, which prolongs the test procedure in clinic situations.

To pursue more effective and convenient STA compensation techniques, there is a basic question that needs to be answered: does STA have inter-subject similarity? The answer of this question will guide us to different directions. If the answer is “NO” and STA is totally a subject-specific movement, we will have to pursue subject-specific models to describe and compensate for STA; but if the answer is “YES” and STA does have inter-subject similarity, it will be possible to develop generic or semi-generic models from the data of a small population and use them for a larger population. Considering most people have similar anatomical structures and limb coordination during the same motor task, it will be reasonable to expect that STA has certain inter-subject similarities. If this is true, the problem could be solved by the second approach discussed above.

In the framework of this dissertation, we will explore the behavior of soft tissue movement and demonstrate that STA has inter-subject similarity, which is contrary to the prevailing opinion. Based on this funding, a “universal” STA model will be developed using *in vivo* STA data from six different subjects. This STA model will be used in an “evidence-based” strategy to formulate a more effective and convenient STA compensation technique for skin marker-based motion analysis.

Anterior Cruciate Ligament (ACL) Injury and Knee Osteoarthritis

The human anterior cruciate ligament (ACL) plays an important role in controlling knee joint stability, not only by limiting tibia anterior translation but also by controlling knee axial rotation and varus movement (Andersen and Dyhre-Poulsen, 1997; Markolf et al., 1995). Rupture of the ACL is a common knee injury in athletic and young population, especially in females. Every year, approximately 80,000 to 250,000 ACL injuries occur in the United States (Griffin et al., 2006). The vast majority of the affected

individuals are aged from 15 to 45 years old (Griffin et al., 2000), and more than 50% of all those sustaining ACL injury are in young athletes from 15 to 25 years old (Griffin et al., 2006). Female athletes are even more vulnerable to ACL injury, with epidemiological data showing that females are two to eight times more likely than males to sustain such an injury (Arendt and Dick, 1995). Both contact and noncontact mechanism during sport participation can result in ACL injury, and the latter one is considered with even higher incidence (Griffin et al., 2000). After the rupture of the ACL, knee joint stability and load-bearing pattern between contact joint surfaces could be altered, resulting in abnormal loading on the cartilage during activities (Chaudhari et al., 2008; Li et al., 2006). This biomechanical environment change has been associated with cartilage degeneration and progressive development of knee joint osteoarthritis (Andriacchi et al., 2006; Andriacchi and Mundermann, 2006; Stergiou et al., 2007; Wu et al., 2000). The theory has been supported by both animal and human studies (Baliunas et al., 2002; Brandt et al., 1991; Neyret et al., 1993; Papaioannou et al., 2004; Pond and Nuki, 1973). For untreated ACL-deficient (ACL-D) knees, the risk of knee osteoarthritis development has been reported as high as 44% after eleven years (Noyes et al., 1983), and over 50% of cases have led to total knee arthroplasty before age 63 (Nebelung and Wuschech, 2005).

To restore the knee joint stability and function after ACL injury, ACL reconstructive surgery typically is recommended. However, the effectiveness of ACL reconstruction in preventing cartilage degeneration and osteoarthritis development remains controversial (Jones et al., 2003; Lohmander and Roos, 1994). Studies have found that even after constructive surgery, early cartilage degeneration cannot be successfully prevented and

premature knee osteoarthritis can still develop (Asano et al., 2004; Daniel et al., 1994; Lohmander et al., 2004; Seon et al., 2006). These studies evaluated the articular cartilage of ACL-reconstructed (ACL-R) knees with sample sizes of from 41 to 105 patients. The results showed a high prevalence of knee osteoarthritis after a period of 5 to 12 years post surgery, and a significant degeneration of cartilage was observed as early as 15 months after surgery. These findings indicated that current reconstructive surgeries are not able to effectively reduce the risk of early cartilage degeneration and osteoarthritis development for ACL-D knees, which has been considered by many researchers as a consequence of that knee joint kinematics has not been fully restored through the reconstructive surgeries and following rehabilitation programs (Brandsson et al., 2002; Papannagari et al., 2006). The residue abnormalities of joint motion and the resultant contact pattern change between articular surfaces could lead to progressive cartilage degeneration with millions of cycles of joint loading during daily activities. And any existing traumatic damage on articular cartilage or menisci accompanying the ACL injury would deteriorate the situation and speed up the mechanical-biological dynamics even more.

But on the other side, in most motion analysis studies, abnormal kinematics and kinetics were often observed in ACL-D knees but not in ACL-reconstructed (ACL-R) knees. Many studies found the motion and loading patterns of ACL-R knees are close to normal knees (Ferber et al., 2002; Georgoulis et al., 2003). There is an inconsistency between motion analysis data and clinic outcomes. One possible explanation is that although the reconstruction does not fully restore the normal kinematics of ACL-D knees, the difference between ACL-R knees and healthy knees are small and not easy

to be detected by measurements without enough accuracy. The kinematics change of ACL-D knees is usually of several millimeters in translation and several degrees in rotation. The differences between ACL-R knees and the healthy could be even smaller. This small difference is not easily identified using ordinary skin marker-based motion analysis, whose errors caused by STA can easily be greater than 10 mm and 5°. This assumption was also supported by two studies which identified abnormal kinematics of ACL-R knees using radiographic techniques (Brandsson et al., 2002; Papannagari et al., 2006). In these studies, the knee motion was investigated during non-ambulatory activities. To identify the abnormal motion during daily activities, radiographic techniques are not suitable and other techniques which can measure motion in a large spatial volume with adequate accuracy are needed. With the new STA compensation technique that will be developed in this study, we expect skin marker-based stereophotogrammetry will be a qualified approach to achieve this challenging aim.

CHAPTER 2
DOES SOFT TISSUE MOVEMENT HAVE INTER-SUBJECT PATTERNS?

Introduction

As introduced in the first chapter, soft tissue artifact (STA), which is the relative movement between skin markers and the underlying bone, represents a major source of errors in skin marker-based motion analysis (Leardini et al., 2005). Because the accuracy of skin marker-based stereophotogrammetry is largely limited by STA, other invasive or radiation-involved techniques have to be used when a higher accuracy is required (Fleming et al., 2001; Lafortune et al., 1992; You et al., 2001). In order to effectively compensate for the effects of STA and improve the accuracy of skin marker-based motion analysis, it is critical to well understand the behavior and characteristics of soft tissue movement during activities.

Several studies have been conducted to examine human soft tissue movement during different motor tasks. Among them, invasive approaches were most frequently used including intracortical bone pins (Benoit et al., 2006; Fuller et al., 1997; Reinschmidt et al., 1997a; Reinschmidt et al., 1997b), external fixators (Cappozzo et al., 1996) and percutaneous trackers (Holden et al., 1997; Manal et al., 2000). These invasive devices provide a direct and reliable measurement of bony segment movement, but they may constrain and/or alter free soft tissue motion. To overcome this limitation, a few studies used non-invasive radiographic techniques including two-dimensional (2D) X-ray and 3D fluoroscopy (Sati et al., 1996; Stagni et al., 2005). These techniques made it possible to measure bony segment pose and unconstrained skin marker positions at the same time. But the limited field of view of fluoroscopy is difficult to examine ambulatory motor tasks. Consequently, few studies have used a non-

invasive approach to investigate soft tissue movement during walking, while walking is one of the most important human daily activities and the focus of clinical gait analysis.

The purpose of the study in this chapter was to investigate soft tissue deformation on the thigh and shank during level walking using a non-invasive approach on twenty healthy subjects. With the measurement of skin marker clusters, soft tissue deformation during walking was quantified as inter-marker translations and rotations, which reflected the positional and orientational change between different skin locations. By using marker triads in addition to single markers, both rotations and translations of skin surface were analyzed. Inter-subject similarity of the translation and rotation patterns was also evaluated, as well as gender effects on soft tissue deformation magnitudes.

Design and Methods

Subjects

Twenty healthy subjects (ten males and ten females) without previous injuries on lower extremities were recruited for this study (Table 2-1). Informed consent was obtained from each subject and the test was conducted under an Institutional Review Board (IRB) approved protocol.

Table 2-1. Subject information.

Gender	Number	Age (year)	Height (mm)	Weight (kg)	Body Mass Index (kg/m^2)
Male	10	22.2 (SD 2.9)	182.1 (SD 4.3)	77.0 (SD 10.8)	23.2 (SD 2.8)
Female	10	21.0 (SD 1.1)	162.0 (SD 6.0)	54.7 (SD 7.8)	20.8 (SD 2.2)
Total	20	21.6 (SD 2.2)	172.1 (SD 11.5)	65.9 (SD 14.7)	22.0 (SD 2.8)

Marker Placement

To track skin motion on the thigh and shank, a cluster of retro-reflective markers and triads was attached to each segment. For each leg, seven single markers and four triads were placed on the anterolateral side of the thigh and femoral epicondyles; six single markers and four triads were placed on the anterolateral side of the shanks and tibial plateau ridges and malleoli (Figure 2-1). The markers and triads were placed approximately at the same locations on each subject. Triads were small rigid triangular plates made of thermoplastic material with three markers fixed on the vertices. With the three vertex markers, each triad's rotation can be determined for skin surface rotation analysis. On the other hand, a triad has the same skin attachment area as a single marker, thus the center position of the three vertices can be used for skin surface translation analysis. A single marker has a mass of about 4 grams and a triad of about 7 grams. All retro-reflective markers are about 10 mm in diameter.

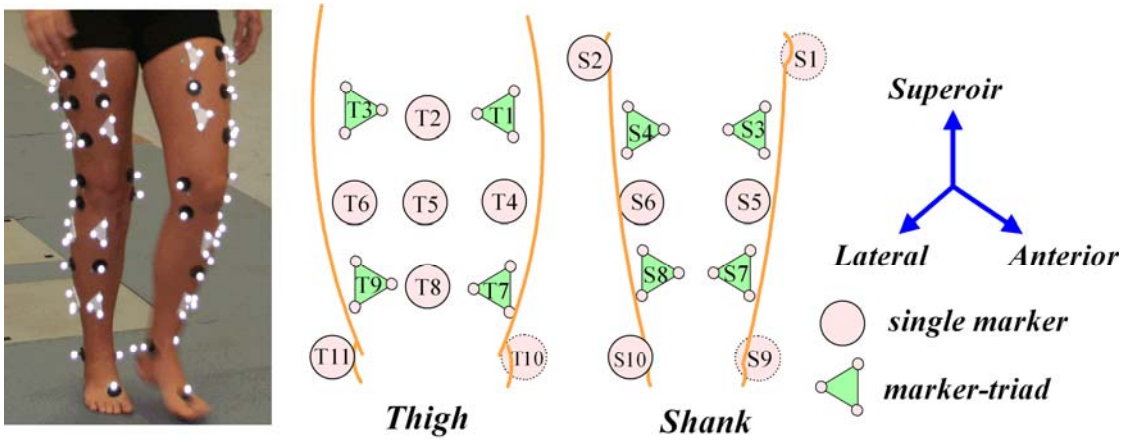

Figure 2-1. Marker placement on the thigh and shank. Seven single markers and four triads were placed on the anterolateral side of the thigh. Six single markers and four triads were placed on the anterolateral side of the shanks. Each triad with three vertex markers was considered as one entity. Marker labels are illustrated for the right leg and are sagittally mirrored for the left leg. [Reprinted with permission from Gao, B., and Zheng, N., 2008, Investigation of soft tissue movement during level walking: Translations and rotations of skin markers: Journal of Biomechanics, v. 41, no. 15, p 3190, Fig.1]

Experimental Setup

An 11-camera stereophotogrammetric system (Motion Analysis Corp., CA) was used to record marker motion at 60 Hz. The average marker tracking error in the 3D measurement space (5.0 m × 2.0 m × 2.5 m) was less than 1 mm after calibration. After a static posture at neutral standing being acquired for anatomical frame definition, each subject was instructed to walk through the measurement space at his/her normal cadence. Five repeated walking trials were collected for each subject.

Analysis Method

The deformation of soft tissue on the thigh and shank was analyzed by quantifying the relative movement between different markers on each segment. One triad on each segment was specified as the reference triad and the movement of other markers with respect to the reference triad was computed. Any triad can serve as the reference triad in principle and the results will reflect a same systematic movement. Here thigh triad T7 and shank triad S3 were selected as the reference triads respectively (Figure 2-1). At the neutral standing posture, local coordinate systems of the reference triads (LCS_{RT}) were defined to parallel with the anatomical reference frames. During walking, other markers' movements relative to the reference triad were expressed as translation vectors and rotation matrices in LCS_{RT} (Figure 2-2).

A marker's translation vector $\vec{V}_i^{RT}$ and a triad's rotation matrix $\left[R_i^{RT}\right]$ in LCS_{RT} can be expressed as:

$$\vec{V}_i^{RT} = [R_{RT}]^{-1}(\vec{p}_i - \vec{O}_{RT}) - \vec{p}_i^{inital} \qquad (2\text{-}1)$$

$$[R_j^{RT}] = [R_{RT}]^{-1}[R_j] \qquad (2\text{-}2)$$

where $\vec{O}_{RT}$ and $[R_{RT}]$ are the position and orientation of the reference triad in the global coordinate system (*GCS*) respectively; $\vec{p}_i$ is the i^{th} marker's position in *GCS* at a dynamic instant; $\vec{p}_i^{initial}$ is the i^{th} marker's position in LCS_{RT} at the initial neutral standing posture; and $[R_j]$ represents the j^{th} triad's orientation matrix in *GCS* at the same dynamic instant. Translation and rotation of each marker relative to the reference triad were decomposed into three directional components. Projection method was used to decompose rotation matrices into three angles in order to avoid the rotation sequence asymmetry.

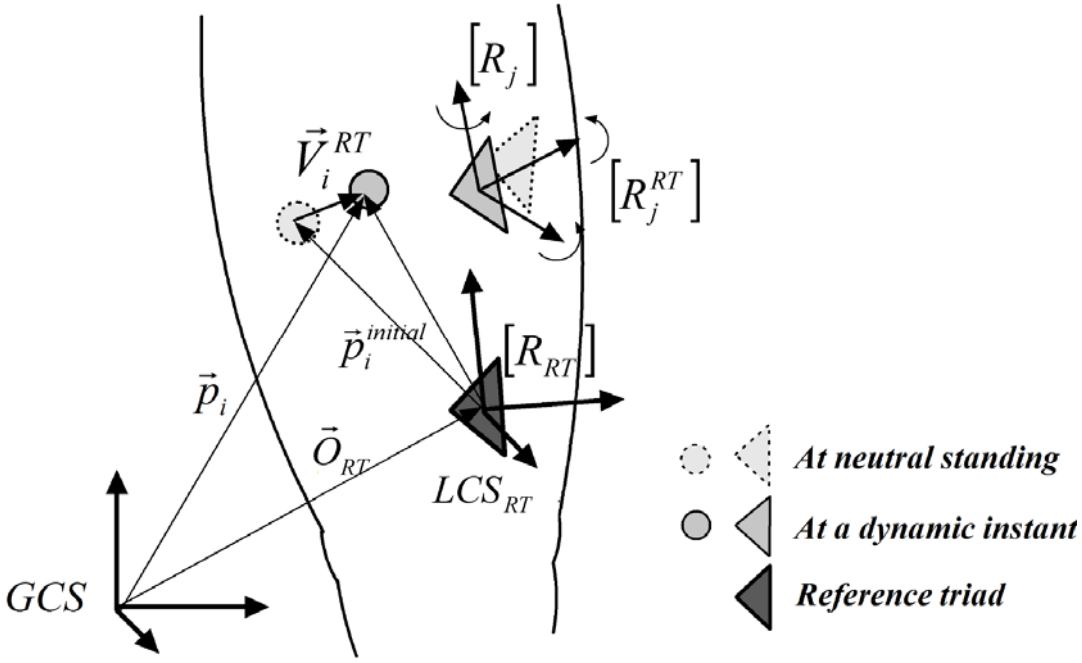

Figure 2-2. Inter-marker soft tissue movement calculation. [Reprinted with permission from Gao, B., and Zheng, N., 2008, Investigation of soft tissue movement during level walking: Translations and rotations of skin markers: Journal of Biomechanics, v. 41, no. 15, p 3191, Fig.2]

All variables were normalized to a gait cycle (from heel strike 0% to heel strike 100%) and then averaged on multiple trials and on left and right legs for each subject.

For each variable at an instant of a gait cycle (*i* %), the average $f_{avg}(i)$ and standard deviation $f_{std}(i)$ of all subjects (n = 20) were calculated. Root mean square (RMS) of $f_{std}(i)$ over a gait cycle represents the average variability of the variable among the subjects. A variable with a strong inter-subject similarity would have similar curves for all subjects, and the maximum and minimum values in a gait cycle would be at the similar timing for all subjects. Therefore, the difference between the maximum and minimum of the averaged curve would be greater. The ratio between the range of $f_{avg}(i)$ and RMS of $f_{std}(i)$ over a gait cycle was used to assess the inter-subject similarity:

$$r = \frac{\max(f_{avg}(i)) - \min(f_{avg}(i))}{\sqrt{\frac{\sum_{i=1}^{100} f_{std}^{2}(i)}{100}}} \qquad (2\text{-}3)$$

For an *r* value greater than 2, it could be considered that the inter-subject average pattern was not overshadowed by the inter-subject variability, i.e., a definite inter-subject similarity existed.

Overall translation/rotation magnitude of a markers/triad was quantified in the form of $R = \sqrt{R_x^2 + R_y^2 + R_z^2}$, where R_x, R_y, R_z were the magnitudes in each spatial direction. The effects of gender on each marker/triad's overall translation/rotation magnitude were examined using one-way analysis of variance (SPSS, Chicago, IL).

Results

Inter-Subject Similarity

The inter-marker movement over a gait cycle was illustrated as mean curves and standard deviations of all subjects (Figure 2-3 to Figure 2-5). Although variability existed

across subjects who had different genders and body heights/weights, inter-subject similarities were definite for most variables. For the thigh, all 30 translation variables and 8 out of 9 rotation variables had definite inter-subject similarities (Figure 2-3, 2-5); for the shank, 23 out of 27 translation variables had definite inter-subject similarities (Figure 2-4).

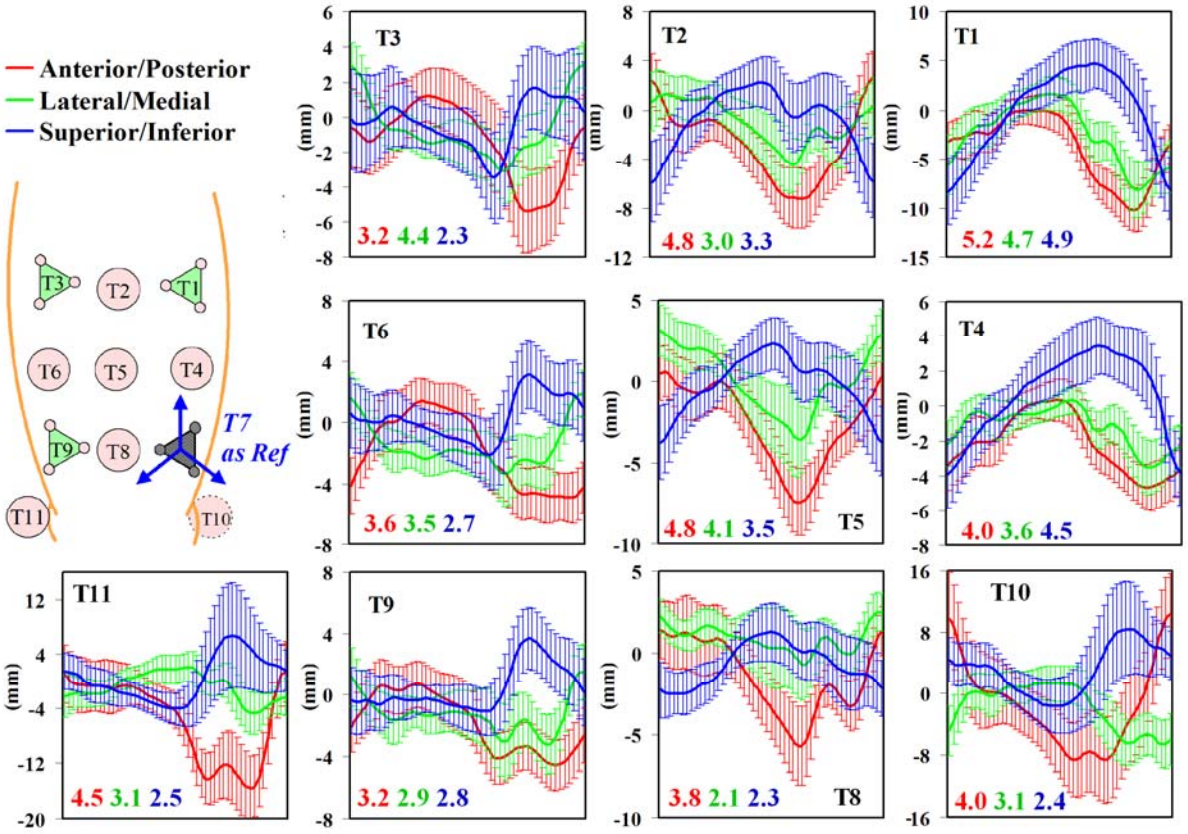

Figure 2-3. Inter-marker translations on the thigh during walking. Triads T7 was specified as the reference triad and other markers' translations relative to it are illustrated as three directional components. The three numbers inside each small graph are the *r* values which indicate the prominence of inter-subject similarities. Horizontal axis of each graph represents 0~100% gait cycle (from heel strike to heel strike). Anterior, lateral, and superior directions are shown as positive. [Reprinted with permission from Gao, B., and Zheng, N., 2008, Investigation of soft tissue movement during level walking: Translations and rotations of skin markers: Journal of Biomechanics, v. 41, no. 15, p 3190, Fig.3]

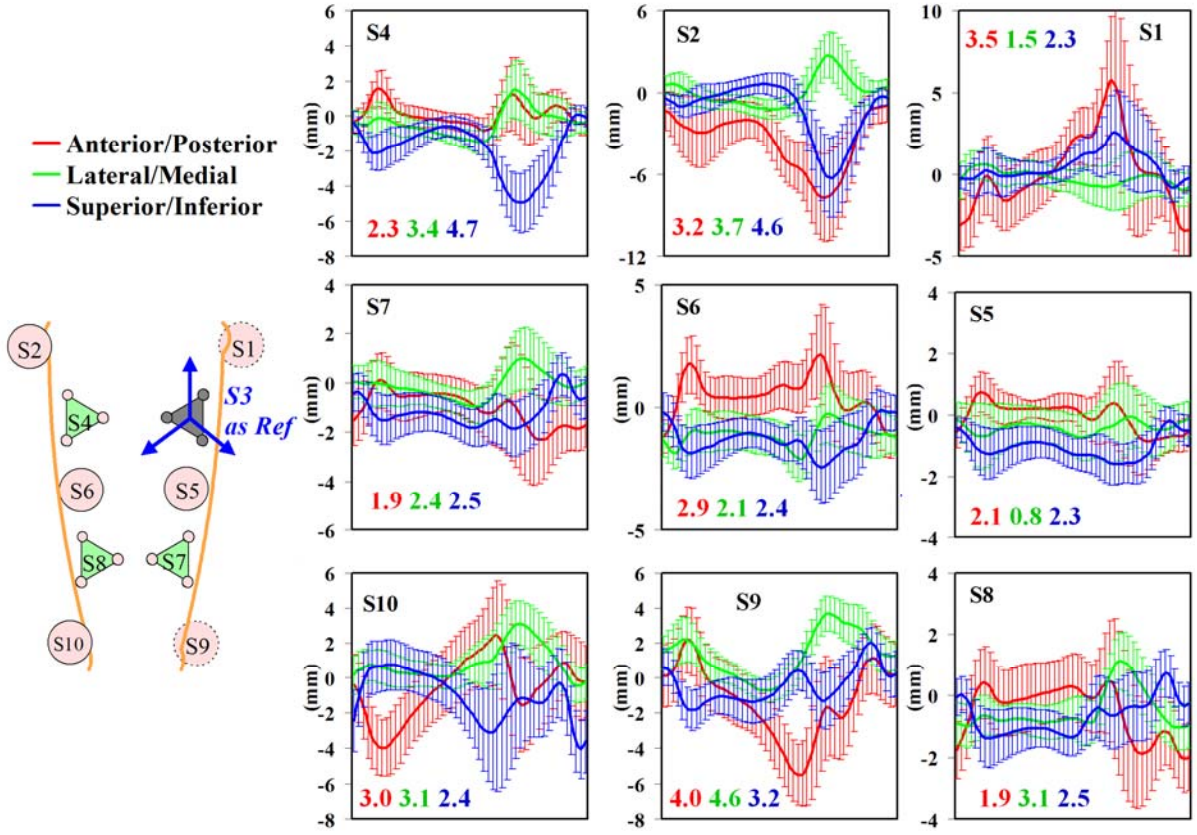

Figure 2-4. Inter-marker translations on the shank during walking. Triads S3 was specified as the reference triad and other markers' translations relative to it are illustrated as three directional components. The three numbers inside each small graph are the *r* values which indicate the prominence of inter-subject similarities. The horizontal axis of each graph represents 0~100% gait cycle (from heel strike to heel strike). Anterior, lateral, and superior directions are shown as positive. [Reprinted with permission from Gao, B., and Zheng, N., 2008, Investigation of soft tissue movement during level walking: Translations and rotations of skin markers: Journal of Biomechanics, v. 41, no. 15, p 3192, Fig.4]

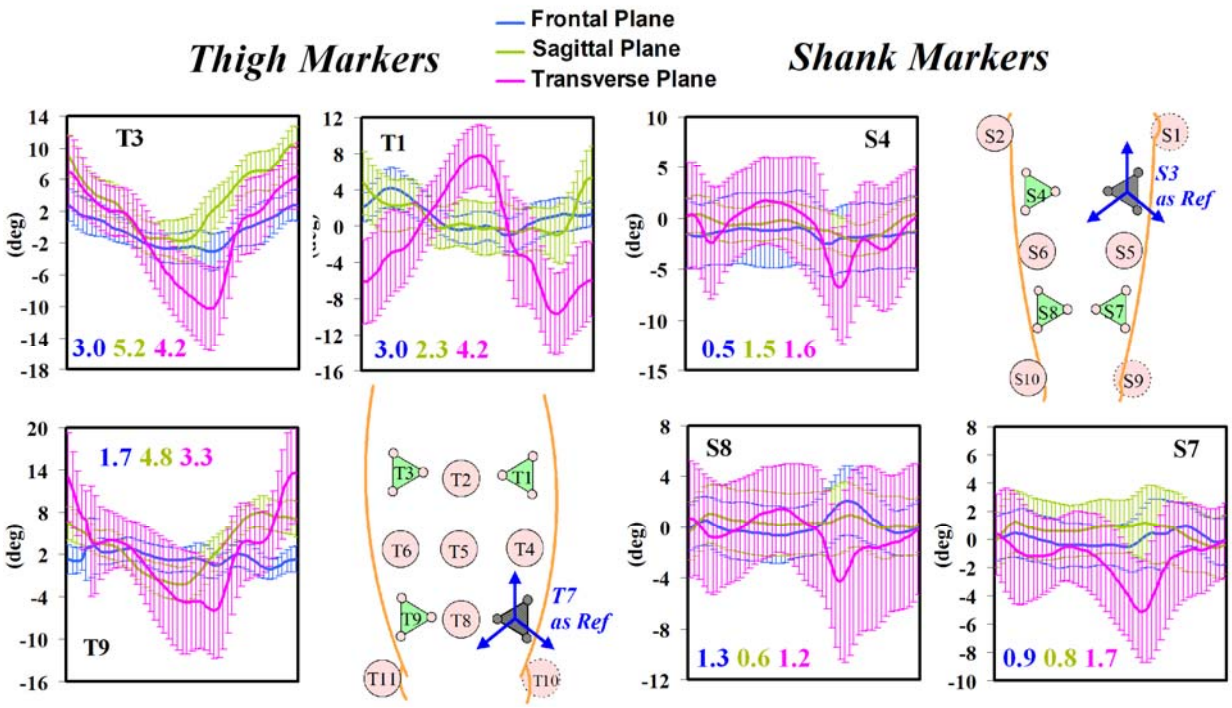

Figure 2-5. Inter-marker rotations during walking. Triads T7 and S3 were specified as the reference triads on the thigh and shank, respectively. Other markers' rotations (_rot) relative to the reference triads are illustrated as three components. The three numbers inside each small graph are the *r* values which indicate the prominence of inter-subject similarities. Horizontal axis of each graph represents 0~100% gait cycle (from heel strike to heel strike). Positive directions are illustrated in the diagram as arrows on the reference triad axes. [Reprinted with permission from Gao, B., and Zheng, N., 2008, Investigation of soft tissue movement during level walking: Translations and rotations of skin markers: Journal of Biomechanics, v. 41, no. 15, p 3192, Fig.5]

Soft Tissue Movement Behavior

From the inter-marker translations and rotations, a 4D image of the soft tissue deformation (3D space and time) on the thigh and shank during a gait cycle can be perceived, with translations showing skin stretching and rotations showing skin tilting between two surface locations. For example, from T1's translations (Figure 2-3) and rotations (Figure 2-5), it can be seen that the skin translation between T1 and T7 occurred mostly in superior/inferior (SI) direction and rotation occurred mainly in the

transverse plane. While a gait cycle progressed, the skin surface between the two locations was elongated in SI direction from heel strike to maximum knee flexion and then was shortened until the next heel strike; meanwhile, it also rotated externally during the first half of the gait cycle and then rotated back internally after that. The elongation/shortening range between T1 and T7 was about 13 mm in SI direction and the rotation range was about 18° in the transverse plane. Similar information can be read for every marker on both thigh and shank.

Soft tissue deformation on the thigh exhibited similar patterns for markers on a same vertical column (Figure 2-3). Translation patterns of T3 were similar to those of T6 and T9; translation patterns of T2 were similar to those of T5 and T8; and translation patterns of T1 were similar to those of T4. But these three subgroups were not similar to each other. Such features also existed for rotations: T3 had similar rotation patterns to T9 but not to T1 (Figure 2-5). No such trends were apparent for shank markers (Figure 2-4).

Soft tissue deformation was generally larger on the thigh than on the shank. Inter-marker translations and rotations occurred in all three directions but the magnitudes were not uniform along all directions (Figure 2-6). For thigh markers (average of 20 subjects), the maximum range of motion (ROM) of translation reached 19.1 mm in anterior/posterior (AP) direction, 9.8 mm in lateral/medial (LM) direction, and 13.0 mm in SI direction; the maximum ROM of rotation was 5.9° in the frontal plane, 12.0° in the sagittal plane, and 19.6° in the transverse plane. For shank markers, the maximum ROM of translation was 9.3 mm in AP direction, 4.4 mm in LM direction, and 6.9 mm in SI direction; the maximum ROM of rotations was 2.7° in the frontal plane, 2.6° in the

sagittal plane, and 8.6° in the transverse plane. Translations were relatively larger in AP and SI directions than in LM direction; rotations were greater in transverse plane than in frontal and sagittal planes. Markers placed on joints (T10, T11, S1, S2, S9, and S10) generally exhibited larger movement than other markers.

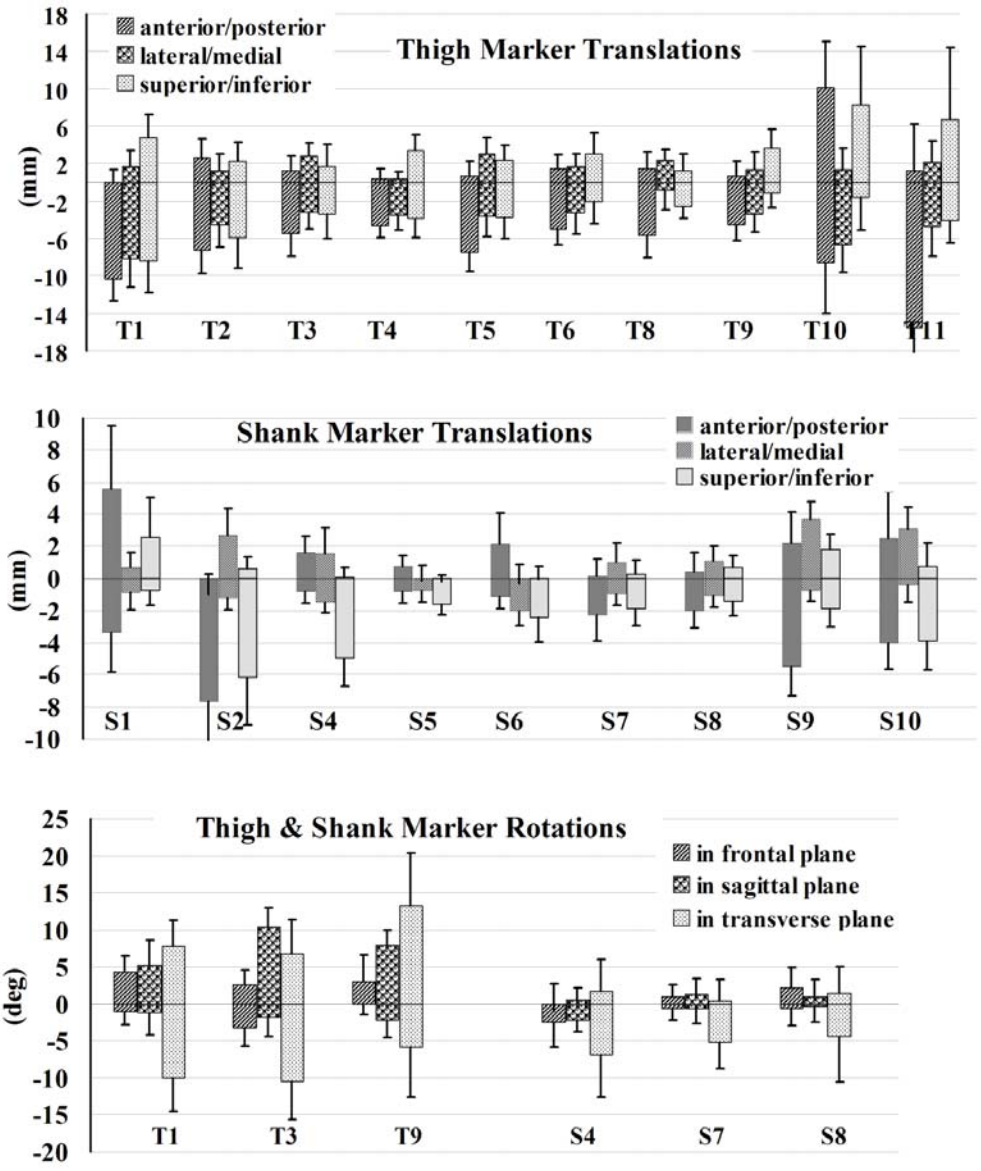

Figure 2-6. Maximums and minimums of inter-marker translations and rotations in a gait cycle. The zero line corresponds to the neutral standing posture. [Reprinted with permission from Gao, B., and Zheng, N., 2008, Investigation of soft tissue movement during level walking: Translations and rotations of skin markers: Journal of Biomechanics, v. 41, no. 15, p 3193, Fig.6]

Gender Differences

For most translation and rotation variables, no significant differences between males and females were detected. The few variables detected with statistical differences between gender groups included translations of T10 and T11, and rotation of T1 and T3 (Table 2-2). Females exhibited smaller inter-marker translations but larger inter-marker rotations.

Table 2-2. Variables that showed statistical differences between gender groups (*P<0.05, ** P<0.01).

Variable	Male	Female	P
Trans_T10	30.1 ± 5.3	24.4 ± 6.4	*
Trans_T11	29.6 ± 6.1	20.9 ± 3.3	**
Rot_T1	20.4 ± 4.7	24.2 ± 2.9	*
Rot_T3	23.3 ± 5.2	28.5 ± 5.1	*

Discussions

The purpose of this chapter was to investigate soft tissue movement on the thigh and shank during level walking using a non-invasive approach. This purpose was achieved using a novel analysis method. By quantifying inter-marker translations and rotations on each segment, the soft tissue deformation was depicted in a 4D picture. The results revealed quantitative information about morphological dynamics of soft tissue profile during walking in forms of positional and orientational changes between different skin locations. Compared with STA reported in a previous study (Stagni et al., 2005), the inter-marker translations measured in the present study were of similar magnitudes. Little data has been published previously to which our results of skin marker rotations during walking can be compared. Inter-marker rotations were found to

be up to 5.9°, 12.0°, and 19.6° in the frontal, sagittal and transverse planes on the thigh, respectively, and up to 2.7°, 2.6°, and 8.6° on the shank, respectively (Figure 2-6).

Soft tissue deformation occurred in all three directions but the distribution was not uniform. Translational movements were often more prominent in AP and SI directions than in ML direction. Rotational movements were greater in the transverse plane than in the other two planes, especially for the thigh. These features could be explained by the muscular structures of lower extremity. Most muscles on the thigh and shank orient along SI direction. During their shortening and lengthening, length change of muscle fibers causes skin markers to move along SI direction; the rotations in both frontal and sagittal planes are small. Meanwhile, the cross-sectional area of muscle bundles increases during shortening and decreases during lengthening. The circumference change of muscle bundles could lead to both translational and rotational movement of skin markers in the transverse plane. Another interesting feature found in this study was that soft tissue movement on the thigh exhibited "longitudinal" similarity. For both translations and rotations, markers on the same vertical column (such as T3-T6-T9, T2-T5-T8, or T1-T4) had similar movement patterns. When the quadriceps contracted during the swing phase, T1 and T4 shifted inferiorly, medially, posteriorly and rotated internally; T2, T5 and T8 shifted inferiorly, laterally, and anteriorly; T3, T6 and T9 shifted superiorly, laterally, and rotated externally. These findings indicated the primary role of quadriceps muscle in soft tissue movement on the anterior-lateral thigh. No such trends were apparent for shank markers.

This study analyzed the inter-marker movement on the thigh and shank, but did not directly measure STA which is markers' movement relative to the bone. The

adoption of this alternative approach was partially a result of technical limitations and the nature of the problem. Currently only invasive devices and fluoroscopic techniques can achieve direct measurement of bony segment movement. But invasive methods have the potential to alter free soft tissue movement and are not appropriate for a large healthy subject population. Fluoroscopy is not easy to be used for measuring large ROM motor tasks like ground walking. Another limitation of this study was the narrow range of subject age and BMI. The BMI of the healthy subjects tested in this step of study was in the lower bound of general patient population. With only young healthy subjects, some findings from this study may vary for other age and/or BMI groups. The influences of age and BMI on soft tissue movement behaviors need further investigation.

Another important finding in this study was that soft tissue deformation exhibited inter-subject similarity, i.e., most inter-marker translations and rotations showed similar patterns across different subjects (Figure 2-3 to Figure 2-5). Since inter-marker movement represents the difference of two markers' STA, this result indicates the possibility that markers' STA may also have inter-subject similarity. Considering that most people have similar muscular structures and joint coordination manners during the same activity, this finding is not surprising. However, little related evidence had been reported previously and the current prevailing opinion about STA is that it has no similarity among different people (Leardini et al., 2005). We consider that three possible reasons may go far in explaining the absence of similar findings in previous studies. The first is the study purpose. Many previous studies focused on the evaluation of joint kinematic errors caused by STA rather than STA itself which is the movement of

individual markers (Benoit et al., 2006; Holden et al., 1997; Manal et al., 2000; Reinschmidt et al., 1997a; Reinschmidt et al., 1997b). Kinematic errors caused by STA are not equivalent to STA itself and could be influenced by more factors. Any variation in marker numbers, marker placement locations, and calculation methods of joint kinematics could result in different joint kinematic errors even for the same intrinsic STA. The second reason involves sample size. Most previous studies included no more than seven subjects with unilateral test (Cappozzo et al., 1996; Fuller et al., 1997; Sati et al., 1996; Stagni et al., 2005). With such few subjects, similarity could be overshadowed easily by variability. The third factor concerns the experimental and analysis methods. Very few studies had used a non-invasive method to examine the movement of individual markers. In two such studies, one tested two total knee replacement patients (Stagni et al., 2005) and the other tested three healthy knees (Sati et al., 1996). Both studies examined the overall ROM of skin markers but did not analyze the time/joint angle related patterns nor perform inter-subject comparison. In the present study, twenty healthy subjects were tested bilaterally during walking without any constraint on free soft tissue movement. This was, to our knowledge, the first study to measure movement of individual skin markers in 4D space using a non-invasive approach and to evaluate their inter-subject similarities.

One importance of that STA has inter-subject similarity is that this may provide a new strategy for STA effect compensation and motion analysis accuracy improvement, as one person's STA profile can possibly be predicted from that of other persons of similar ages and body conditions. Compared with current STA compensation techniques which treat STA as a random or arbitrary noise (Alexander and Andriacchi,

2001; Andriacchi et al., 1998; Cheze et al., 1995; Lu and O'Connor, 1999; Soderkvist and Wedin, 1993; Spoor and Veldpaus, 1980), this may lead to more efficient STA compensation methods by allowing construction of generic or semi-generic STA models from a small group of people and to apply to a large population. Although results in this work indicate the potential of this approach, further studies on direct STA measurement and inter-subject assessment will be needed to completely prove the hypothesis and explore the efficacy.

Conclusions

By using a non-invasive approach to analyze skin marker movement in a relatively large, healthy subject sample, the study in this chapter provided detailed 4D information of soft tissue deformation on the thigh and shank during level walking. Both qualitative and quantitative information is helpful in understanding STA behavior and exploring better marker configurations for gait analysis. Contrary to the prevailing opinion, this study also suggested the possibility that soft tissue movement has inter-subject similarity. This new finding may lead to more effective strategies for STA effect compensation and accuracy improvement in skin marker-based motion analysis. In the next two chapters, we will further explore the behavior of STA *in vivo* using a simultaneous fluoroscopic and stereophotogrammetric experiment. The findings from these studies will lead us to a new strategy of STA compensation.

CHAPTER 3
IN VIVO ASSESSMENT OF SOFT TISSUE ARTIFACT

Introduction

In the previous chapter we demonstrated that soft tissue movement is not a random noise but is a natural movement and has inter-subject similarity. This indicates that “soft tissue artifact (STA)”, which is the relative movement between the markers and the underlying bone, is also not a random “artifact”. Similar to soft tissue deformation or inter-marker movement which was studied in the previous chapter, STA may also have certain patterns which are related to adjacent joint positions and motor tasks. If these natural patterns of STA can be directly identified, we can use this information to develop more specific STA compensation techniques, which will be much more effective than current compensation techniques that treat STA as random noise.

However, to directly assess STA, the movement of both skin markers and the underlying bone needs to be measured at the same time. Comparing to the measurement of skin marker movement, the measurement of bone motion is much more challenging. As being discussed in Chapter 2, most studies that measured *in vivo* bone movement used invasive/semi-invasive methods, including intracortical bone pins (Benoit et al., 2006; Fuller et al., 1997; Reinschmidt et al., 1997a; Reinschmidt et al., 1997b), external fixators (Cappozzo et al., 1996) and percutaneous trackers (Holden et al., 1997; Manal et al., 2000), etc. For the purpose of assessing STA behavior, intracortical bone pin method has apparent disadvantages. First, the invasive pins can cause significant discomfort and potential infection risk to the tested subjects. Second, the pins could constrain and alter the free movement of the soft tissue, and the discomfort could even alter normal skeletal movement. External fixators have similar

drawbacks. They could produce even more constraint on free soft tissue movement than intracortical pins. Percutaneous trackers are less invasive, but they can only be used to measure tibial movement, where the effect of STA is much less than on the thigh.

So far only a few studies used non-invasive techniques to evaluate free soft tissue movement relative to the underlying bone in living people (Garling et al., 2007; Sangeux et al., 2006; Sati et al., 1996; Stagni et al., 2005). These studies used medical imaging techniques to measure the bone position, including magnetic resonance imaging (MRI) and fluoroscopy. MRI provides a radiation-free option for marker and bone pose tracking, but it is not suitable for dynamic measurements due to the low speed of image acquisition. Fluoroscopy techniques have been widely used in the biomechanical community to measure *in vivo* poses of orthopedic prostheses and/or bones during different motor tasks (Banks et al., 2003; Komistek et al., 2003; Kozanek et al., 2009; Stiehl et al., 1995). This “dynamic X-ray” technique can usually reach an imaging acquisition rate of 7 to 30 frames per second, which is much faster than MRI imaging and is sufficient for many low or middle speed activities. However, unlike MRI or computer tomography (CT), fluoroscopy only produces a series of 2D images but does not directly provide the 3D pose measurement. To obtain the 3D pose of the tested object from the 2D images, a 2D-3D registration is needed. This registration could be achieved using an edge based matching (Banks and Hodge, 1996) or image intensity based matching (Penney et al., 2001). With such a registration, even a single view fluoroscopy can be used to obtain the 3D pose of the tested object. This technique has been validated and shown the capability to achieve an accuracy of about 1° and 1 mm

for in-plane motion measurement. The out-plane motion measurement accuracy is lower when using a single plane fluoroscopy technique. More recently, double plane fluoroscopy has also been implemented to reduce out-plane motion measurement errors (Bingham and Li, 2006; Li et al., 2006). Because of its non-invasive nature and the capability to measure skeletal pose in a dynamic manner, fluoroscopic technique provides a suitable approach for the aim of our study.

To track skin marker motion along with tracking bone pose using fluoroscopic technique, there are two options: using fluoroscopy itself (Garling et al., 2007; Sati et al., 1996) or using a separate stereophotogrammetric system (Akbarshahi et al., 2009; Stagni et al., 2005). Using fluoroscopy itself to track the marker position simplifies the experimental configuration to using only one system, but it is difficult to track many markers distributed on a large area of the body segment due to the limited view field of fluoroscopy. Using a separate stereophotogrammetric system to track marker positions is a more flexible approach. It allows the measurement of large number of markers in a large space. But both spatial and temporal synchronizations between the stereophotogrammetric system and the fluoroscopic system need to be achieved. Then the movement of the markers and the bone can be expressed in a uniform spatiotemporal space, and relative movement (STA) can be analyzed.

For the purpose to assess free movement of large number of skin markers relative to the underlying bone, a simultaneous fluoroscopy and stereophotogrammetry method was used in this chapter. Six male subjects who had total knee arthroplasty (TKA) prostheses were tested during a series of knee flexion/extension movements and a stepping-up activity.

Design and Methods

Subjects

With the permission of the institutional review board (IRB) of the University of Florida (UF), six male subjects who had accepted a primary TKA surgery were recruited in this study (Table 3-1).

Table 3-1. TKA subject information.

Subject #	1	2	3	4	5	6
Age (year)	60	69	64	67	65	65
Height (m)	1.74	1.68	1.64	1.79	1.78	1.70
Weight (kg)	95	75	81	95	78	80
Body mass index (kg/m^2)	31.4	26.6	30.1	29.6	24.6	27.7
TKA side	Right	Left	Left	Right	Right	Left
Time after surgery (months)	52	35	25	42	12	60
Top Thigh Circumference (cm)	68	52	56	58	53	50
Mid Thigh Circumference (cm)	60	48	48	50	45	44
Maximum Calf Circumference (cm)	43	39	39	40	39	35
Thigh skinfold thickness (cm)	35	11	28	26	15	8
Shank skinfold thickness (cm)	24	16	13	17	6	9

The inclusive criteria of subject recruitment were:

- Gender: male
- Being younger than 70 years old
- Being active in daily life and having no difficulties to perform daily activities
- Body mass index (BMI) less than 32
- Completion of the TKA surgery at least one year before participating in this study

A signed consent form was obtained from each subject and the test was conducted using an IRB approved protocol.

Experimental Setup

A fluoroscopic system (SIEMENS AXIOM-Artis) in the Orthopaedics and Sports Medicine Institute of UF & Shands Hospital was used to record the radiographic images of knee joint movement. The images were captured at a frequency of 7.5 Hz and the shutter speed was 10 ms. The fluoroscopic system has an image intensifier of 14 inch and the image size was 1024-by-1024 pixels. The distance between the X-ray source and the intensifier was about 1.1 m (Figure 3-1).

Figure 3-1. Simultaneous fluoroscopy and stereophotogrammetry setup.

A stereophotogrammetric system with five Eagle cameras (Motion Analysis Corp., CA, USA) was set up around the functional space of the fluoroscopic system to capture

the movement of reflective markers (Figure 3-1). The 3D residue of marker position tracking of the stereophotogrammetric system was less than 0.4 mm after calibration. The stereophotogrammetric system was running at 60 Hz and shutter speed was 1 ms.

Marker Placement

The subject was required to wear an athletic short that allowed good exposure of both thigh and shank and had little constraint on the movement of skin markers. On the TKA side of the subject, eleven retro-reflective markers (10 mm in diameter) were attached to the thigh (Figure 3-2). Nine markers (T1 to T9) were placed to cover the anterolateral side of the thigh, and another two markers (T10 and T11) were placed on the medial and lateral epicondyles of the femur. Eleven markers were attached to the shank (Figure 3-2). Two markers (S1 and S2) were placed on the medial and lateral ridges of the tibial plateau. Six markers (S3 to S8) were placed on the anterolateral side of the shank. Two markers (S9 and S10) were placed on the medial and lateral malleoli. Another marker (S11) was placed on the tibial tubercle. These markers were used to measure the skin motion at 22 locations.

Four markers were placed on the pelvis (Figure 3-1). These markers were used to measure the pelvic orientation and to calculate hip flexion angle during movement. Since the pelvic markers were not used to measure skin motion, their specific positions were not critical. They were usually placed on the locations that had no large displacement and had good exposure to the stereophotogrammetric cameras. Another marker was placed on the patella to facilitate the temporal synchronization between the fluoroscopic and stereophotogrammetric systems (see next sections for details). In addition, four markers were attached to the image intensifier and five markers were attached to the C-arm of the fluoroscopic unit. These markers were used to track the

movement of C-arm during test and to determine the spatial synchronization between the fluoroscopic and stereophotogrammetric systems (see next sections for details).

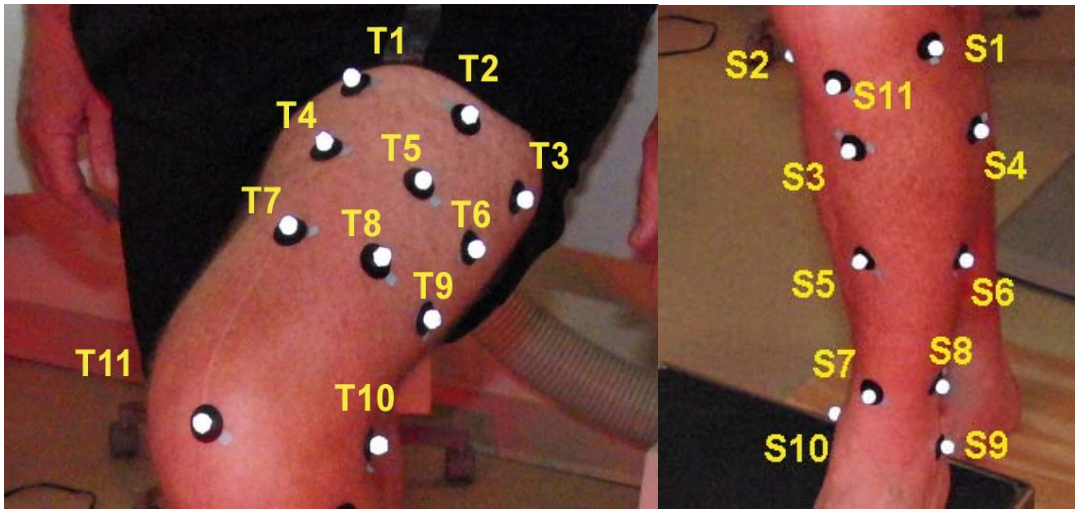

Figure 3-2. Marker placement on the thigh and shank.

Motor Tasks

Due to the limited field of view of the fluoroscopy, it was not suitable to measure motor tasks occurring in a large space like ground walking. Thus, we designed a series of knee flexion movements at different hip flexion angles to cover the sagittal-plane range of motion (ROM) of both hip and knee joints during basic daily activities. Five knee flexion trials were performed by the subject, with a hip flexion angle at -15°, 15°, 30°, 45°, and 60° respectively (for description convenience, we referred “15° hip extension” to as “-15° hip flexion” in this manuscript). At each knee flexion trial, the subject performed a few repeats of knee extension-flexion-extension movements, while maintaining the hip flexion angle which was instructed by a researcher using a goniometer. Figures 3-3 and 3-4 illustrate a subject performing the knee flexion/extension movements at -15° and 45° of hip flexion. Other trials were essentially similar.

Figure 3-3. A subject performing knee flexion/extension movement at -15° of hip flexion.

Figure 3-4. A subject performing knee flexion/extension movement at 45° of hip flexion.

With the series of knee flexion/extension movements, a combination ROM of hip flexion angle (about from -15° to 60° in a discrete manner) and knee flexion angle (about 0° to 90° in a continuous manner) could be covered. Ankle flexion angle was not intentionally controlled considering its low influence on shank STA (Cappozzo et al., 1996). Retrospective analysis showed that the ankle plantarflexion angle covered in the series of movements was about -10° to 30°. From these trials, STA on the thigh and its dependency on hip and knee flexion angles could be analyzed. STA on the shank and its dependency on knee and ankle flexion angles could be analyzed.

In addition to the five knee flexion/extension movements, a stepping-up activity was also performed by each subject (Figure 3-1). This activity was tested as an example of functional motor task during daily living. The step was about 25 mm in height. In the stepping-up trial, the tested subject slowly stepped his foot of the TKA side onto the step, and followed by the other foot.

Test Procedure

First, the fluoroscopic unit was configured for knee joint imaging and the C-arm was positioned horizontally. A custom-built calibration jig was assembled onto the image intensifier of the C-arm and an X-ray image was taken. This image was used to obtain the calibration parameters of the fluoroscopy (e.g. pixel size, source-intensifier distance, image center position) and to correct geometric distortion of the fluoroscopic images. The stereophotogrammetric cameras were positioned around the testing space and the positions of the cameras were adjusted to reach a good coverage on the TKA side of the tested subject. The stereophotogrammetric system was then calibrated with a seed calibration followed by a wand calibration.

Four markers were attached to the image intensifier plane of the fluoroscopic unit, and another five markers were attached to the C-arm (Figure 3-5). These markers were used to track the C-arm position during test and to facilitate spatial synchronization between the two systems. A custom-built L-frame which had four markers attached to a rigid plate was mounted on a tripod and placed between the C-arm (Figure 3-5). An X-ray image was taken on the L-frame by the fluoroscopic system (Figure 3-6), and the 3D positions of all these markers were taken by the stereophotogrammetric system at the same time (Figure 3-7). The 4 markers on the L-frame and the 4 on the intensifier panel were seen by both the fluoroscopic and stereophotogrammetric systems thus could be used to spatially synchronize the two systems. The same procedure was repeated three times, with the L-frame at three different positions and orientations. The three trials were averaged to provide a more reliable synchronization result. After the spatial synchronization procedure, the L-frame was taken out of the functional space and the system was ready for test.

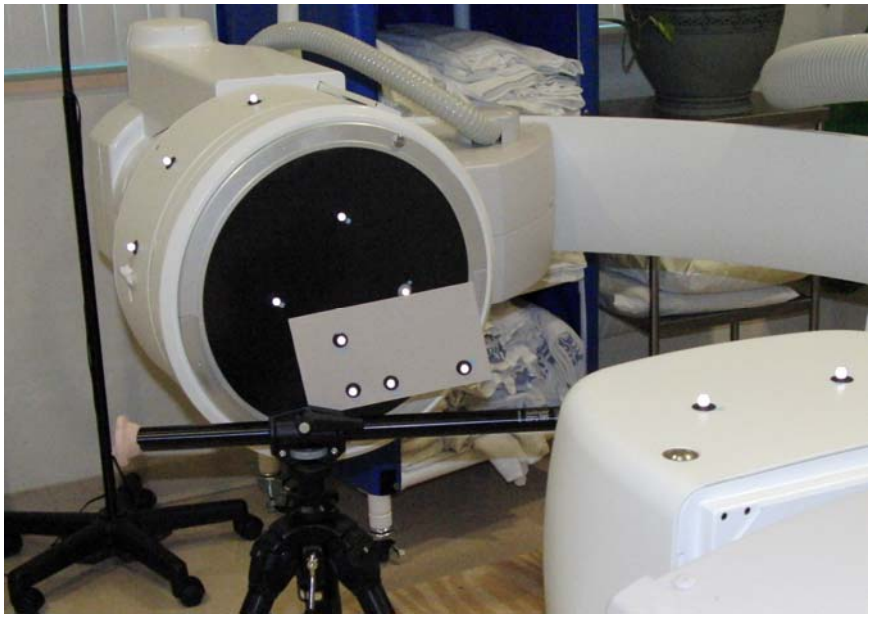

Figure 3-5. L-frame used for spatial synchronization.

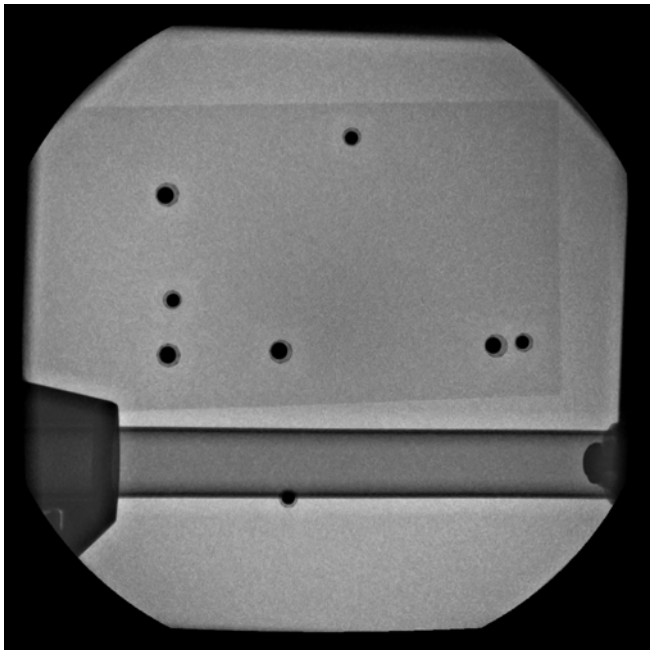

Figure 3-6. X-ray image of the L-frame.

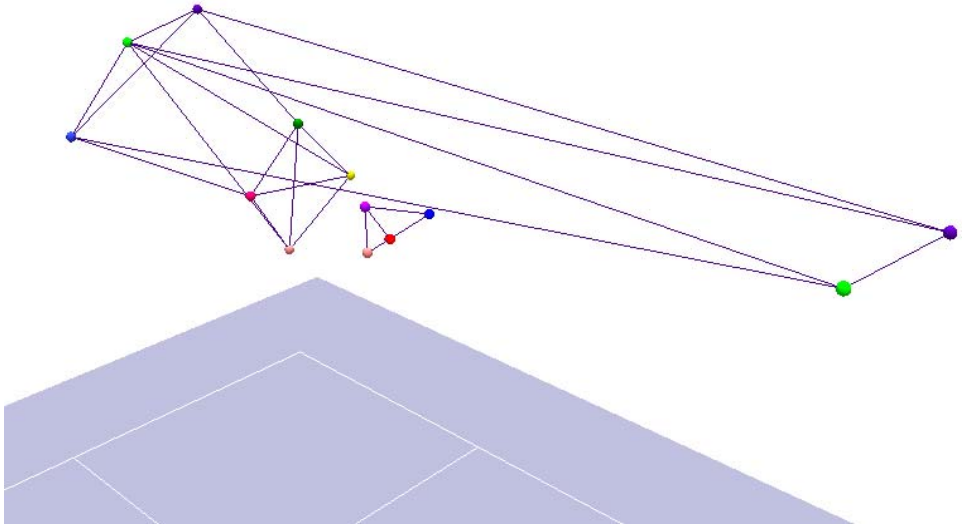

Figure 3-7. Stereophotogrammetric image of the L-frame.

Reflective skin markers were placed on the subject and the test started with a static trial, while the subject was standing still on a pre-designed plate. His foot distance and orientation were controlled by two bars on the plate (Figure 3-8). Both fluoroscopic

and stereophotogrammetric images were taken for this standing posture (Figure 3-9). This trial was used to define the initial anatomical coordinate systems and the initial position of each skin marker relative to the underlying bone. The spatial relationships between the geometrical coordinate systems of the prostheses and the anatomical coordinate systems of the bone were also obtained from this trial.

Figure 3-8. Standing posture on a control plate.

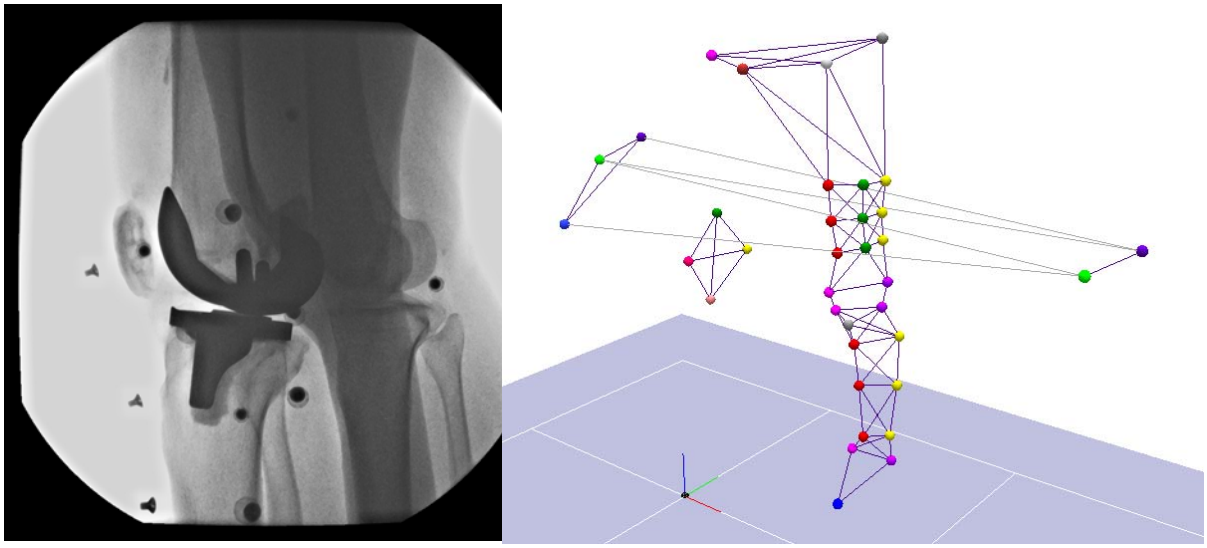

Figure 3-9. Fluoroscopic and stereophotogrammetric images on the standing posture.

After the static trial, the subject performed the series of knee flexion/extension movements. The subject stood on his non-tested foot and was instructed to lift his thigh of the TKA side to a position where the hip flexion angle was measured by a researcher using a goniometer. The subject maintained the hip angle and flexed/extended his knee slowly for several repeats. Enough practice was given before each trial until the subject felt completely comfortable to perform the required task. Hand support was sometime provided to help the subject perform the task, especially for the -15° trial (Figure 3-3). For all the trials, the flexion/extension movement was performed in a slow-speed manner to accommodate to the frame rate of fluoroscopy (7.5 Hz). During data collection of each trial, the stereophotogrammetric system was turned on first and then the fluoroscopic system. Temporal synchronization was not implemented during the experimental stage but in data processing stage (see next sections). At least one complete flexion/extension cycle was recorded by both systems for each trial (each hip flexion angle).

After the five knee flexion/extension trials, the stepping-up trial was performed by the subject. The subject slowly stepped his foot (TKA side) onto the 25 mm high step, and followed by the other foot. The fluoroscopic and stereophotogrammetric data were collected in a similar manner as the flexion/extension movements.

Image Processing

All the fluoroscopic images were first converted from DICOM format to TIFF format using a MATLAB (MathWorks Inc., MA, USA) program. The fluoroscopic calibration image was used to compute the major parameters of the fluoroscopy (e.g. pixel size, source intensifier distance, image center position, distortion coefficients) by another MATLAB program developed by former students in the lab (Figure 3-10). These

parameters were then used to process all the fluoroscopic images for geometric distortion correction, and in later shape-matching procedure.

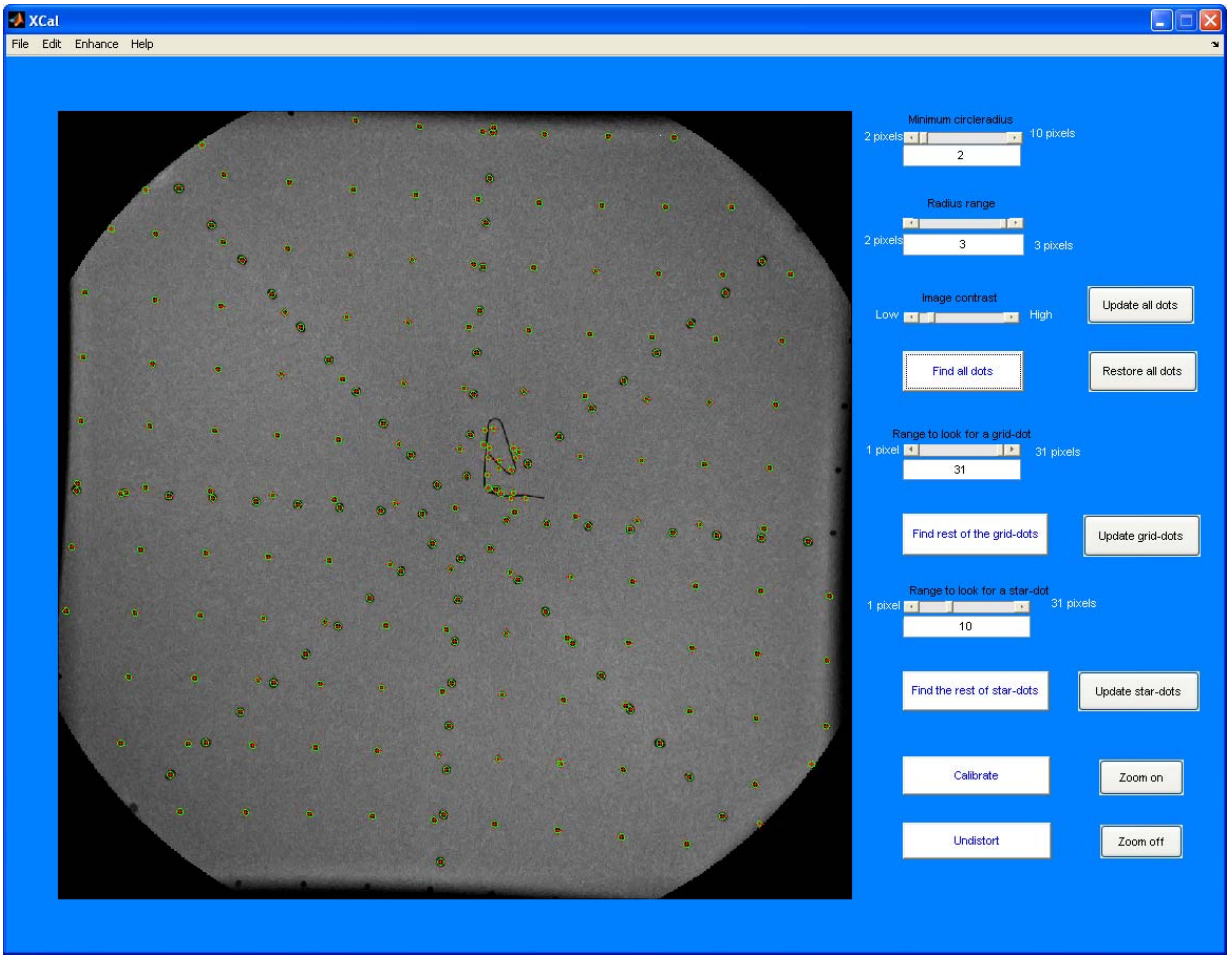

Figure 3-10. Program used to obtain parameters of the fluoroscopy and correct edge distortion of fluoroscopic images.

3D models of both femoral and tibial components of the TKA prostheses in STL format were imported into a custom-developed software (JointTrack, Mu, University of Florida). Controlled by the calibration parameters obtained from the previous step, the 2D projections of the models were generated. With the undistorted fluoroscopic images on the background, an edge-based shape-matching procedure was performed to determine the 3D poses of the prostheses at each fluoroscopic image (Figure 3-11).

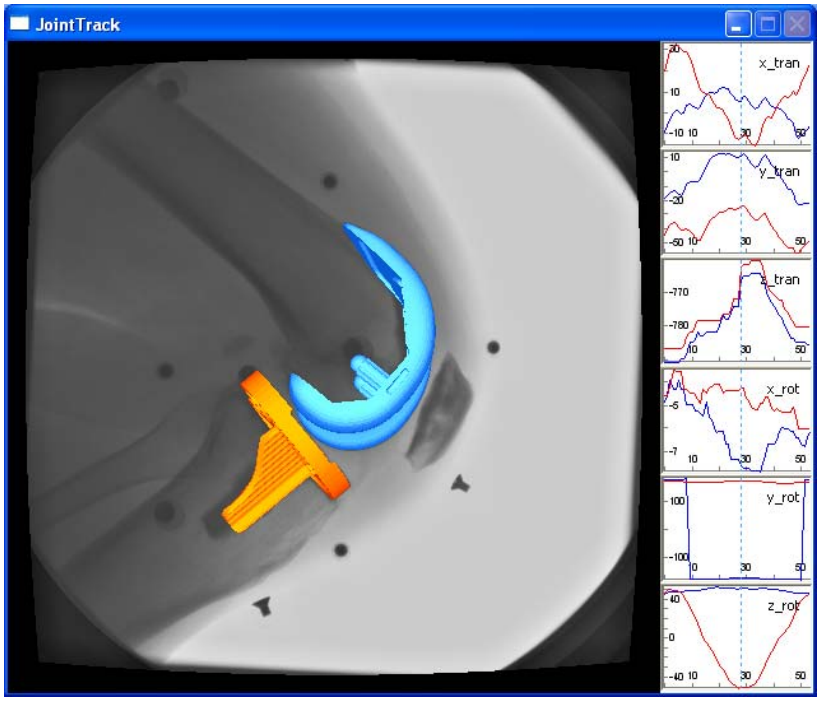

Figure 3-11. JointTrack used to determine the 3D poses of the TKA prostheses at each fluoroscopic image.

Spatial and Temporal Synchronization

The stereophotogrammetric and fluoroscopic images recorded at the spatial synchronization trials (Figures 3-5 to 3-7) were used to determine the spatial relationship between the coordinate systems of the two systems. For each trial, the 3D positions of the eight markers (4 on the image intensifier panel and 4 on the L-frame) were first determined from the stereophotogrammetric system (Figure 3-7). An STL model of the eight markers was created and imported into JointTrack. A shape-matching process was performed between the marker cluster model and the fluoroscopic image (Figure 3-12). Differing to the method only using markers on the image intensifier for spatial synchronization (Stagni et al., 2005), we also included the L-frame markers to form the marker cluster model. By involving markers spreading along the in/out image plane axis, this modified approach resulted in more reliable spatial

synchronization. As shown on the left picture of Figure 3-12, the four markers on the image intensifier seem to be matched well with the fluoroscopic image, but from the four markers on the L-frame we can tell the match was not precise. On the right picture of Figure 3-12, all the eight markers are matched well and the results are more reliable.

From the matching result, the marker cluster's 3D pose in the fluoroscopic space was obtained. Since the marker cluster's 3D pose in the stereophotogrammetric space was also known, the spatial relationship between the fluoroscopic space and the stereophotogrammetric space was able to be determined. The average result was taken from the three spatial synchronization trials. The eight-marker spatial synchronization method demonstrated good repeatability for the multiple trials. The standard deviation (STD) of spatial synchronization results obtained from the three trials were usually less than 0.2° for rotations and 0.6 mm for in-plane translations and 3 mm for out-plane translation.

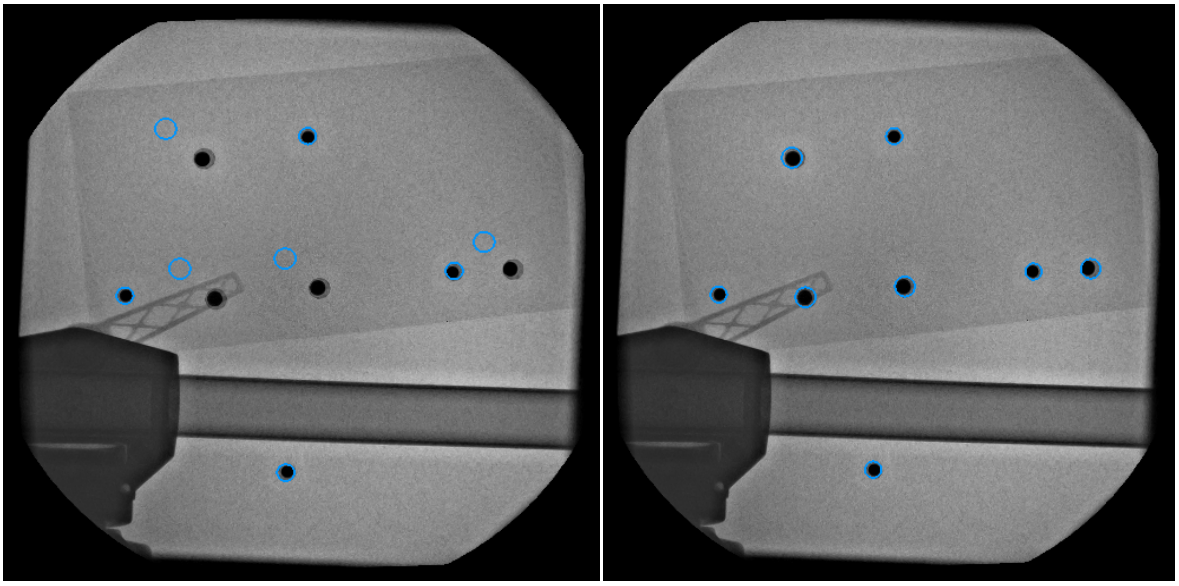

Figure 3-12. Shape-matching between marker clusters and the fluoroscopic image. Left: only the four markers on the image intensifier being matched; Right: all the eight markers being matched.

Since the spatial relationship between the fluoroscopic coordinate system and the markers fixed on the C-arm was constant during the test, the spatial relationship between the fluoroscopic coordinate system and the stereophotogrammetric coordinate system was able to be determined by tracking the markers attached to the C-arm even the C-arm moved during the test.

Temporal synchronization between the fluoroscopic and the stereophotogrammetric systems was achieved by using a single “target marker”, which was usually the patella marker or the tibial tubercle marker (depending on the fluoroscopic images of a specific trial). Since the target marker was tracked by the stereophotogrammetric system and it was also visible in the fluoroscopic image, the motion trajectory of this marker determined by both systems provided direct information to synchronize the two systems temporally. Because the shape-matching process on a sphere shaped single marker lacks good accuracy along the in/out plane direction, we only used the in-plane movement of the target marker to determine the time alignment. The 3D trajectory of the target marker measured from the stereophotogrammetric system was transformed to the fluoroscopic space and projected onto the image plane. Each of the two components of the projected trajectory (X: horizontal component; Y: vertical component) was used to compare to the X or Y translation measured directly from the fluoroscopy (Figure 3-13). The optimization metric used to align the time axes of the two systems was the STD of the difference between the two translational trajectories measured from the two systems. This optimization metric was sensitive to the shape misalignment of the curves but insensitive to the vertical offset between the curves. Since the stereophotogrammetric system had a higher frequency than the

fluoroscopy (60 Hz vs 7.5 Hz), down-sampling (1:8) was applied on the stereophotogrammetric curve in order to perform the curve matching. This method demonstrated good synchronization reliability. For all the trials in this study, the difference between the synchronization results using X and Y components was always no more than one stereophotogrammetric frame (i.e. 1/60 second).

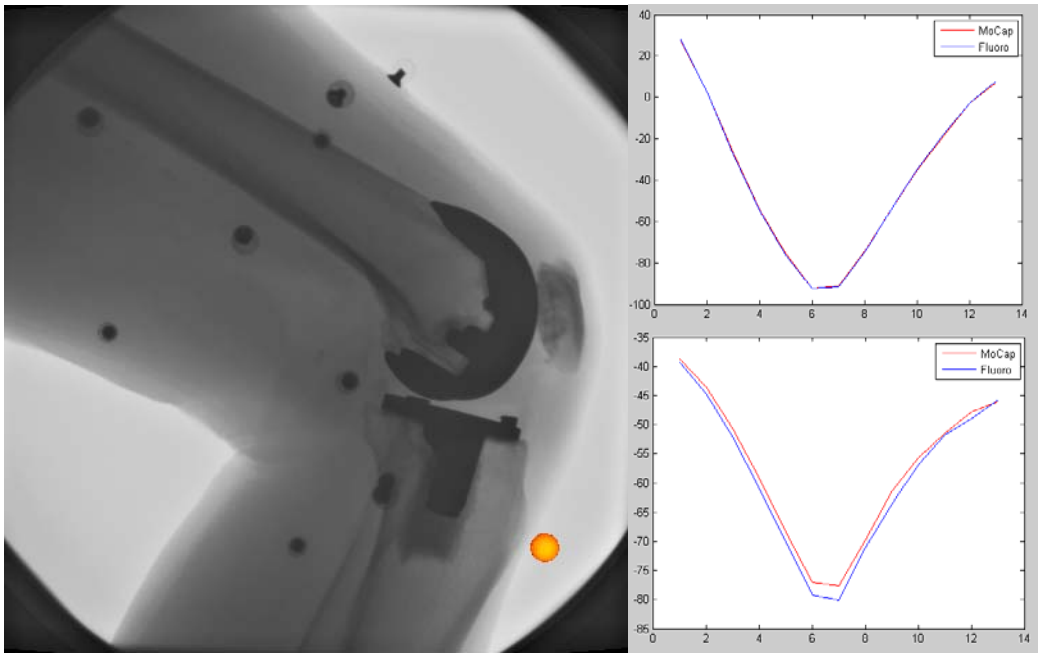

Figure 3-13. Temporal synchronization between the fluoroscopic and the stereophotogrammetric trajectories of the target marker.

STA Computation

Once the spatial and temporal synchronizations between the stereophotogrammetric and fluoroscopic systems were determined for each trial, the movement of both skin markers and prostheses/bone could be analyzed in a uniformed spatiotemporal space. The movements of individual markers relative to the underlying bone were determined, and expressed in the anatomical coordinate system of femur or tibia (Figure 3-14).

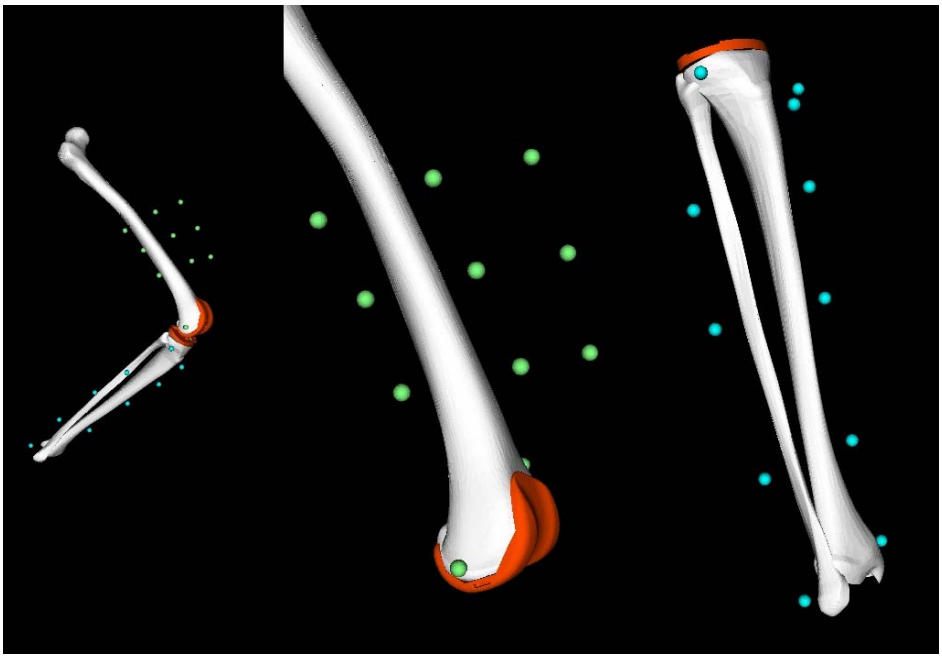

Figure 3-14. The movements of markers and the underlying bones were transformed to a uniform spatiotemporal space thus the relative movements can be analyzed.

The anatomical coordinate systems of the femur and tibial were defined based on the standing posture. The origin of tibia was defined as the midpoint of the medial and lateral ridges of the tibial plateau. The origin of femur was defined as the midpoint of the medial and lateral epicondyles of the femur. The coordinate axes of both femur and tibia were defined parallel to the global coordinate systems at the standing posture, thus all joint angles (hip, knee and angle) were initialized as zero at the neutral standing posture. The dynamic pose of the anatomical coordinate systems of femur/tibia during movement was determined from the fluoroscopic measurement.

Results

STA on the Thigh and Shank of a Representative Subject

Figures 3-15 to 3-20 show the STA (individual marker's displacement relative to the bone) of a representative subject during knee flexions at -15°, 15°, 30°, 45°, 60° of

hip flexion and during stepping up. The marker names can be found in Figure 3-2. The horizontal axis of each subplot is along time. For the knee flexion trials, it starts from an extension position and ends at the peak flexion that followed (usually larger than 90°). For the stepping-up trial, it starts from the knee entering the fluoroscopic view and ends when the movement concluded with the knee fully extended. In some trials some markers were not tracked by the stereophotogrammetric system at some frames. This usually happened on some shank markers and medial knee and ankle markers when the knee joint reached high flexion. The missing data points were not interpolated or extrapolated in these figures, thus the results showing below are truly from experimental data.

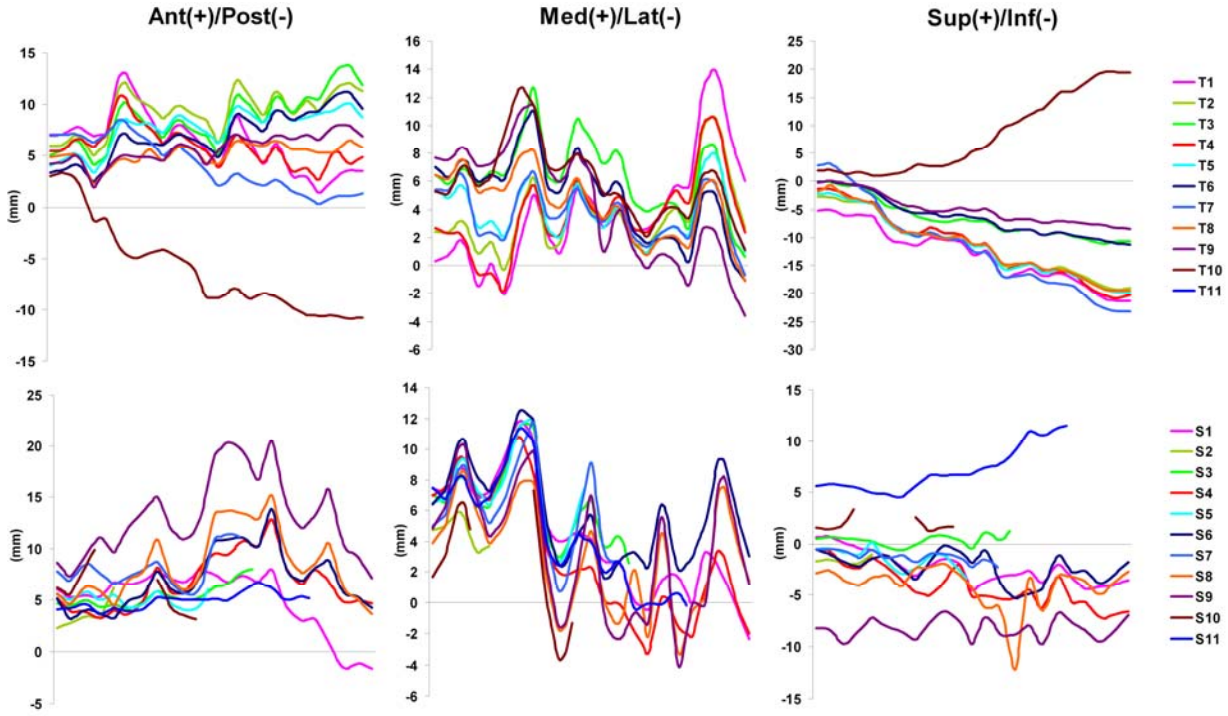

Figure 3-15. STA on the thigh and shank of a representative subject during knee flexion at -15° of hip flexion.

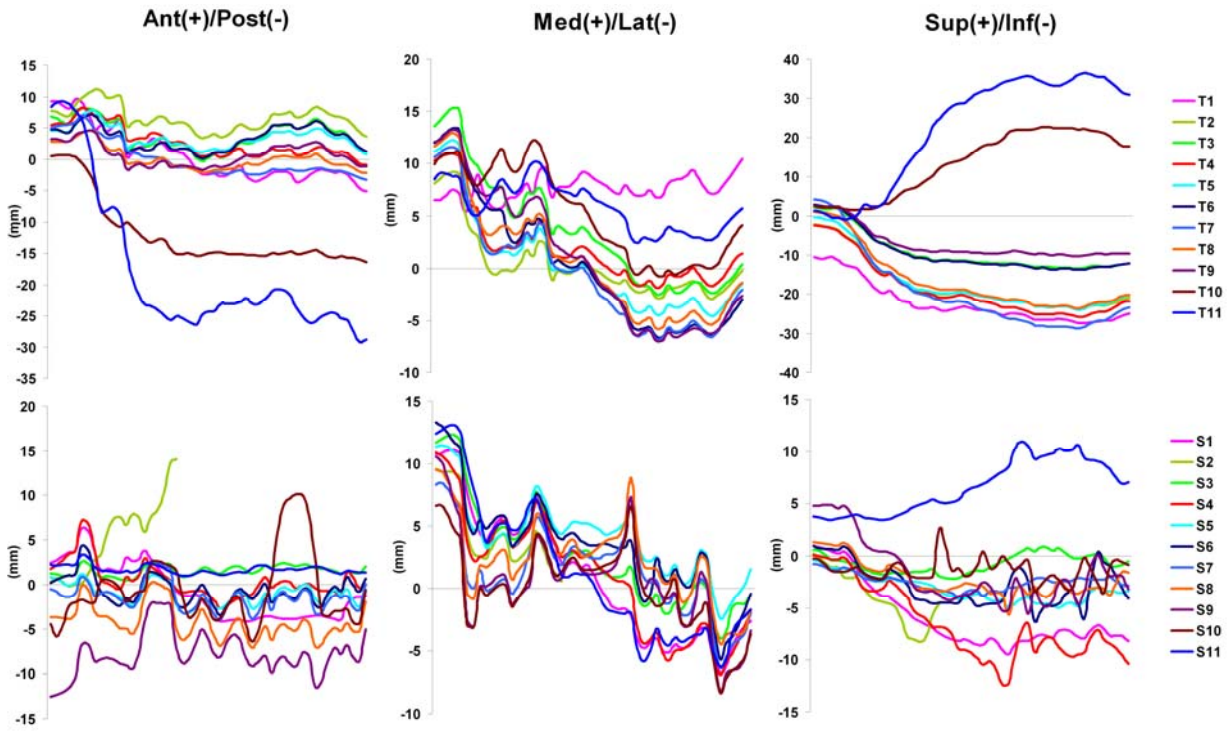

Figure 3-16. STA on the thigh and shank of a representative subject during knee flexion at 15° of hip flexion.

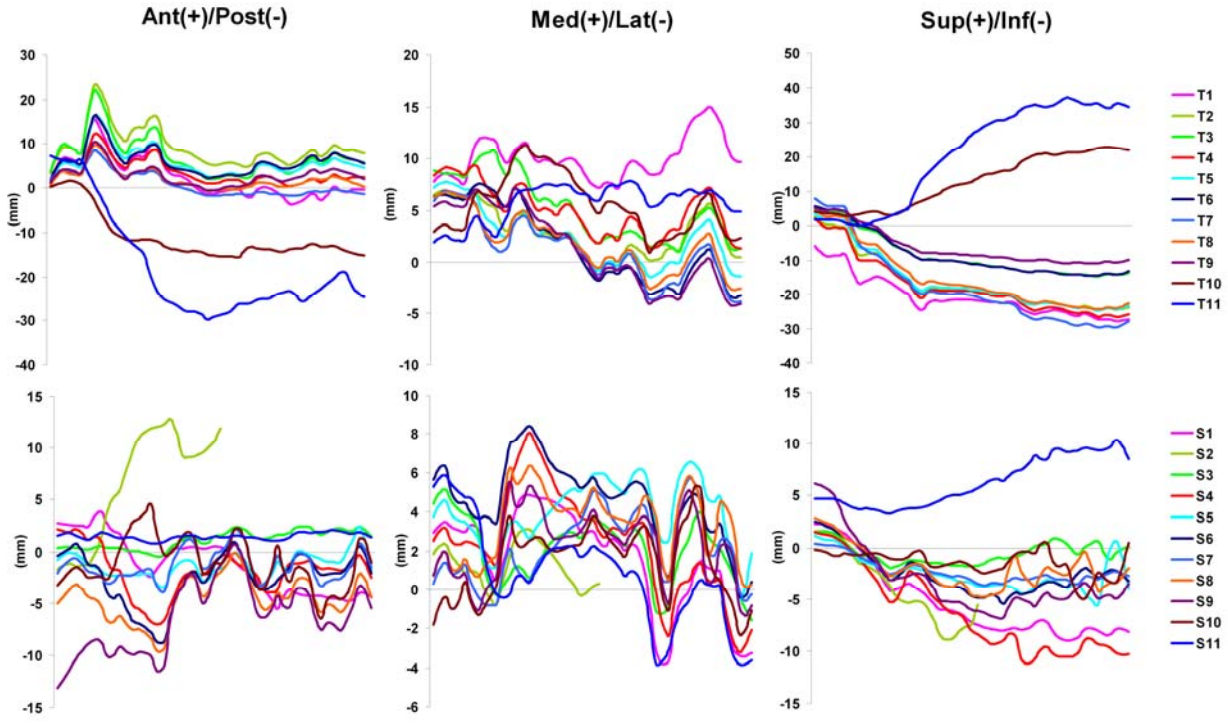

Figure 3-17. STA on the thigh and shank of a representative subject during knee flexion at 30° of hip flexion.

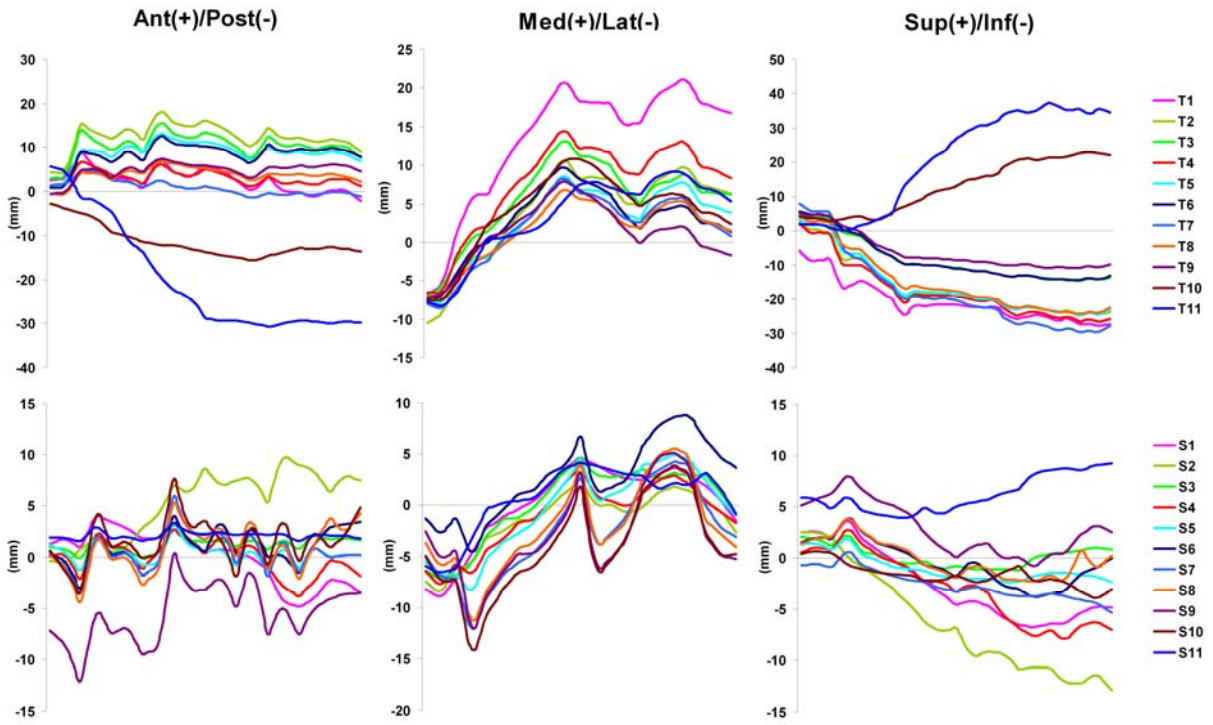

Figure 3-18. STA on the thigh and shank of a representative subject during knee flexion at 45° of hip flexion.

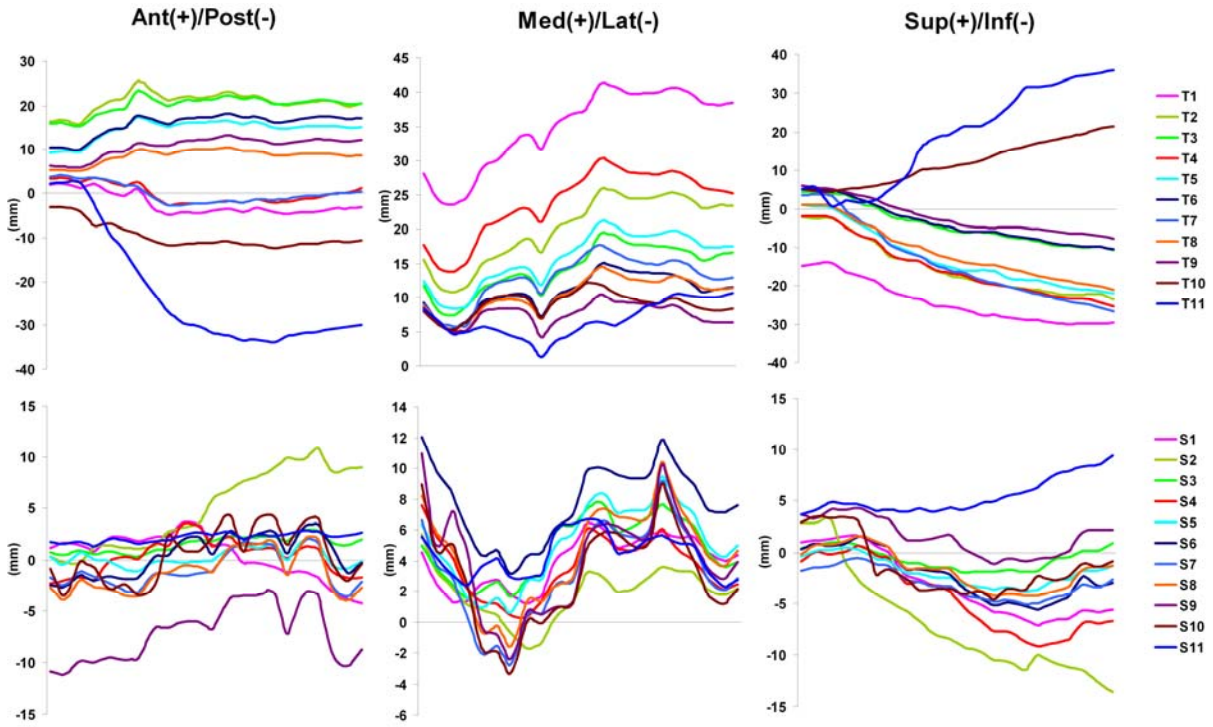

Figure 3-19. STA on the thigh and shank of a representative subject during knee flexion at 60° of hip flexion.

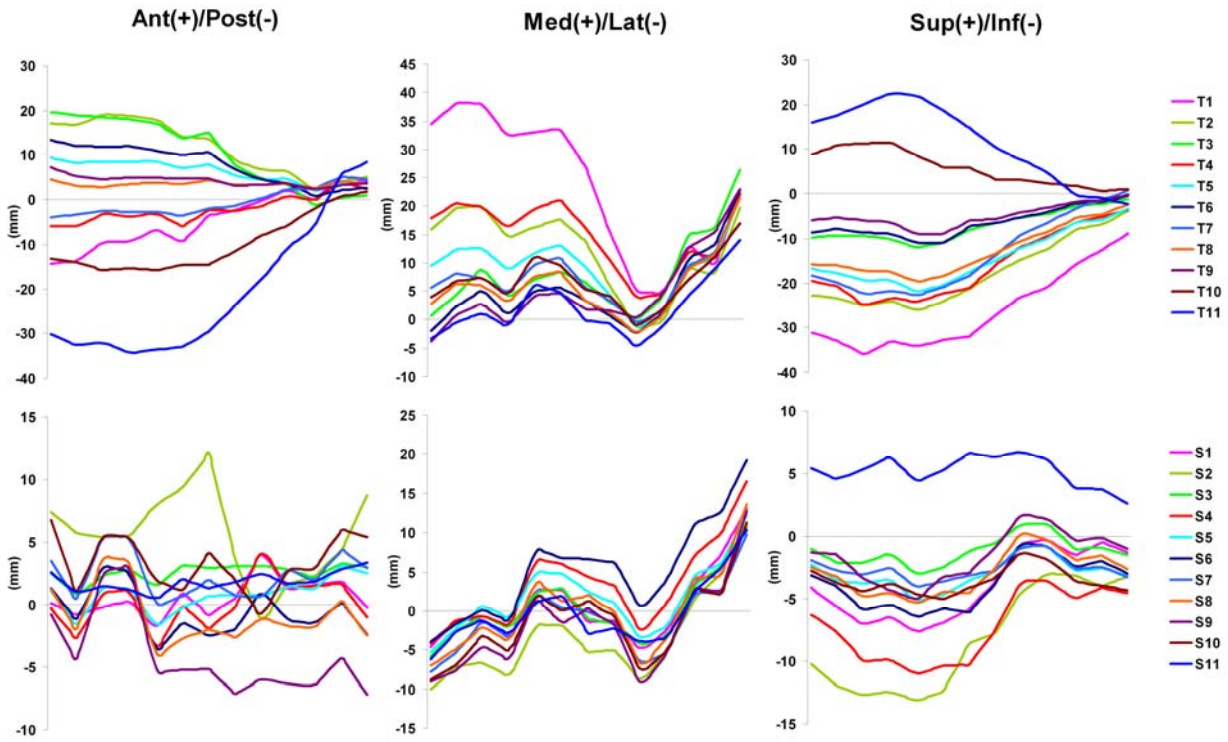

Figure 3-20. STA on the thigh and shank of a representative subject during stepping up.

Inter-Subject Common Patterns of STA on the Thigh

Figures 3-21 to 3-26 show the mean curves and STD of every thigh marker's STA across all the six subjects, during knee flexions at -15°, 15°, 30°, 45°, 60° of hip flexion and during stepping up. For the knee flexion trials, the STA was firstly expresses along knee flexion angle; then the average across all subjects was taken over the range from 10° to 90° of knee flexion. For the stepping-up trial, the average across subjects was taken over time from the frame when the knee entered the fluoroscopic view until the frame when the movement concluded with the knee extended on the step.

Due to the larger error of out-plane translation measurement of single view fluoroscopy technique, the STA along medial/lateral (ML) direction is not reliable and not presented. In each of the following figures, subplots of STA along anterior/posterior

(AP) direction (_X) are shown on the top row, with anterior as positive; subplots of STA along superior/inferior (SI) direction (_Z) are shown on the bottom row, with superior as positive.

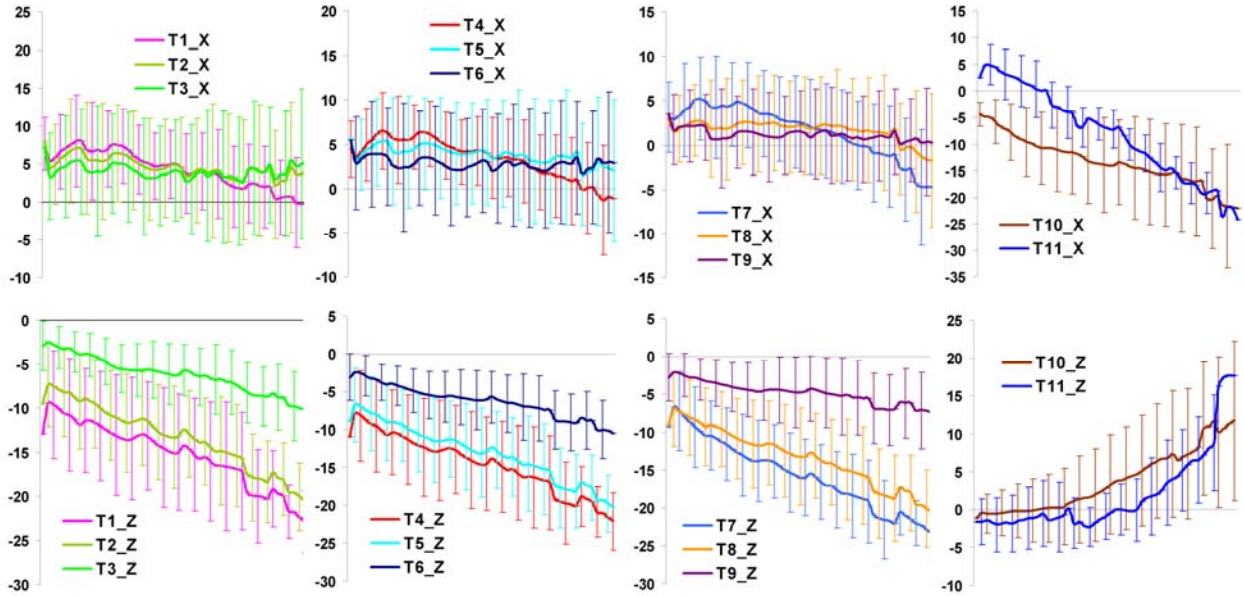

Figure 3-21. Mean curves and standard deviations of thigh STA across all subjects during knee flexion at -15° of hip flexion.

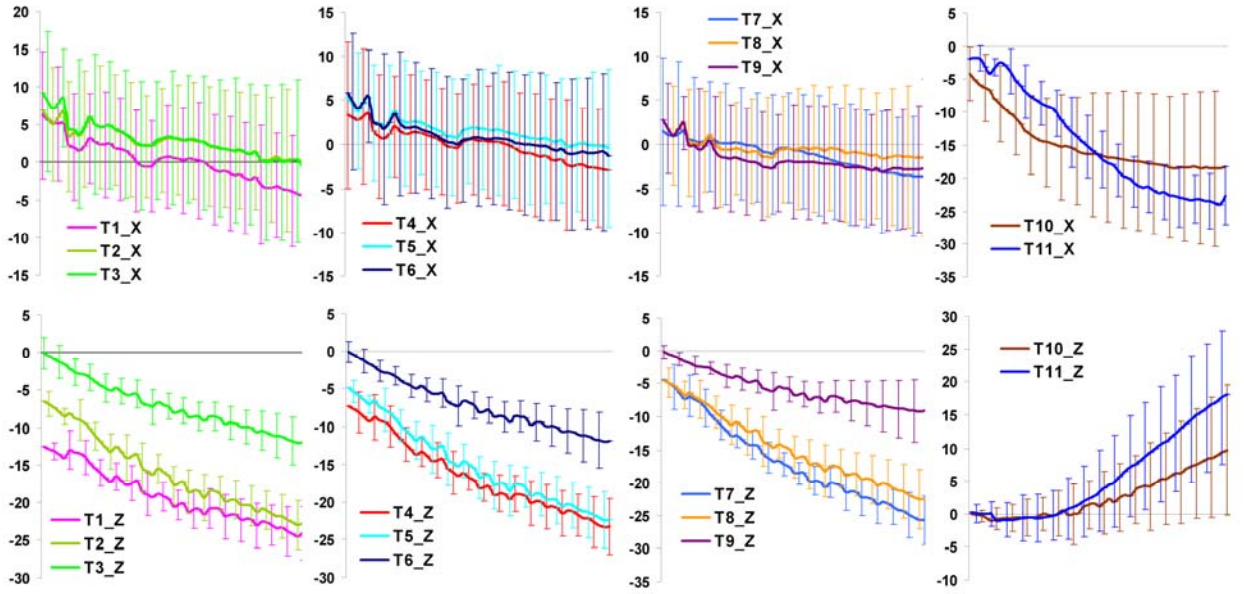

Figure 3-22. Mean curves and standard deviations of thigh STA across all subjects during knee flexion at 15° of hip flexion.

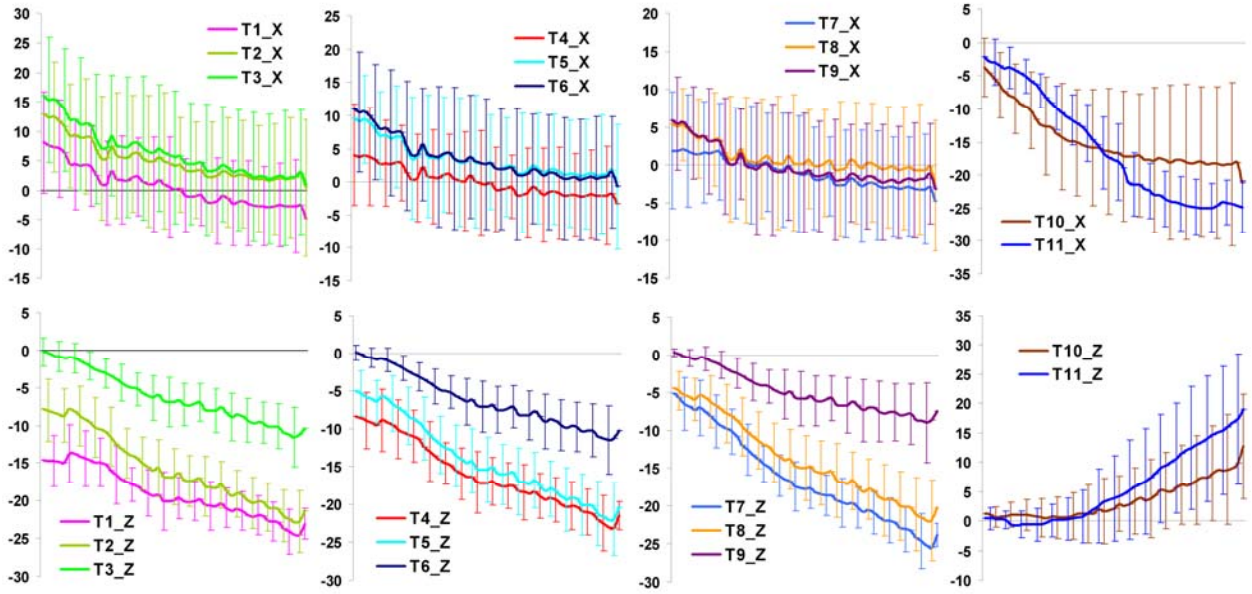

Figure 3-23. Mean curves and standard deviations of thigh STA across all subjects during knee flexion at 30° of hip flexion.

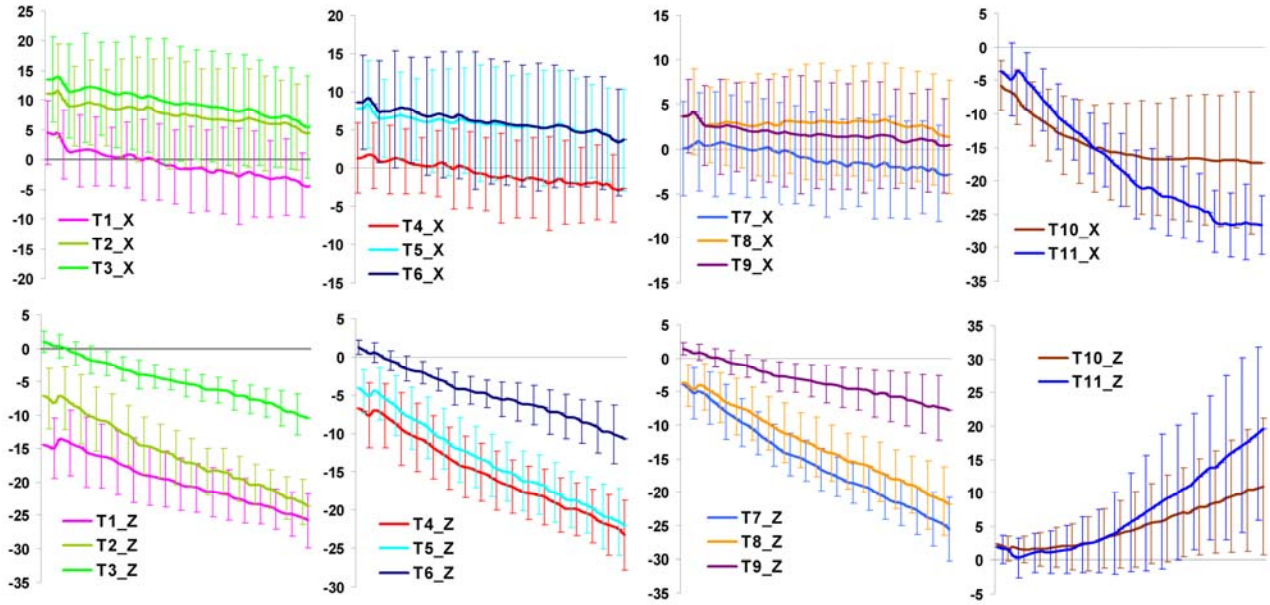

Figure 3-24. Mean curves and standard deviations of thigh STA across all subjects during knee flexion at 45° of hip flexion.

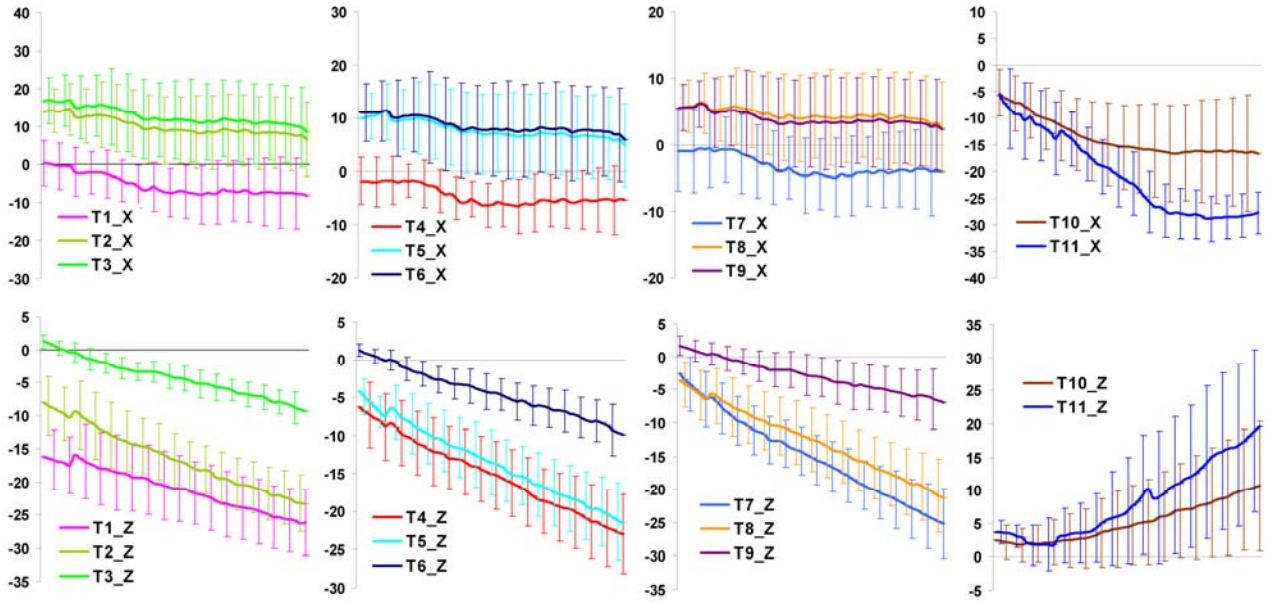

Figure 3-25. Mean curves and standard deviations of thigh STA across all subjects during knee flexion at 60° of hip flexion.

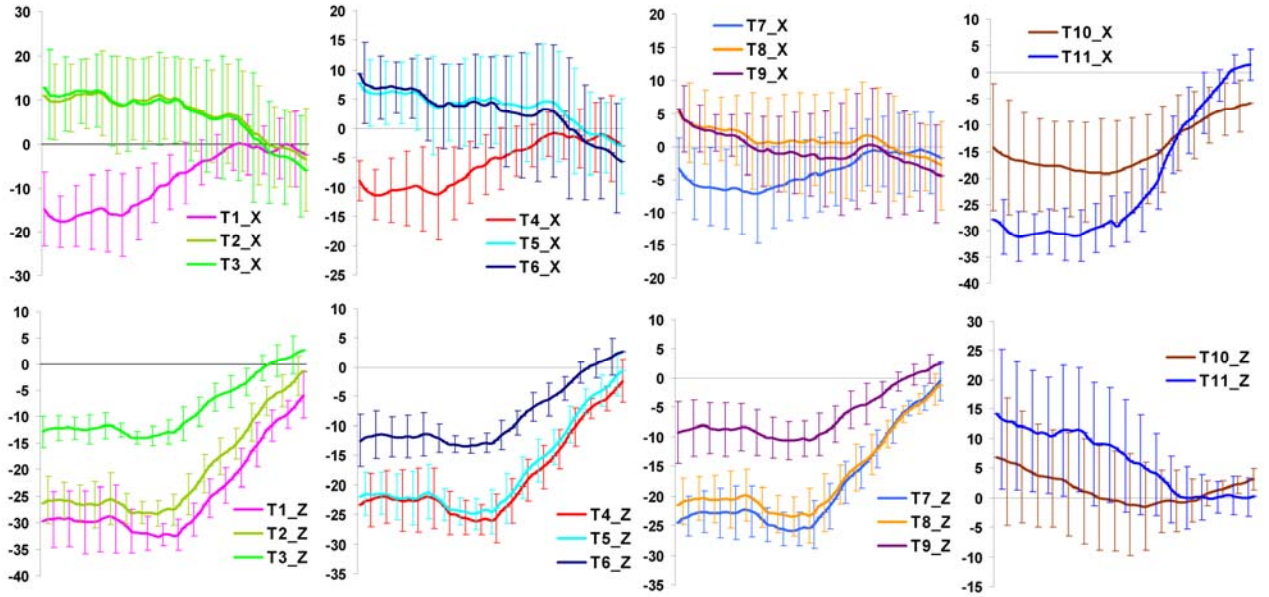

Figure 3-26. Mean curves and standard deviations of thigh STA across all subjects during stepping up.

Inter-Subject Common Patterns of STA on the Shank

Figure 3-27 to 3-32 show the mean curves and STD of each shank marker's STA across all the six subjects, during knee flexions at -15°, 15°, 30°, 45°, 60° of hip flexion and during stepping up. The marker names can be found in Figure 3-2. For the knee flexion trials, the STA was firstly expresses along the knee flexion angle; then the average across all subjects was taken over the range from 10° to 90° of knee flexion. For the stepping-up trial, the average across subjects was taken over time from the frame when the knee entered the fluoroscopic view until the frame when the movement concluded with the knee extended on the step.

The STA along ML direction are not presented due to the lower accuracy of out-plane translation measurement of single view fluoroscopy. In each of the following six figures, subplots of STA along AP direction (_X) are shown on the top row, with anterior as positive; subplots of STA along SI direction (_Z) are shown on the bottom row, with superior as positive.

In the trials at -15° of hip flexion, some skin markers on the shank were not completely tracked during the whole movement by the stereophotogrammetric cameras, thus there are some incompletion or discontinuities showing on the curves. For most other trials, this was not an issue.

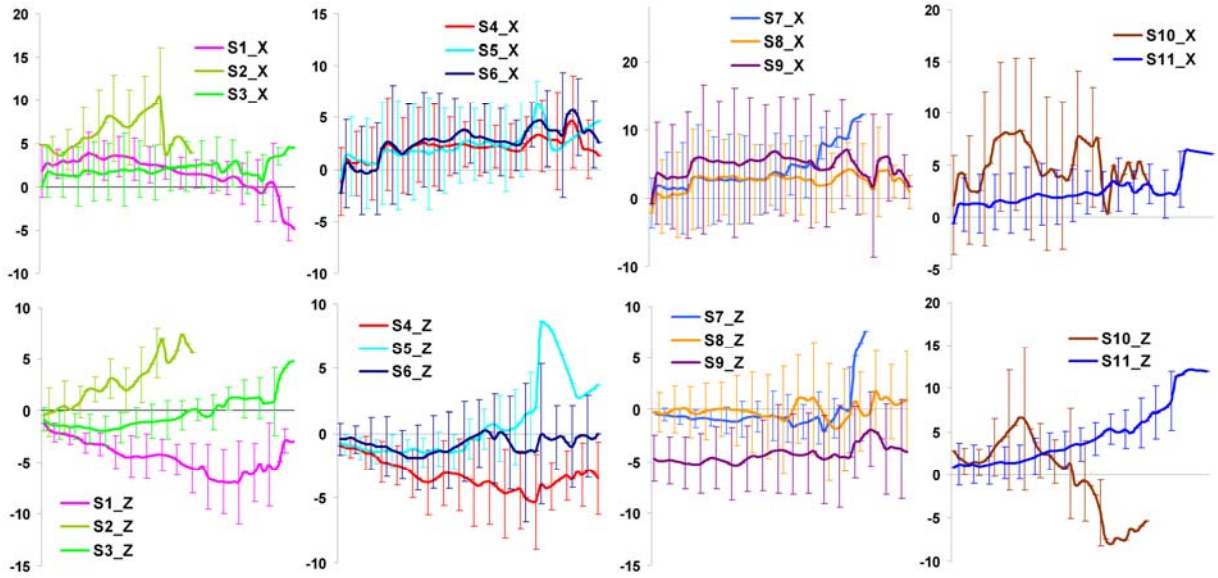

Figure 3-27. Mean curves and standard deviations of shank STA across all subjects during knee flexion at -15° of hip flexion.

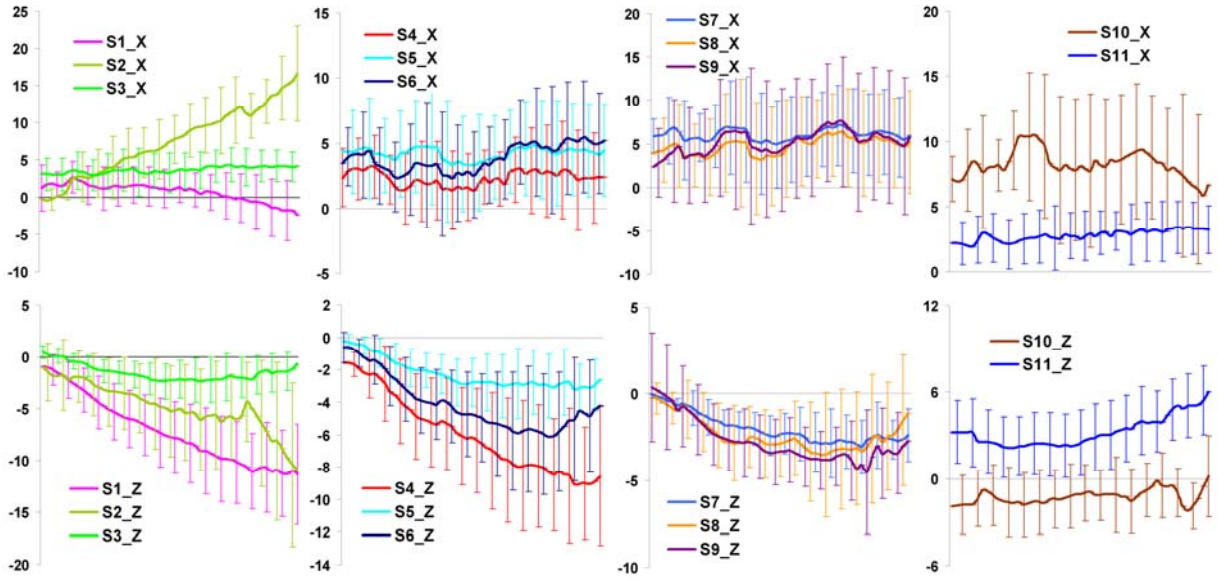

Figure 3-28. Mean curves and standard deviations of shank STA across all subjects during knee flexion at 15° of hip flexion.

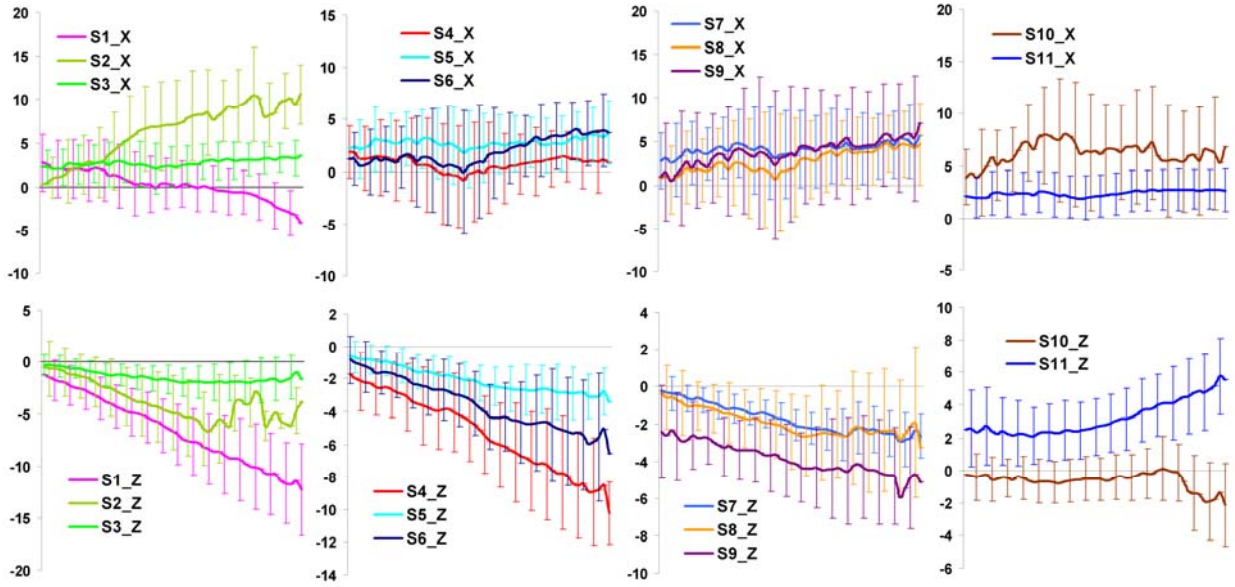

Figure 3-29. Mean curves and standard deviations of shank STA across all subjects during knee flexion at 30° of hip flexion.

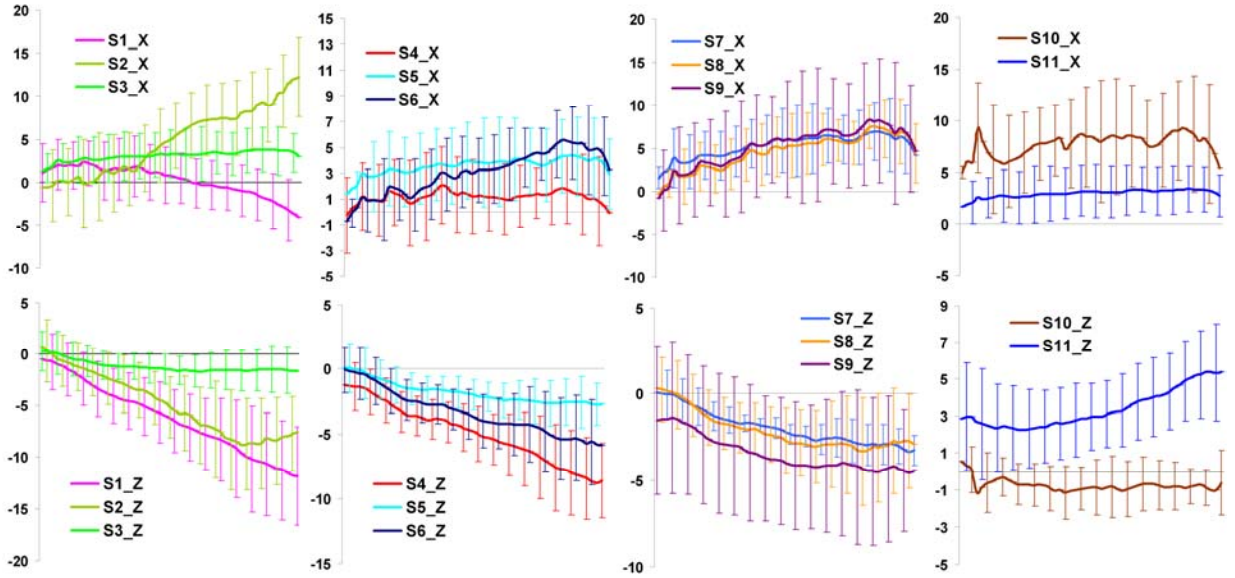

Figure 3-30. Mean curves and standard deviations of shank STA across all subjects during knee flexion at 45° of hip flexion.

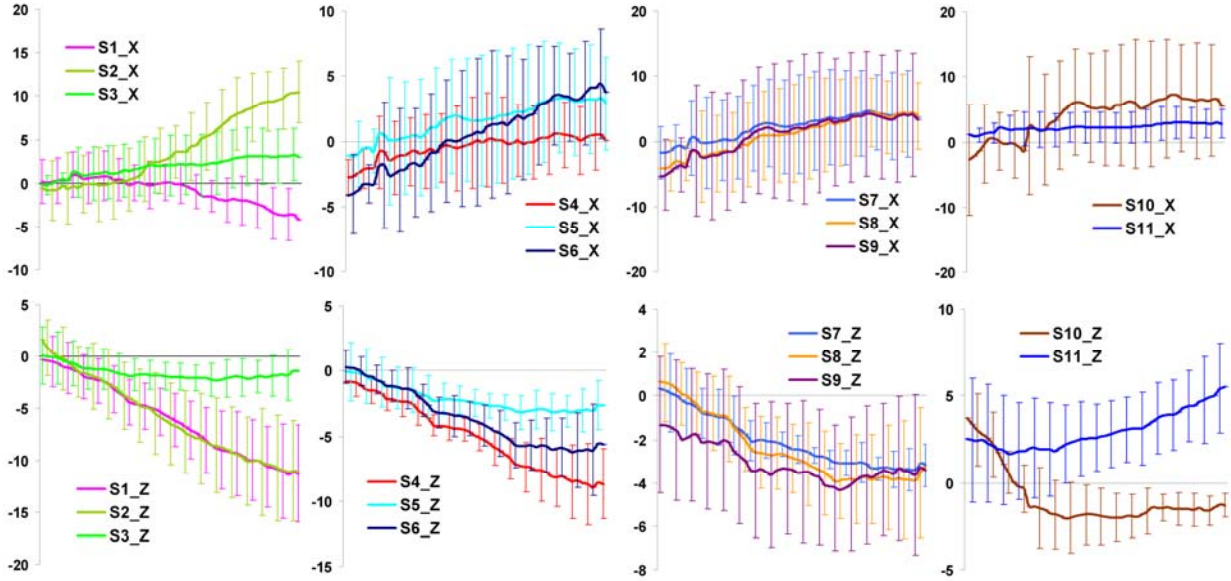

Figure 3-31. Mean curves and standard deviations of shank STA across all subjects during knee flexion at 60° of hip flexion.

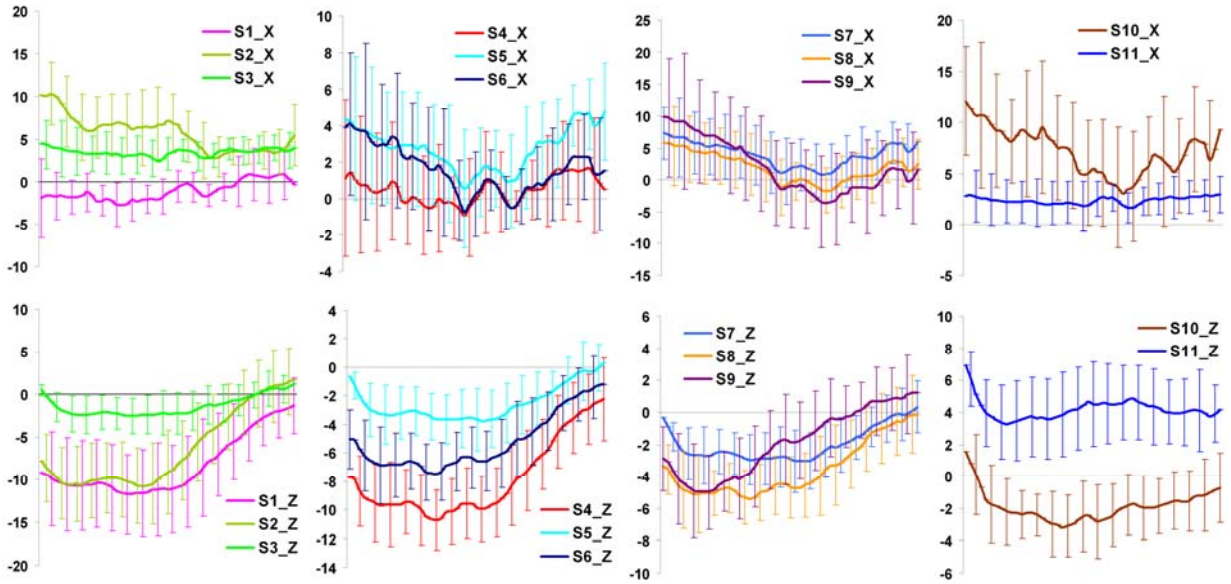

Figure 3-32. Mean curves and standard deviations of shank STA across all subjects during stepping up.

Discussions

In this step of study, the STA of individual markers on both thigh and shank was measured *in vivo* without any constraints by invasive apparatus. At a very first glance, it is apparent that STA is not random noise but is systematic movement that related to the activity and joint positions. For the knee flexion/extension movements, STA increased with increasing knee flexion (deviating from the standing posture where the markers' initial local positions were determined). For the stepping-up activity, STA started with large values when the knee first entered the fluoroscopic view field (usually at over 70° of knee flexion and over 50° of hip flexion); STA decreased as the knee extended and finally reached close to zero when the movement concluded at knee extension. From Figures 3-15 to 3-32, it can be seen that STA on the thigh was generally much larger than STA on the shank. A skin marker's movement on the thigh relative to the femur sometimes can be over 30 mm at high flexion. STA on the shank was usually less than 15 mm in any direction. This observation was expected considering the muscular structures on the thigh and the shank.

The magnitudes and profiles of STA varied along different anatomical directions. STA was generally larger along SI direction than along the other two directions, and this feature was more prominent on the thigh. On the thigh, STA along SI direction exceeded 20 mm for many markers at high flexion, while STA along AP direction was usually less than 15 mm. STA along ML direction was not able to be reliably measured due to the relatively low accuracy of out-plane translation measurement using single view fluoroscopy. Based on the ML results we obtained, STA along ML direction was lower than along SI direction, but a little higher than along AP direction for most

markers. On the shank, STA along AP direction was usually less than 10 mm for most markers, and was a little larger along SI direction.

STA was not uniformly distributed on different markers at different locations. On the thigh, most markers shifted slightly posteriorly while the knee flexed, but the two markers on the femoral epicondyles (T10 and T11) exhibited much larger posterior displacement than other markers. The three markers on the anterior side (T1, T4 and T7) exhibited the smallest anterior displacement. All the thigh markers except for T10 and T11 moved inferiorly during knee flexion, while T10 and T11 moved in the superior direction. Among T1 to T9, the three markers on the lateral side (T3, T6 and T9) exhibited the smallest inferior displacement, while the three markers on the anterior side (T1, T4 and T7) exhibited the largest inferior displacement. Overall, the markers on "bone landmarks" (T10 and T11) showed larger STA than other thigh markers. Anterior markers (T1, T4 and T7) were more reliable in AP direction, while lateral markers (T3, T6 and T9) were more reliable in SI direction.

On the shank, most markers tended to slightly shift anteriorly during knee flexion except for the marker on the lateral ridge of the tibial plateau (S1), which moved in the posterior direction. The marker on the medial ridge of tibial plateau (S2) exhibited larger anterior displacement than most other markers. All shank markers except for the one on the tibial tubercle (S11) moved inferiorly during knee flexion. The two markers on the ridges of tibial plateau (S1 and S2) exhibited the largest inferior displacement. The three markers on the anterior tibia (S3, S5 and S7) showed the smallest inferior displacement (less than 2 mm). Overall, S3, S5 and S7 had small STA on both AP and SI directions. S11 had small STA on AP direction but not on SI direction. The commonly used "bone

landmarks" (S1, S2, S9, and S10) did not exhibited smaller STA than other shank markers.

Another interesting observation was that STA exhibited similar patterns for markers that were on a same "column" (vertical line). This was very prominent on the thigh. The nine markers on the anterolateral thigh (T1 to T9) can be categorized into three subgroups: 1) T1, T4 and T7; 2) T2, T5 and T8; and 3) T3, T6 and T9. The three markers in each subgroup showed similar STA patterns along both AP and SI directions. But the similarity for markers on a same "row" (horizontal line) was lower. Such similarity was also visible for markers on the shank, although less prominent. Markers S3, S5, and S7 exhibited similar STA patterns, as well as the subgroup S4, S6 and S8. This observation is consistent with the findings in Chapter 2, and is reasonable considering most muscles' contraction directions are generally along SI direction during knee flexion movement.

STA patterns exhibited inter-subject similarity, which can be seen in Figures 3-21 to 3-32. Although there was some variability, STA on most markers was in similar profiles across subjects. The similarity is most prominent for STA along SI direction, which showed clear mean curves and small STD across subjects. The common patterns along AP direction had higher STD than along SI direction, but still apparent. Because there were unavoidable marker placement inconsistency on different subjects, and the STA was more sensitive to location change along AP direction than along SI direction (based on the findings in the previous paragraph), the higher STD on AP direction could result more from the marker placement inconsistency than from the real inter-subject variability of STA. The effect of location sensitivity on the STA variability

was more evidenced by the epicondyle markers (T10 and T11). Since the location sensitivity of STA is higher close to the joint where large amount soft tissue deformation occurs during knee flexion, the STA patterns of T10 and T11 exhibited higher inter-subject variability than other markers. Considering subjects' anthropometric variability and marker placement inconsistency on different subjects, the observed common patterns across subjects strongly demonstrated that STA is not totally subject-dependent. This study is the first, to our knowledge, to provide direct evidence supporting this concept. This finding indicates the possibility that STA models can be developed from some subjects and used for others, with major behaviors being reflected.

In addition to that STA has inter-subject similarity which was demonstrated in this study, another widely accepted concept that STA is totally motor task-dependent is also being challenged by the findings in this study. First, from Figures 3-21 to 3-32 it can be easily identified that the STA patterns were similar during the series of knee flexion movements, with small differences likely caused by the difference of hip flexion angles. In addition, for the stepping up activity, the STA exhibited comparable behavior to the knee flexion movements if we consider the movement of adjacent joints. For example, the SI components of thigh STA during stepping up are generally consistent with those during knee flexion at 60° of hip flexion, imaging that the knee joint angle changed from 90° to 0°. Based on this observation, we hypothesized that a large portion of STA is determined by the joint position or simply the adjacent joint angles. If the relationship between STA and the adjacent joint angles can be determined, a "universal" STA model could be developed for different motor tasks. If this hypothesis is proved, we no longer

have to pursue STA models for each specific motor task. Rather than this, the "universal" STA model will be sufficient to represent the basic behavior of STA during different motor tasks. In the next chapter, we will validate this hypothesis and demonstrate that STA also has inter-motor-task similarity in addition to inter-subject similarity. Based on this knowledge, a "universal" STA model will be developed and two new evidence-based STA compensation methods will be implemented and their effectiveness over conventional method will be evaluated.

CHAPTER 4
DEVELOPMENT OF NEW METHODS FOR SOFT TISSUE ARTIFACT COMPENSATION

Introduction

In the previous chapter, we demonstrated that soft tissue artifact (STA) has inter-subject similarity, and proposed the hypothesis that STA is not totally motor-task-dependent but mainly related to adjacent joint angles. In this chapter, we will test this hypothesis and demonstrate that a large portion of STA can be predicted by adjacent joint position. Further, we will develop a “universal” STA model that reflects the common patters multiple subjects. This STA model that can be represented as functions of adjacent joint angles will be established based on the *in vivo* STA data obtained from the previous chapter. From this model, two new “evidence-based” STA compensation methods will be developed and their performance will be evaluated by comparison to the conventional method.

Development of a “Universal” STA Model

STA in a Two-Dimensional Joint Angle Space

In the last chapter, the STA during each of the series of knee flexion movements has been determined. By combining the results of the series of knee flexion trials (5 trials) together, we are able to obtain an STA map over a wide coverage of combinations of adjacent joint angles. Specifically, the hip, knee and ankle flexion angles during each of the 5 trials were calculated along with the STA measurement. STA on the thigh was examined over hip and knee flexion angles, and STA on the shank was examined over ankle and knee flexion angles.

For example, Figure 4-1 illustrates a 3-dimensional (3D) plot of T1’s STA along superior/inferior (SI) direction of a representative subject, over hip and knee flexion

angles. This plot contains all the data points from the 5 trials of knee flexion movements of this subject. Each dot in the plot represents one fluoroscopic image. A top 2-dimensional (2D) view of this plot reveals the hip and knee angle ranges that were covered by the 5 trials (Figure 4-2). For this subject, the 5 trials covered a hip flexion range about from 10° to 50°, and a knee flexion range about from 0° to 100°. It was noted that the actual hip flexion angles during these trials may deviate from the intended value (i.e., -15°, 15°, 30°, 45°, and 60°). Especially for the -15° trial, the actually hip flexion angle was positive but not negative. This phenomenon happened on almost every subject. The cause was retrospectively identified as that when the subject performed this motor task his pelvis usually tilted forward and this reduced the intended hip extension angle (the forward pelvic titling can be observed in Figure 3-3). Reasonable amount of hip angle fluctuation during individual trials was also observed (Figure 4-2). A left view of Figure 4-1 shows the relationship between this STA component and hip flexion angles (Figure 4-3). With hip flexion angle increased, STA increased along negative direction (i.e., marker T1 moved inferiorly). The spread along vertical axis in Figure 4-3 indicates this STA component was not purely related to hip flexion angle but also knee flexion angle. This is shown in Figure 4-4 which is a front view of Figure 4-1. Figure 4-4 clearly reveals a negative slope between this STA component and knee flexion angle (i.e. with knee flexed more, marker T1 shifted inferiorly more). Figures 4-3 and 4-4 demonstrate that the SI component of T1's STA is related to both hip and knee flexion angles.

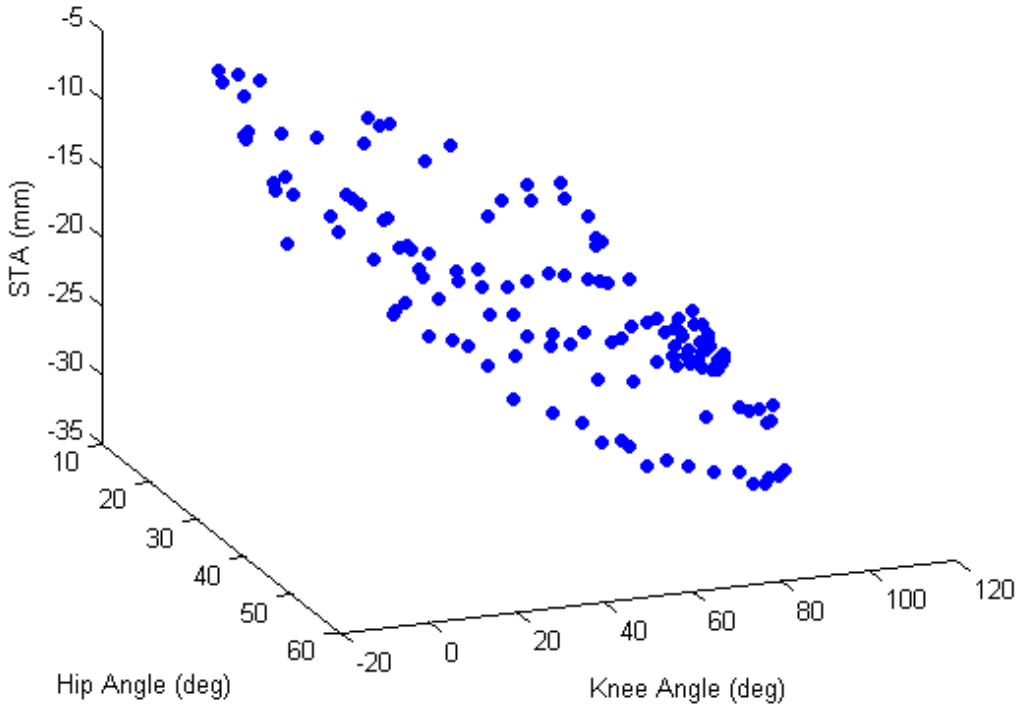

Figure 4-1. 3D plot of marker T1's STA (SI component) of a representative subject over hip and knee flexion angles.

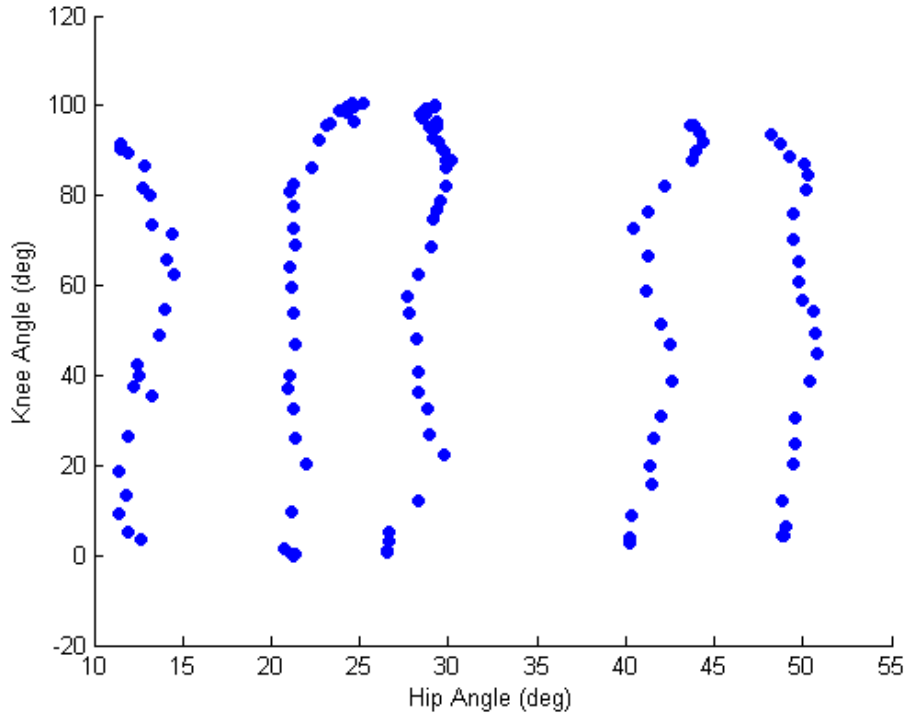

Figure 4-2. 2D plot showing the hip and knee angle coverage by the series of knee flexion movements of a representative subject.

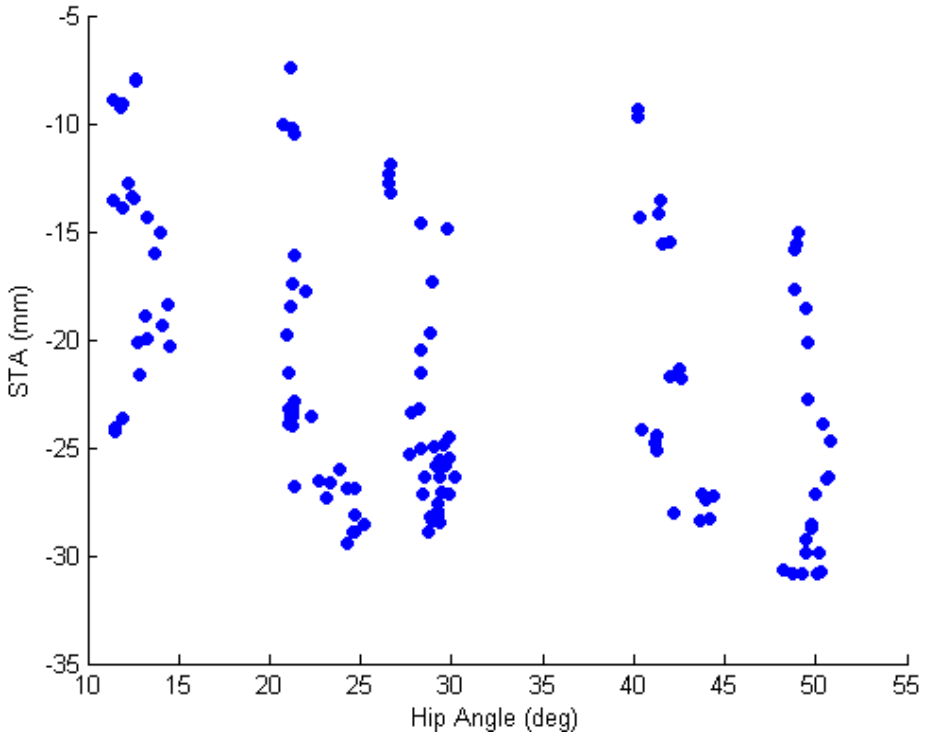

Figure 4-3. 2D plot showing the relationship between the STA component and hip flexion angle.

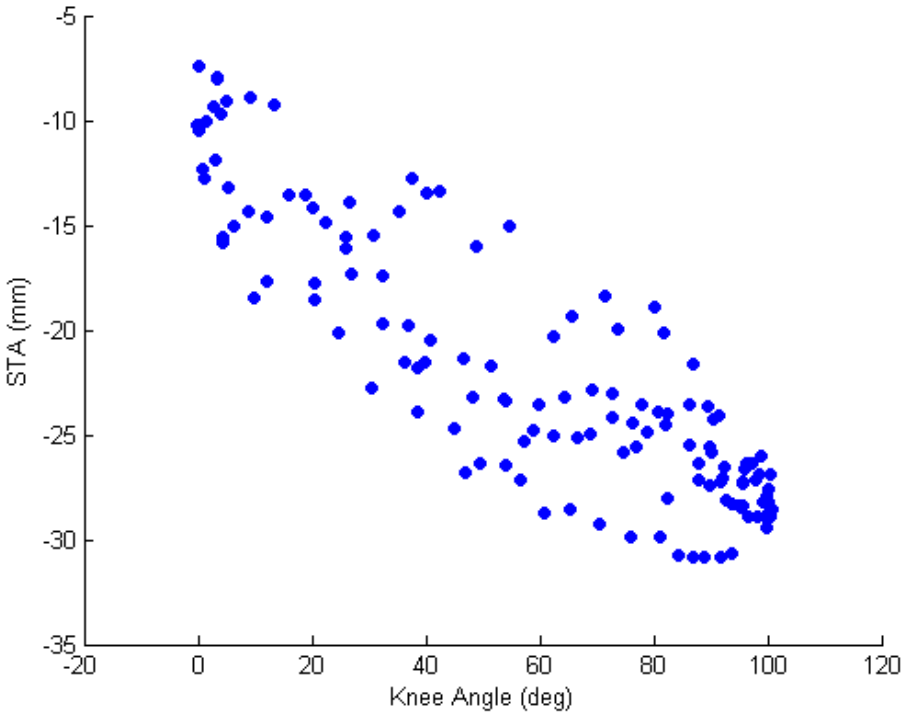

Figure 4-4. 2D plot showing the relationship between the STA component and knee flexion angle.

Similar procedures can be performed on shank STA to examine its relationship to both ankle and knee flexion angles. Figure 4-5 illustrates the 3D plot of the SI component of S4's STA of the same subject, over ankle and knee flexion angles. A top view of Figure 4-5 reveals the ankle and knee angle ranges that were covered by the series of trials (Figure 4-6). It shows the trials covered an ankle flexion range of about from 10° dorsiflexion to 35° plantarflexion. A left view of Figure 4-5 shows the relationship between this STA component and ankle flexion angle (Figure 4-7). A slight positive trend indicates marker S4 tended to shift superiorly while the ankle plantarflexed. Differing to this weak correlation with the ankle joint angle, a more prominent correlation between this STA component and knee joint angle was observed (Figure 4-8). A clear negative trend can be seen, indicating that marker S4 tended to move inferiorly while the knee flexed.

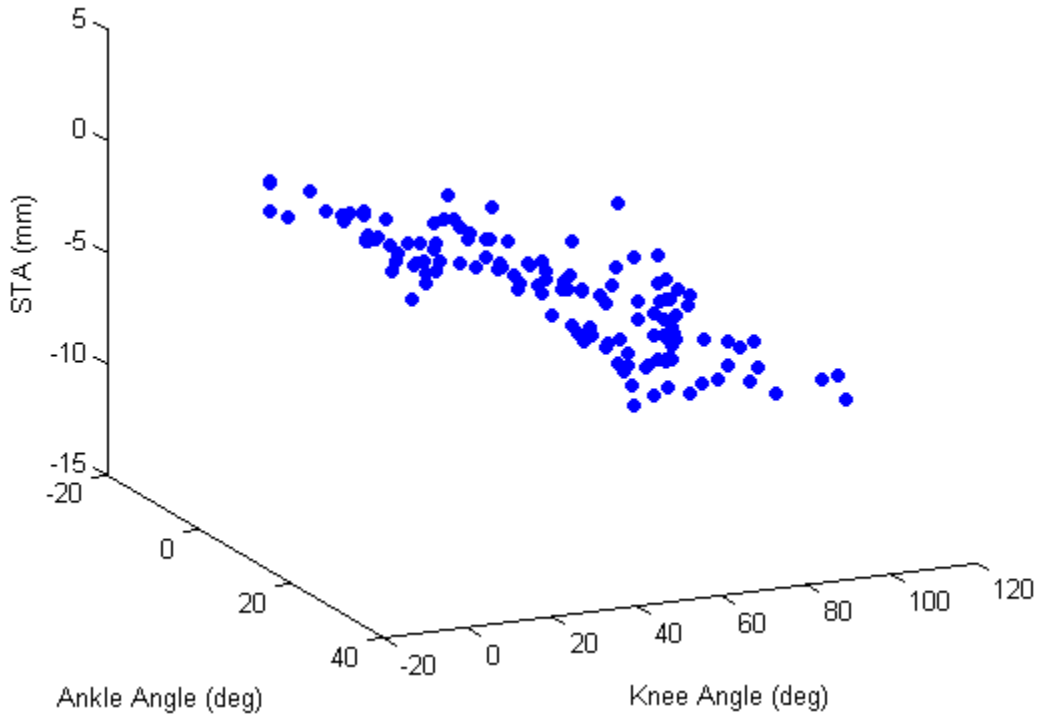

Figure 4-5. 3D plot of marker S4's STA (SI component) of a representative subject over ankle and knee flexion angles.

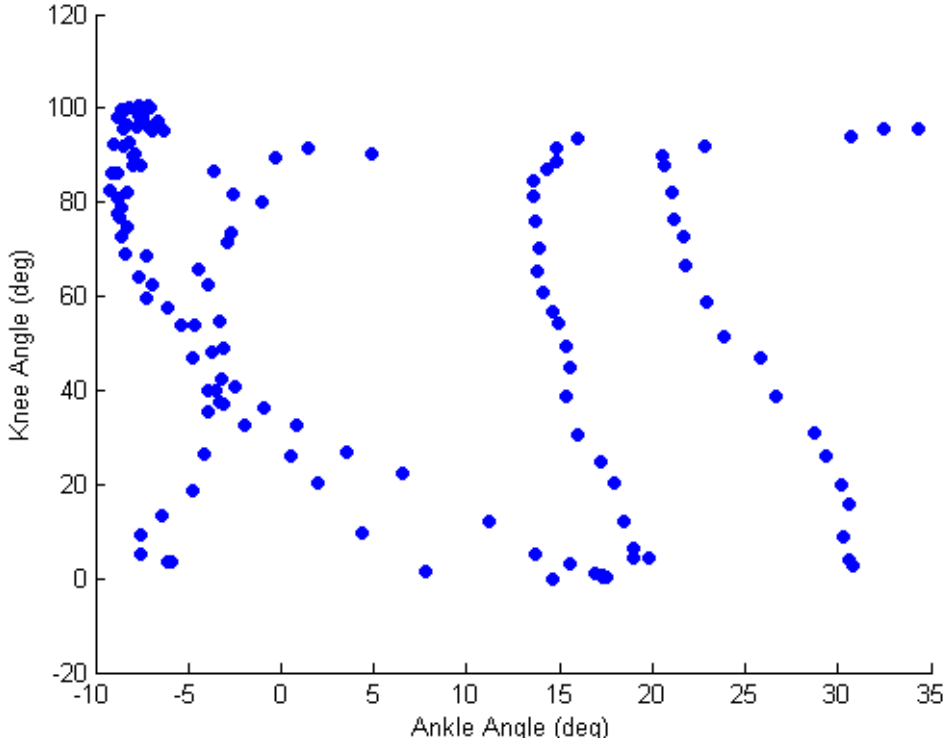

Figure 4-6. 2D plot showing the ankle and knee angle coverage by the series of knee flexion movements of a representative subject.

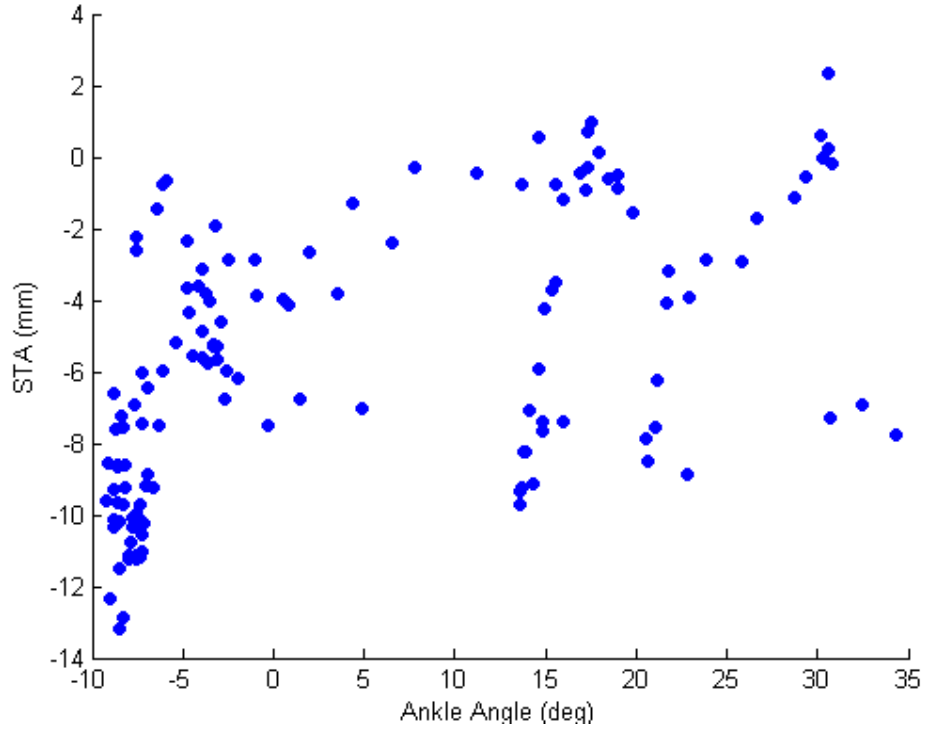

Figure 4-7. 2D plot showing the relationship between the STA component and ankle plantarflexion angle.

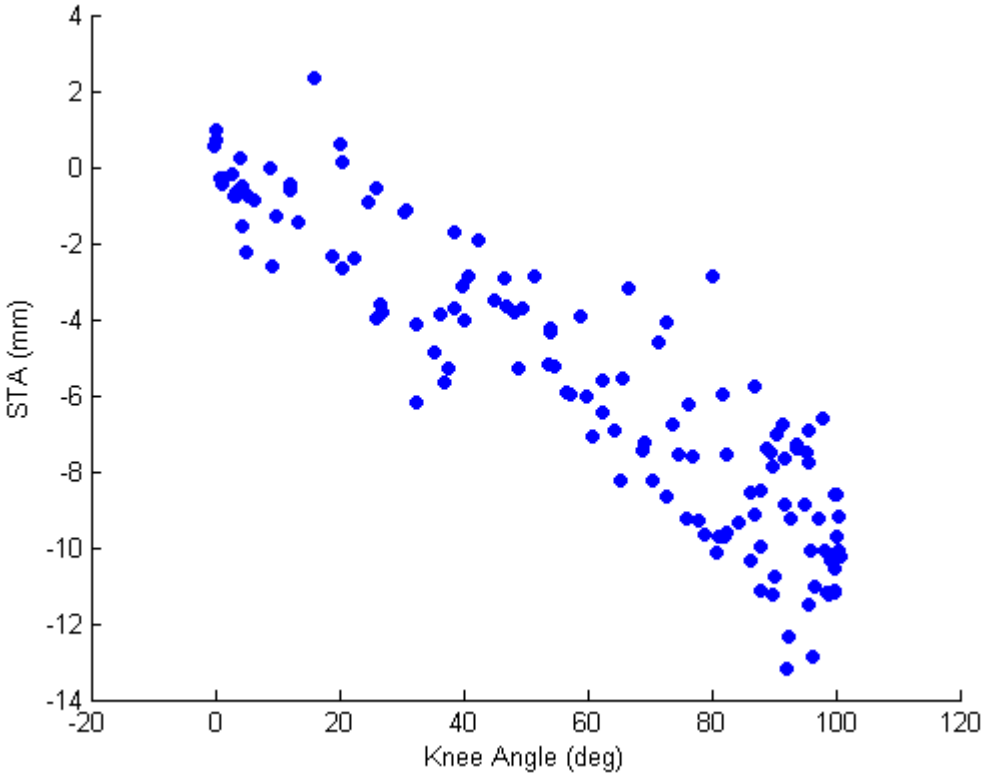

Figure 4-8. 2D plot showing the relationship between the STA component and knee flexion angle.

Mathematical Expression of STA

To express the relationship between STA and adjacent joint angles mathematically, multiple linear regression was used to construct the 2-variable function for each directional component of each marker's STA. To perform the multiple linear regression, there are many different options to design the terms of independent variables (here the independent variables are the adjacent joint angles). We have tested linear and quadratic options for this process. Due to the acceptable effectiveness and the simplicity, we decided to use linear terms in this step. Another benefit of using linear models is the intuitiveness of mathematical description. Each of the three coefficients obtained from the regression has an intuitive meaning in a linear model. The first two

coefficients are the slopes of the STA to each adjacent joint angle, while the third coefficient is an offset value at the neutral position in the model.

Specifically, a thigh marker's STA vector $\vec{V}^{i}_{STA\_thigh}$ was modeled as a multilinear function of hip and knee flexion angles (α_{hip} and α_{knee}), and a shank marker's STA vector $\vec{V}^{i}_{STA\_shank}$ was modeled as a multilinear function of ankle and knee flexion angles (α_{ankle} and α_{knee}):

$$\vec{V}^{i}_{STA\_thigh} = \begin{bmatrix} a_1 & b_1 & c_1 \\ a_2 & b_2 & c_2 \\ a_3 & b_3 & c_3 \end{bmatrix} \times \begin{bmatrix} \alpha_{hip} \\ \alpha_{knee} \\ 1 \end{bmatrix} \qquad (4\text{-}1)$$

$$\vec{V}^{i}_{STA\_shank} = \begin{bmatrix} a_1 & b_1 & c_1 \\ a_2 & b_2 & c_2 \\ a_3 & b_3 & c_3 \end{bmatrix} \times \begin{bmatrix} \alpha_{ankle} \\ \alpha_{knee} \\ 1 \end{bmatrix} \qquad (4\text{-}2)$$

The number index (1, 2, or 3) represents each of the three directional components of the STA vector: anterior/posterior (AP), medial/lateral (ML) and SI. Coefficient a and b reflects the sensitivities of the STA component to each of the two adjacent joint angles, and coefficient c is an offset. The 2-variable function shows geometrically as a plane in 3D. By using this model, the relationship between each marker's STA and the adjacent joint angles can be fully described simply by using a 3-by-3 matrix. Once this matrix is determined, the 3D STA vector of the specific marker at any combination of adjacent joint angles can be predicted.

As an example, by running the multilinear regression on the data points shown in Figure 4-1 (SI component of T1 marker's STA), we obtained for marker T1:

$$\begin{bmatrix} a_3 & b_3 & c_3 \end{bmatrix} = \begin{bmatrix} -0.181 & -0.165 & -6.8 \end{bmatrix} \qquad (4\text{-}3)$$

The R-squared value was 0.89 and the root-mean-square (RMS) residual error was 2.06 mm. Thus the SI component of T1's STA as a function of the adjacent joint angles can be expressed as:

$$V^{1}_{STA\_thigh\_3} = -0.181 \times \alpha_{hip} - 0.165 \times \alpha_{knee} - 6.8 \qquad (4\text{-}4)$$

The intuitive explanation of Equation 4-4 is: for each degree of hip flexion increase, the marker T1 tended to move inferiorly by 0.181 mm; for each degree of knee flexion increase, the marker T1 tended to move inferiorly by 0.165 mm. The small offset (6.8 mm) could come from both modeling deviation and the actual difference between dynamic movement and the static standing posture. Figure 4-9 geometrically shows this function in 3D. Figure 4-10 shows the 2D projections of the 3D plane to demonstrate its dependency on hip and knee joint angles. From these figures, it can be seen the multilinear STA model provides as a good representation of experimental data points.

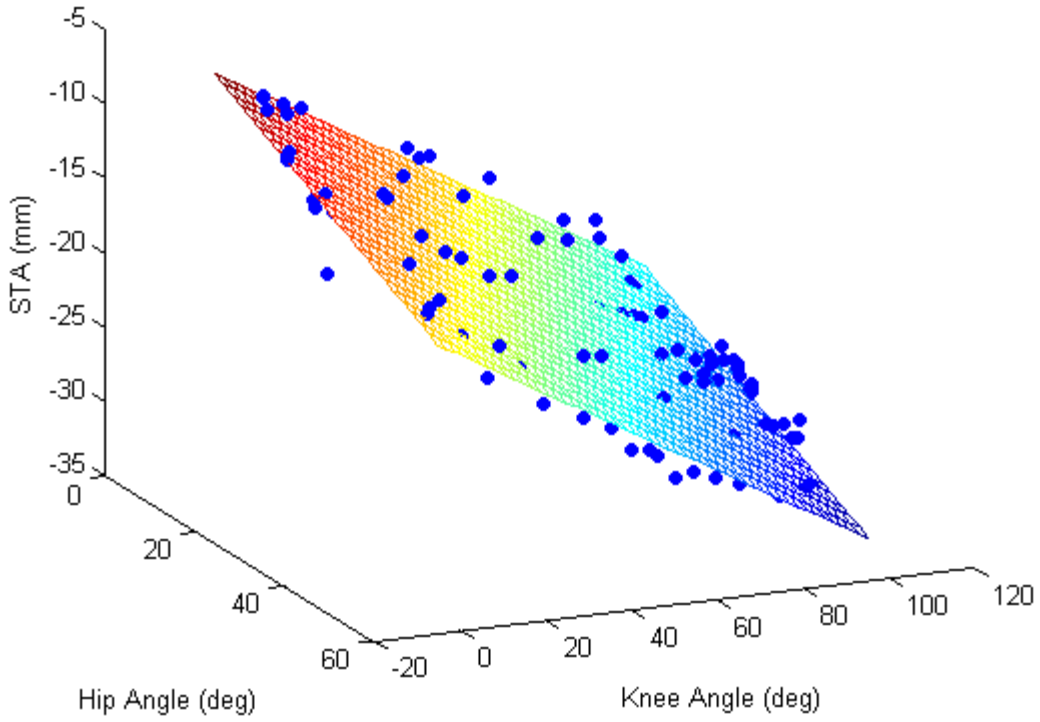

Figure 4-9. Multilinear regression on the data points of the SI component of T1's STA.

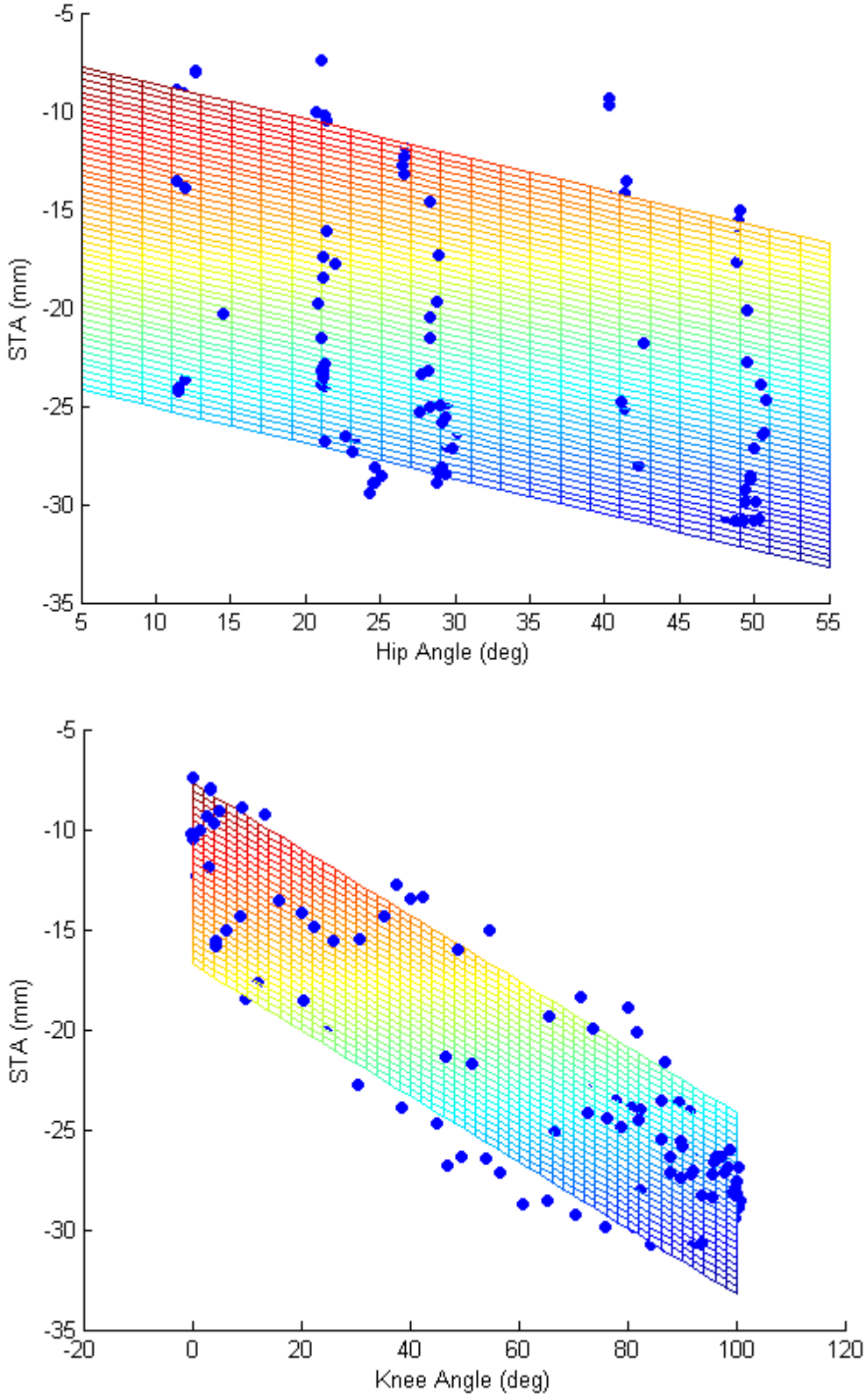

Figure 4-10. 2D projections of the regression model showing the dependency of the SI component of T1's STA to hip and knee joint angles.

Similarly, by performing the multilinear regression on the data points shown in Figure 4-5 (SI component of marker S4's STA), we obtained for marker S4:

$$\begin{bmatrix} a_3 & b_3 & c_3 \end{bmatrix} = \begin{bmatrix} 0.061 & -0.092 & -0.55 \end{bmatrix} \qquad (4\text{-}5)$$

The R-squared value was 0.87 and the RMS residual error was 1.36 mm. Thus the SI component of T1's STA as a function of ankle and knee angles can be expressed as:

$$V^4_{STA\_shank\_3} = 0.061 \times \alpha_{ankle} - 0.092 \times \alpha_{knee} - 0.55 \qquad (4\text{-}6)$$

The intuitive explanation of Equation 4-6 is: for each degree of ankle plantarflexion increase, the marker S4 tended to move superiorly by 0.061 mm; for each degree of knee flexion increase, the marker S4 tended to move inferiorly by 0.092 mm. The offset is almost zero. Figure 4-11 geometrically shows this function in 3D. Figure 4-12 shows the 2D projections of the 3D plane to illustrate its dependency on ankle and knee joint angles.

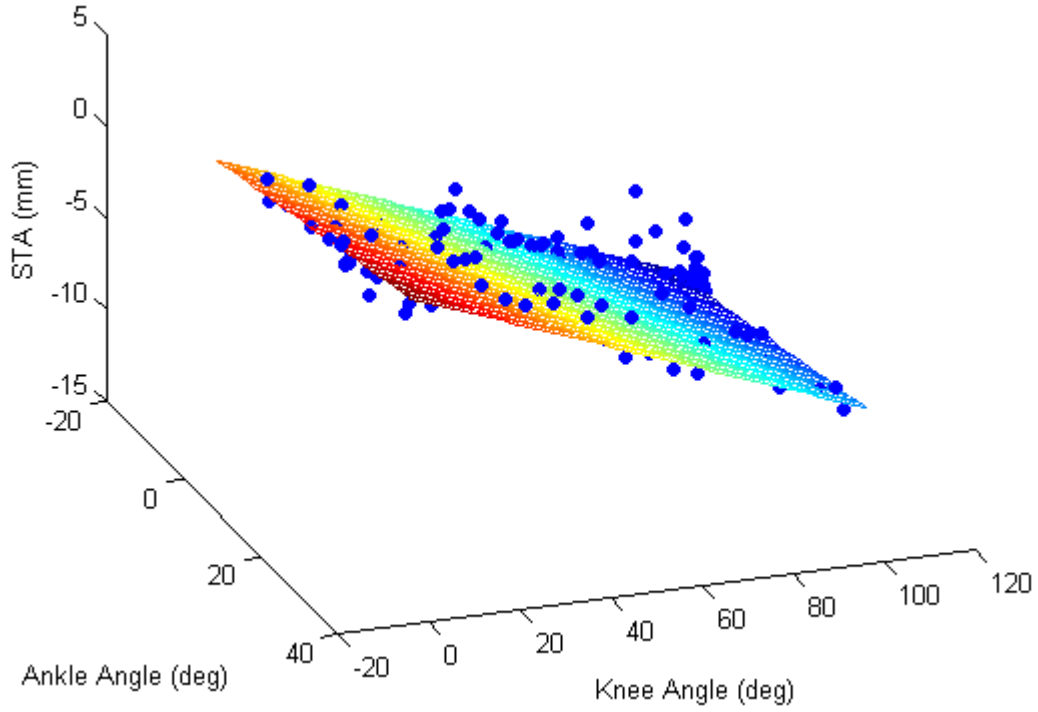

Figure 4-11. Multilinear regression on the data points of the SI component of S4's STA.

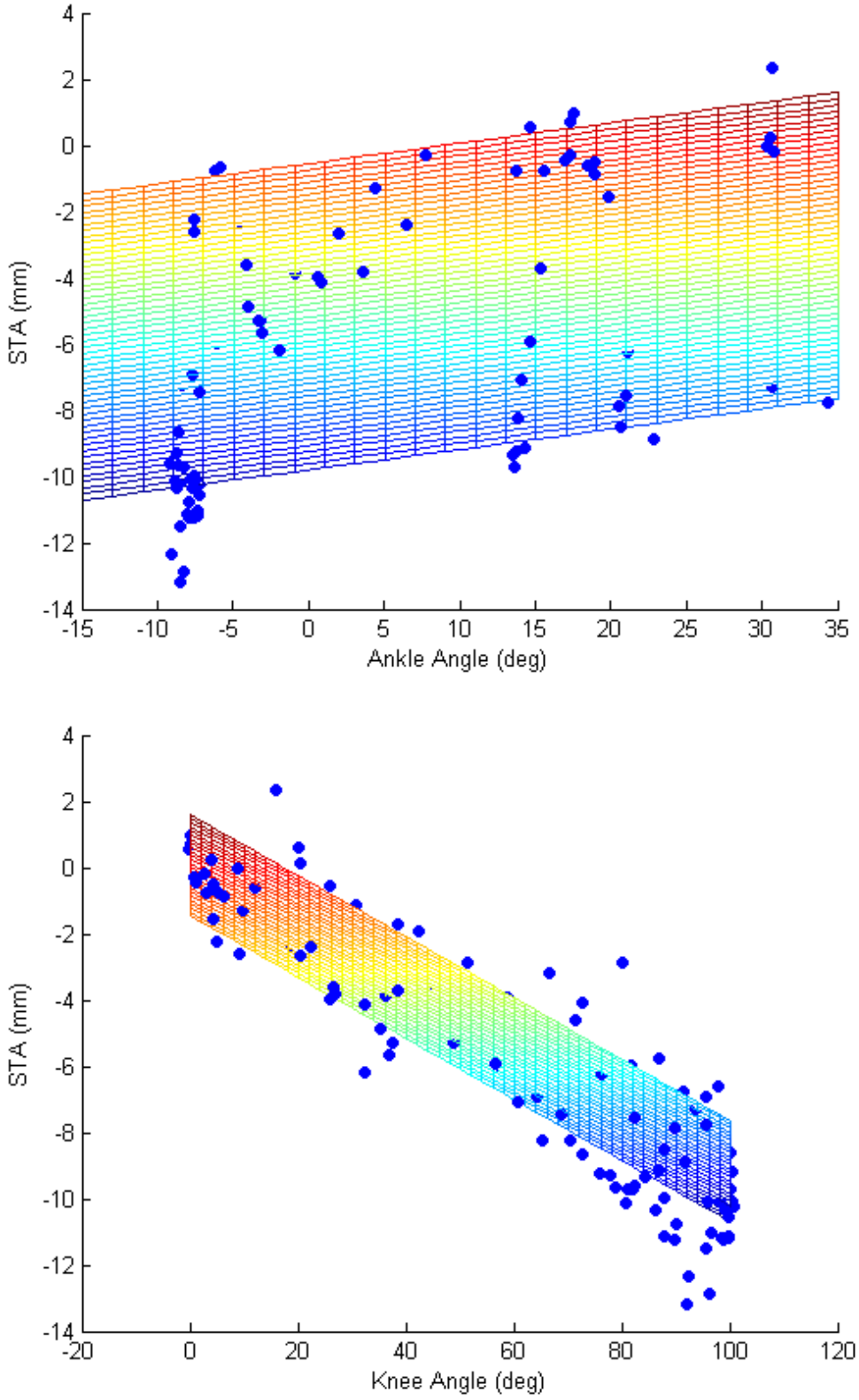

Figure 4-12. 2D projections of the regression model showing the dependency of the SI component of S4's STA to ankle and knee joint angles.

The same procedures were then performed on every component of every marker, and a series of 3-by-3 matrices were obtained for the thigh markers and the shank markers. Thus a complete set of STA models was established for this representative subject.

Inter-Motor-Task Similarity of STA

In the beginning of this chapter, we hypothesized that STA is not totally motor-task-dependent and a large portion of STA can be determined by the angles of the adjacent joints. In this section, we will test this hypothesis by using the STA models established based on the data from the series of knee flexion movements, to predict the STA in the stepping-up trial and compare the predicted STA to the experimental measurements.

To perform this comparison, the hip, knee, and ankle flexion angles during the stepping-up trial of the same subject were first computed. Then at each frame of the stepping-up trial, the instant hip and knee flexion angles were used to compute the "predicted STA" for every thigh marker; the ankle and knee flexion angles were used to compute the "predicted STA" for every shank marker. The computation was performed using Equations 4-1 and 4-2 and the matrices determined in the previous step.

Figures 4-13 and 4-14 show the comparisons of predicted STA (dashed lines) and the experimentally measured STA (solid lines) of thigh markers during the stepping-up trial, along AP and SI directions, respectively. It can be seen that the predicted STA successfully reflect the major patterns of real STA. The trends and the distributions among different markers of the predicted STA are fairly close to the experimentally measured results. The prediction residual errors are much smaller than the STA itself. In Figures 4-15 and 4-16, the prediction residuals (dashed lines), which are the

differences between the predicted STA and the measured STA, are plotted against the original STA (solid lines). The prediction residuals are usually less than 10 mm for most markers. This comparison indicates the feasibility of using the STA models established from the knee flexion movements to compensate for STA in the stepping-up movement.

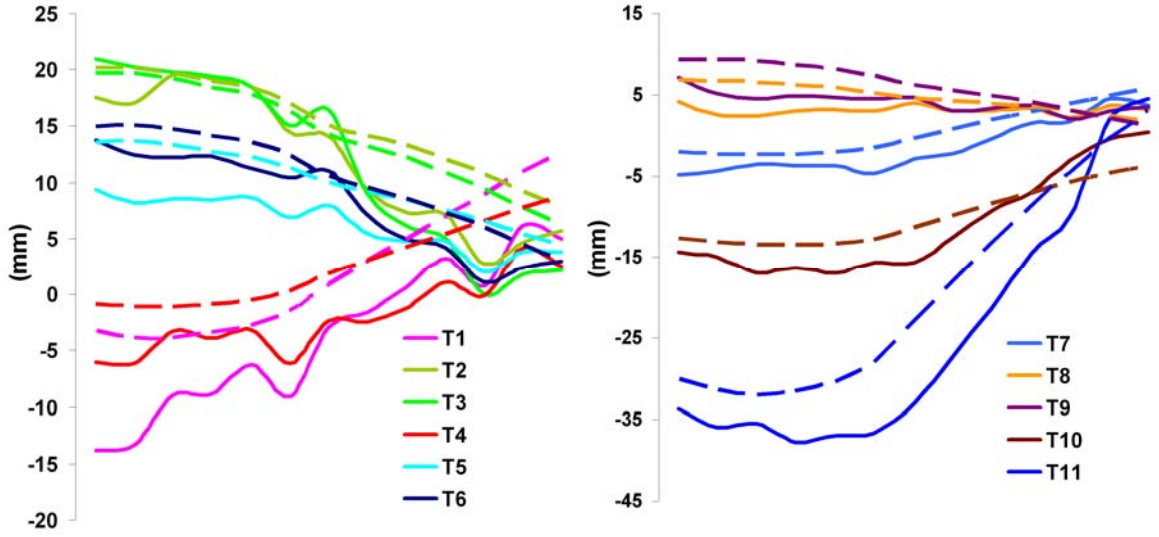

Figure 4-13. Measured (solid lines) and predicted (dashed lines) AP component of thigh STA during stepping-up activity.

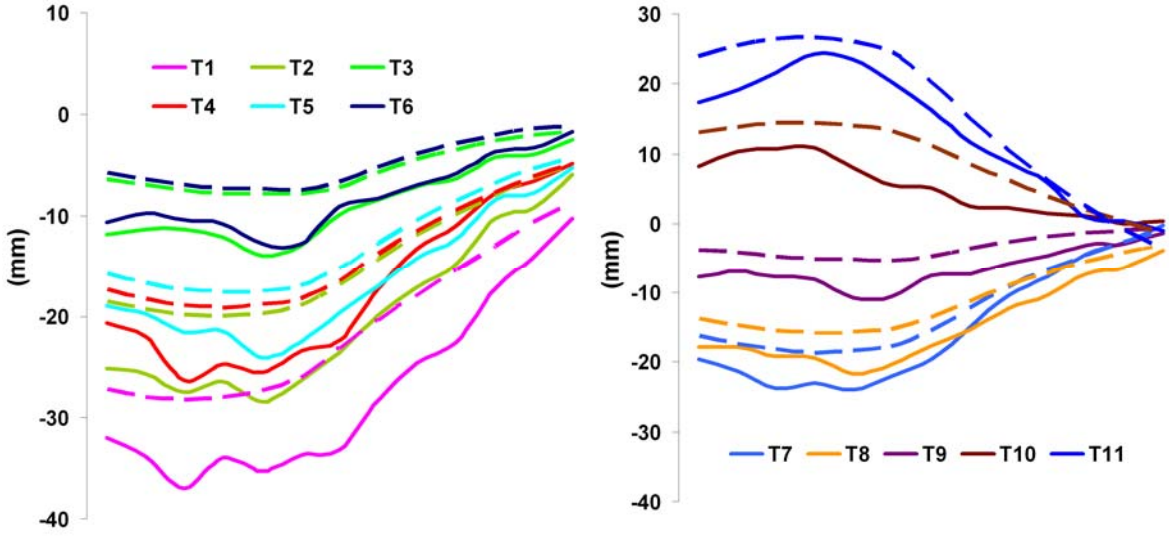

Figure 4-14. Measured (solid lines) and predicted (dashed lines) SI component of thigh STA during stepping-up activity.

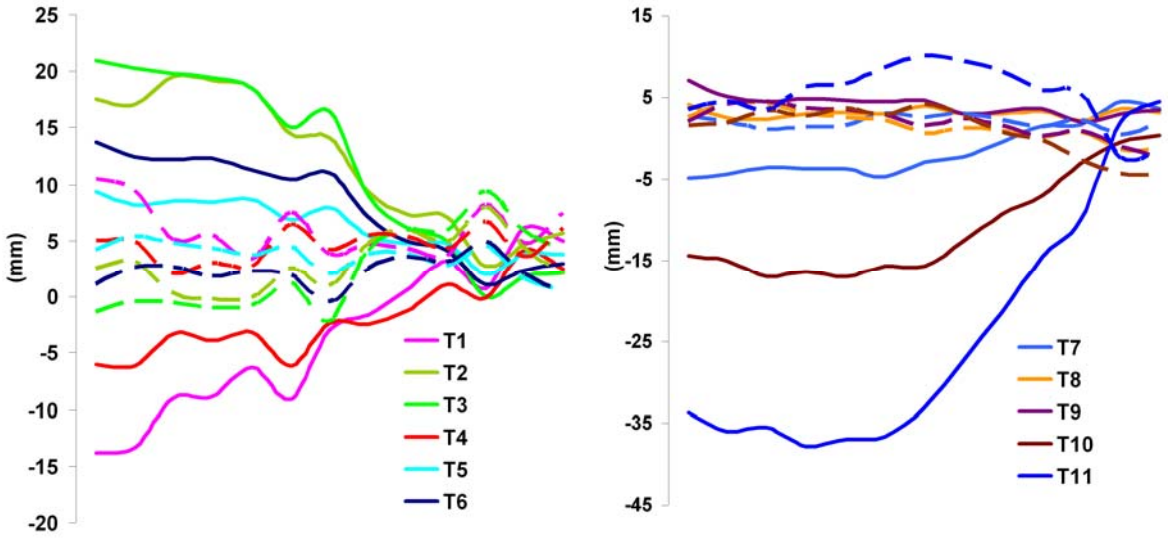

Figure 4-15. Comparison between the prediction residuals (dashed lines) and the STA of thigh markers along AP direction (solid lines) during stepping-up activity.

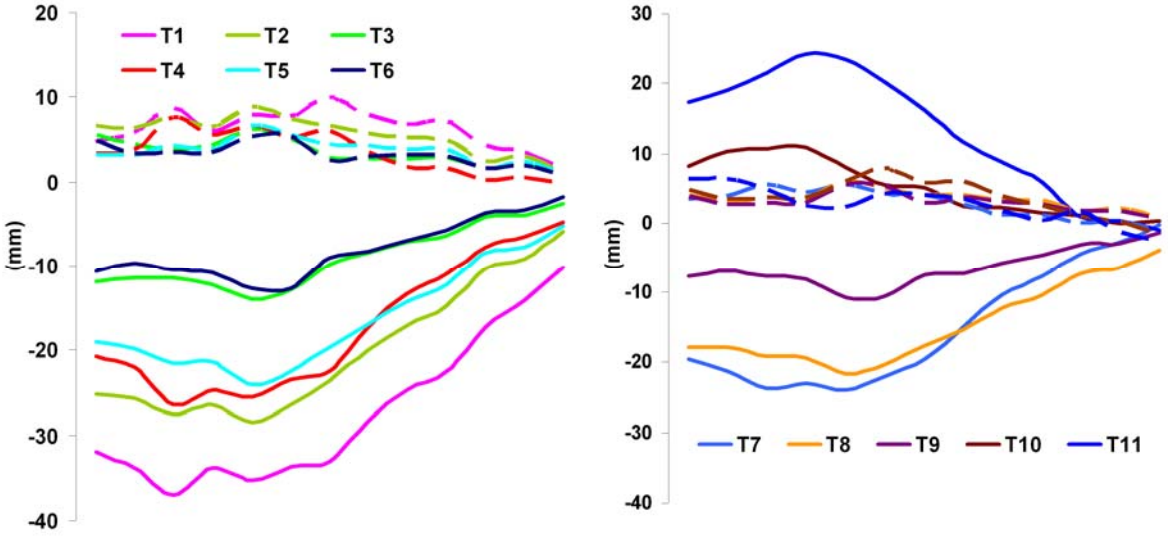

Figure 4-16. Comparison between the prediction residuals (dashed lines) and the STA of thigh markers along SI direction (solid lines) during stepping-up activity.

Figures 4-17 and 4-18 show the comparisons of predicted STA (dashed lines) and the measured STA (solid lines) of shank markers during the stepping-up movement, along AP and SI directions, respectively.

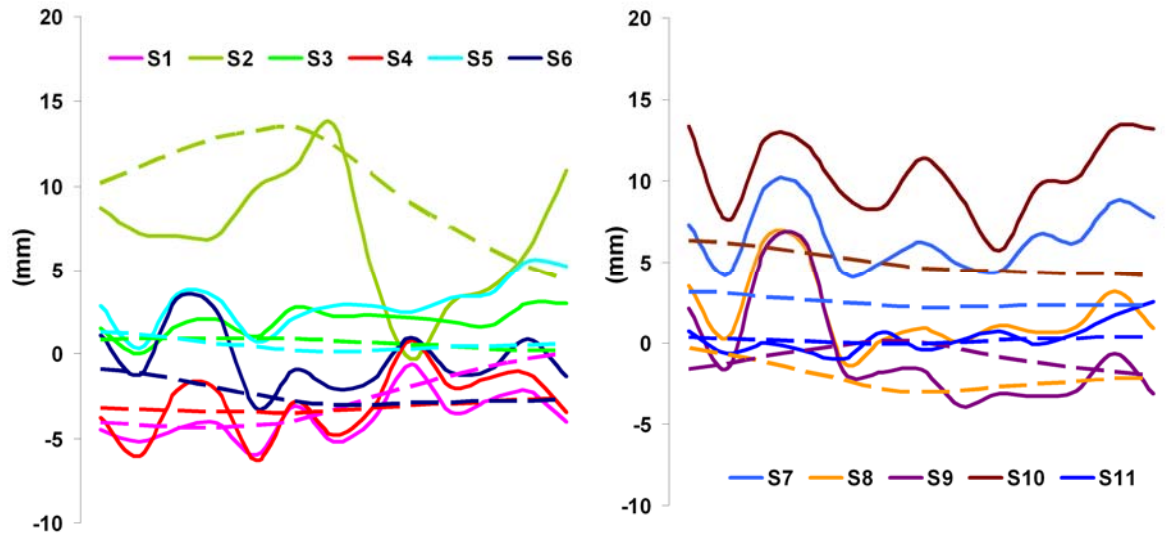

Figure 4-17. Measured (solid lines) and predicted (dashed lines) AP component of shank STA during stepping-up activity.

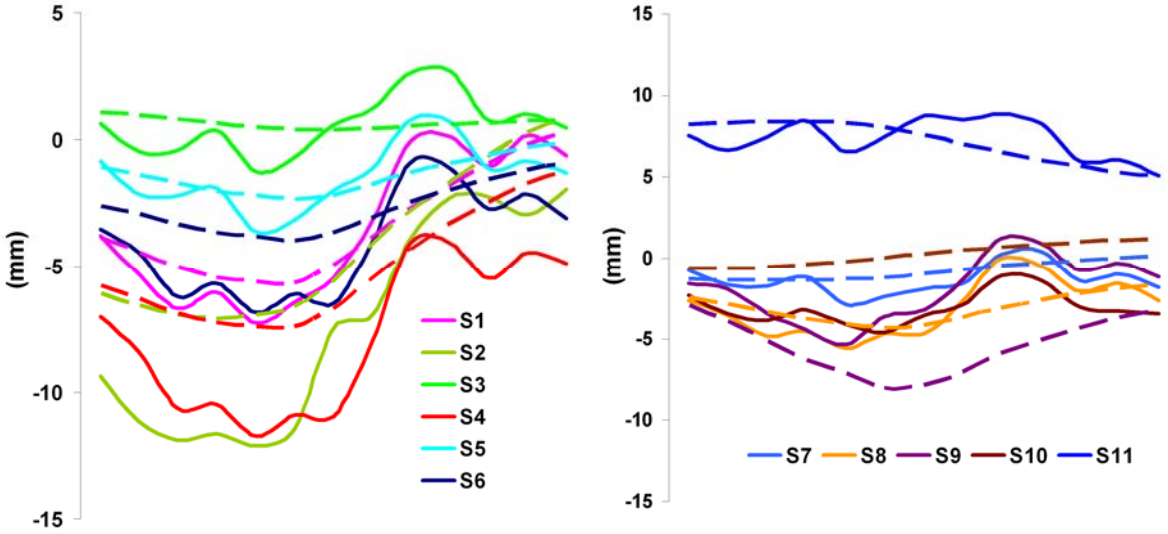

Figure 4-18. Measured (solid lines) and predicted (dashed lines) AP component of shank STA during stepping-up activity.

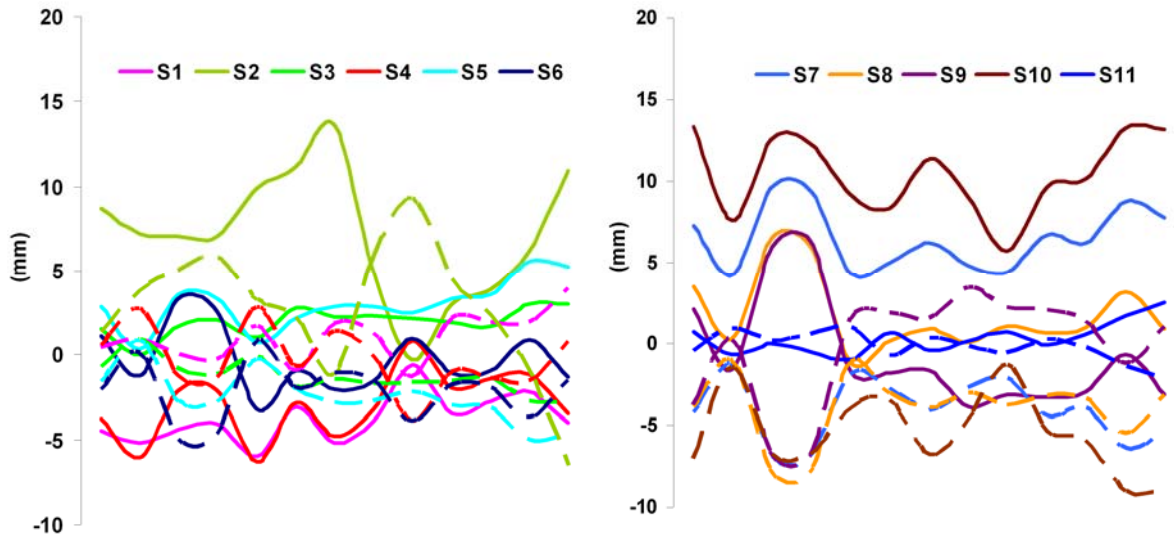

Figure 4-19. Comparison between the prediction residuals (dashed lines) and the STA of shank markers along AP direction (solid lines) during stepping-up activity.

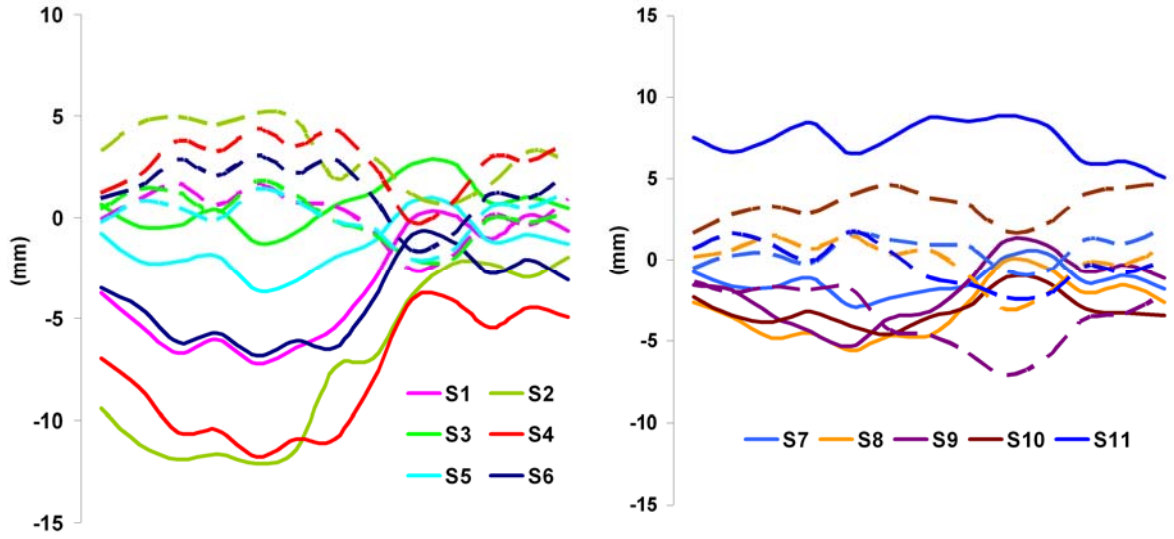

Figure 4-20. Comparison between the prediction residuals (dashed lines) and the STA of shank markers along SI direction (solid lines) during stepping-up activity.

Again, the predicted STA reflected major trends and the distributions of real STA for many markers. Because the STA magnitudes on the shank are much smaller than on the thigh, similar amount of prediction errors could cause the predicted STA looks

less alike the measured STA. This phenomenon was more or less prominent for different markers. However, prediction residuals are still smaller than the original STA magnitudes. Figures 4-19 and 4-20 plot the prediction residuals (dashed lines) against the original curves of STA (solid lines). The prediction residuals for shank markers are usually less than 5 mm.

Figures 4-13 to 4-20 revealed the inter-motor-task similarity of STA and demonstrated the possibility to predict STA during a motor task based on data obtained from other motor tasks.

A "Universal" STA Model of All Subjects

So far we have demonstrated that STA has both inter-subject and inter-motor-task similarities. Based on this knowledge, a "universal" STA model could be established based on multiple subjects' data.

As examples comparable to Figures 4-1 to 4-8, the SI component of marker T1's STA of all the six subjects are plotted over hip and knee angles (Figures 4-21 to 4-24); the SI component of marker S4's STA of all subjects are plotted over ankle and knee angles (Figures 4-25 to 4-28). In these figures, each color represents each subject.

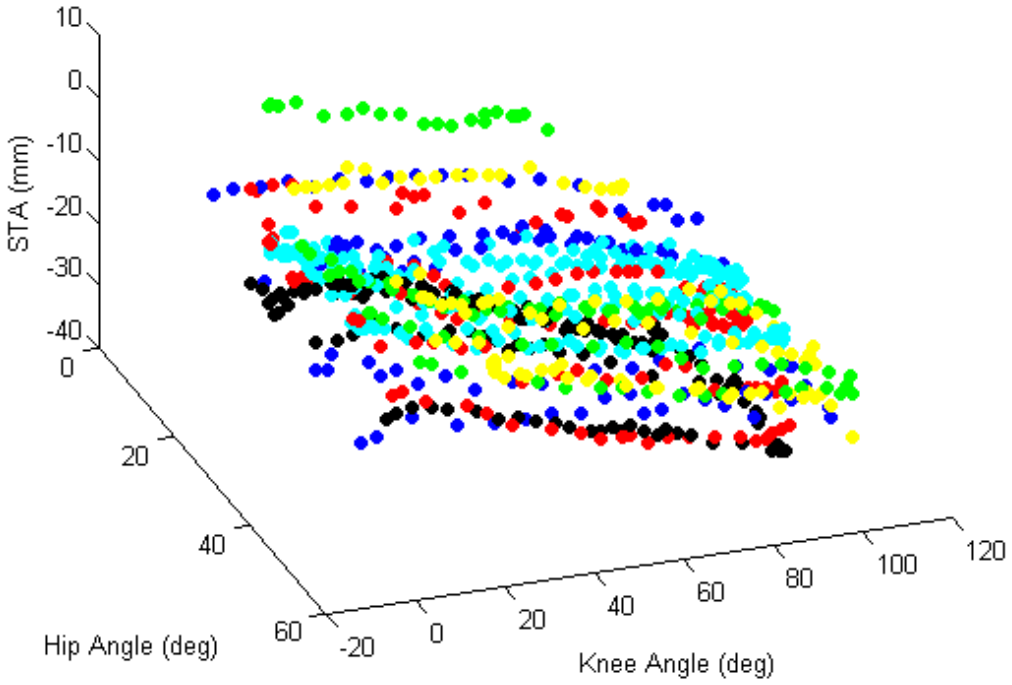

Figure 4-21. 3D plot of marker T1's STA (SI component) of all subjects over hip and knee flexion angles.

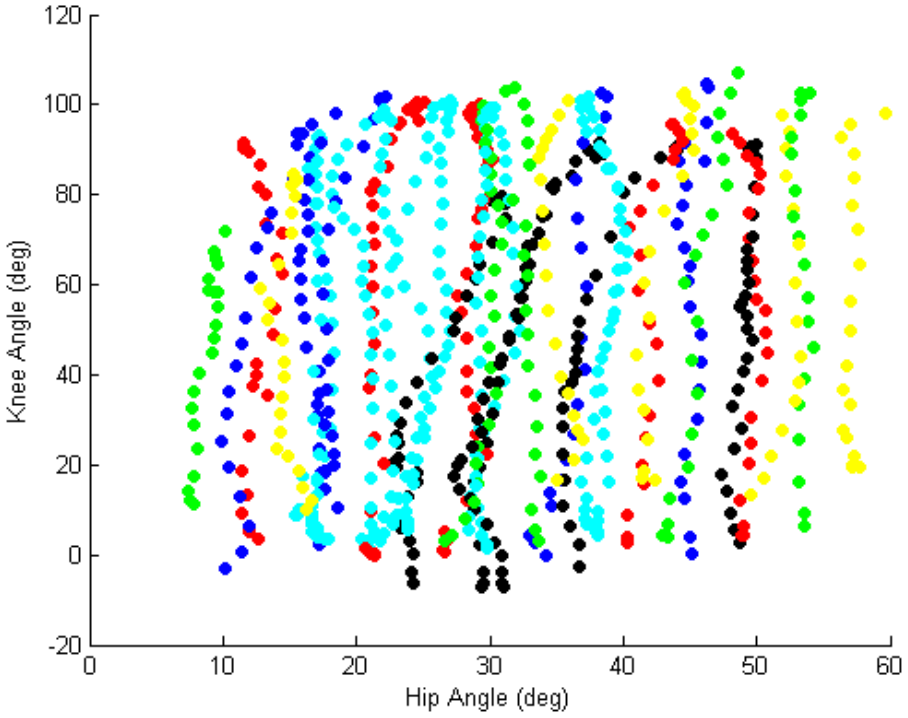

Figure 4-22. 2D plot showing the hip and knee angle coverage by the series of knee flexion movements for all subjects.

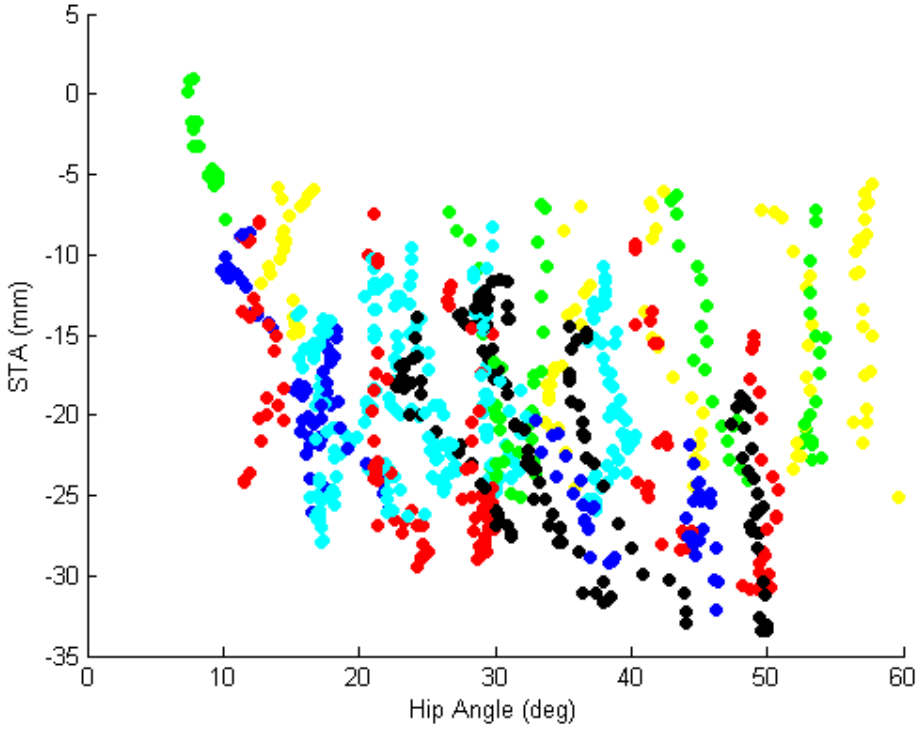

Figure 4-23. 2D plot showing the relationship between the STA component and hip flexion angle for all subjects.

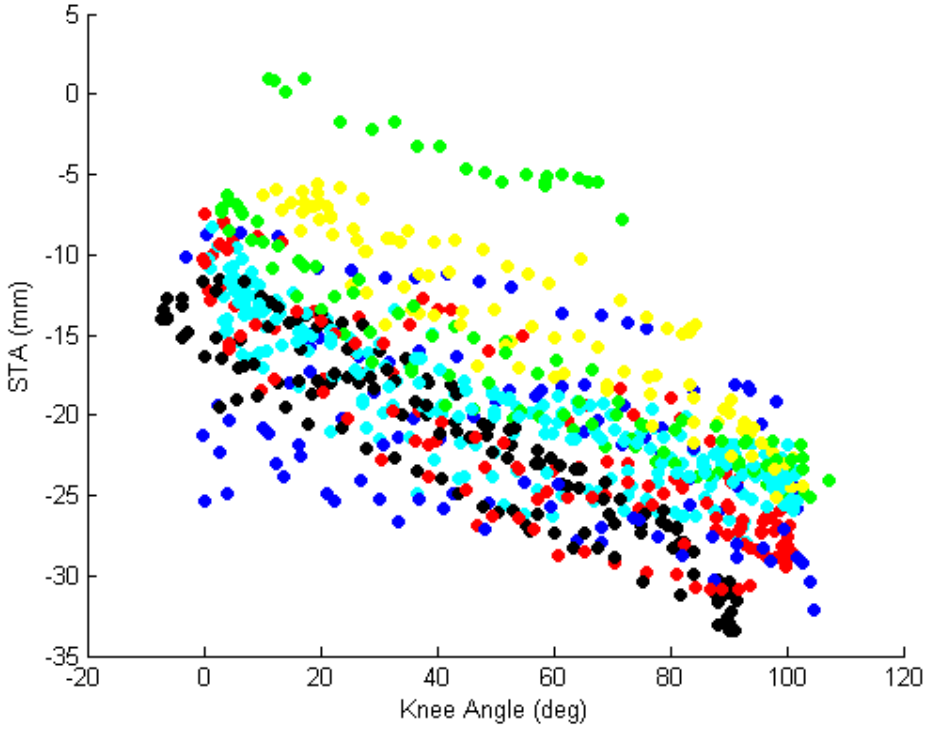

Figure 4-24. 2D plot showing the relationship between the STA component and knee flexion angle for all subjects.

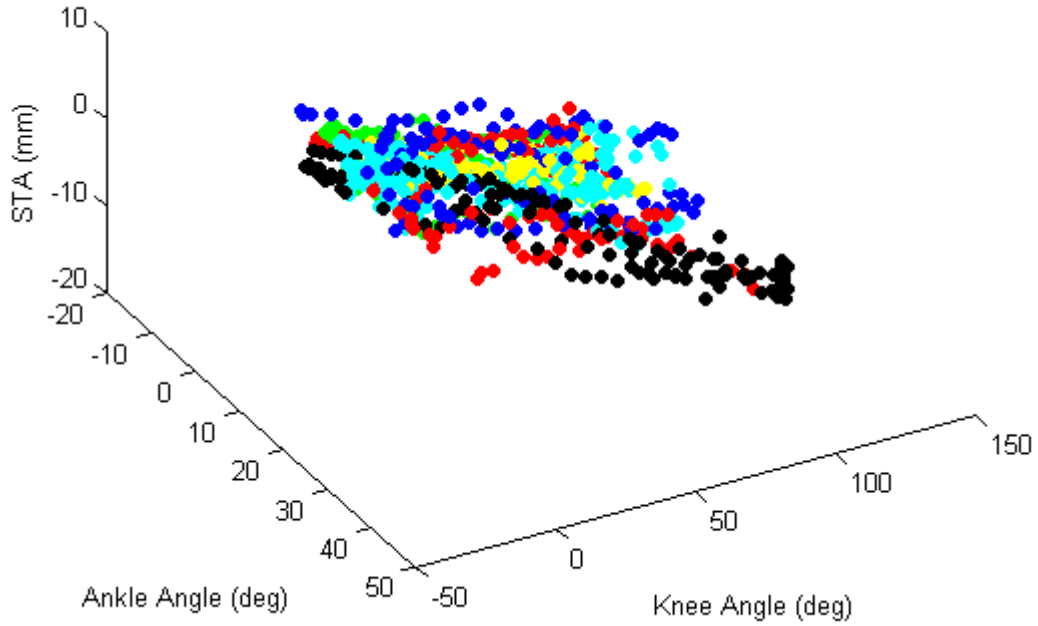

Figure 4-25. 3D plot of the marker S4's STA (SI component) of all subjects over ankle and knee flexion angles.

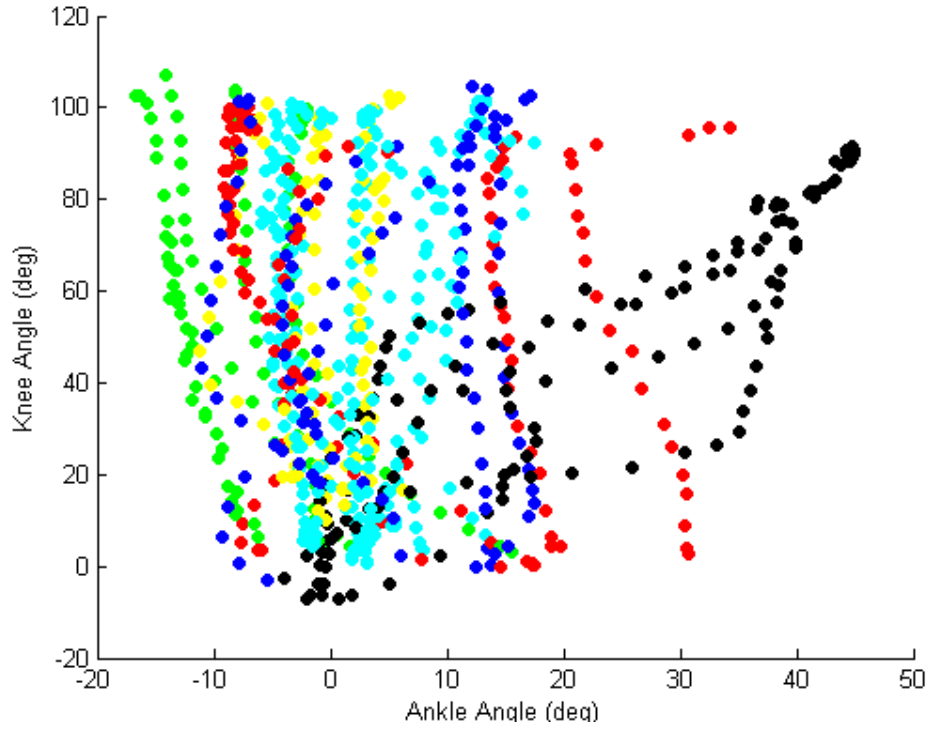

Figure 4-26. 2D plot showing the ankle and knee angle coverage by the series of knee flexion movements for all subjects.

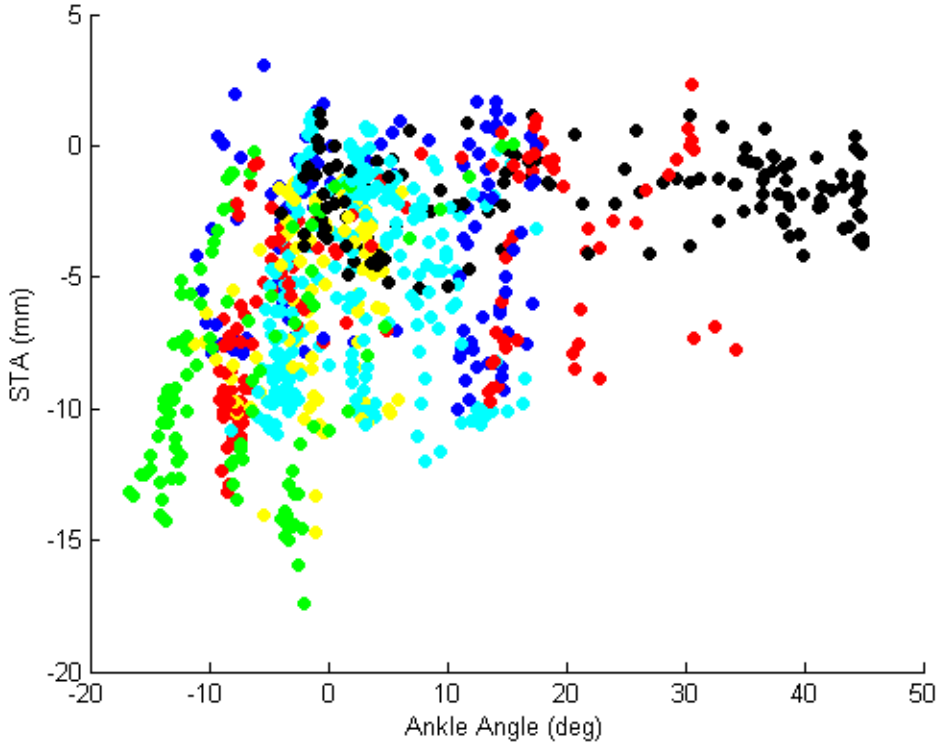

Figure 4-27. 2D plot showing the relationship between the STA component and ankle plantarflexion angle for all subjects.

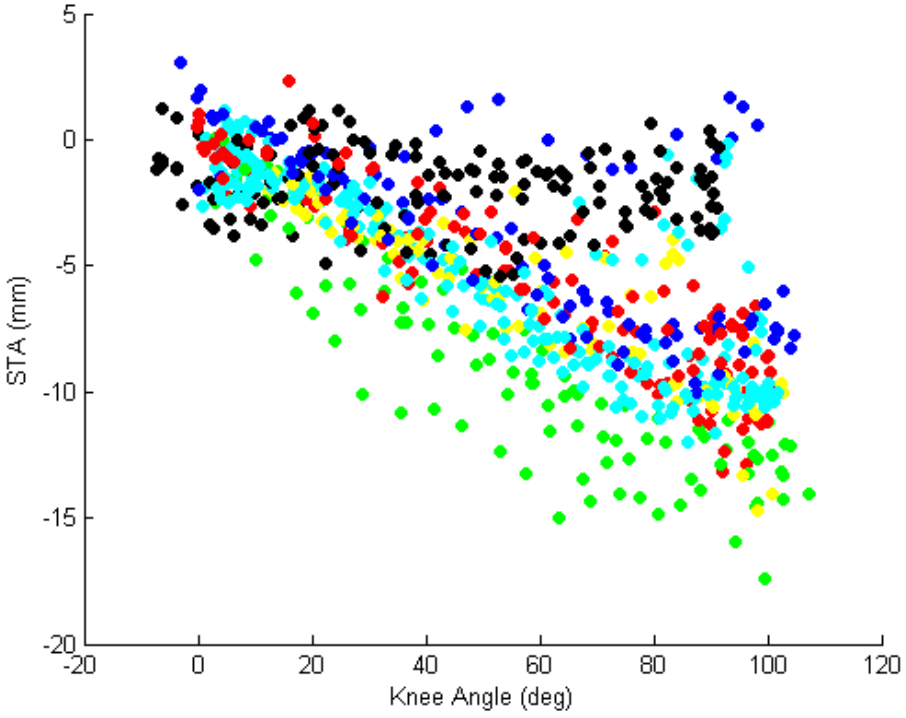

Figure 4-28. 2D plot showing the relationship between the STA component and knee flexion angle for all subjects.

From Figures 4-21 to 4-28, it can be seen the relationships between STA and adjacent joint angles are not exactly the same for all subjects. But the basic trends of these relationships are similar. If we used all the data points from all subjects to perform the multilinear regression procedure described in earlier sections, the resultant functions should be an overall representation of all the six subjects.

For the example in Figure 4-21, by running the multilinear regression on all data points from six subjects for the SI component of T1 marker's STA, we obtained for marker T1:

$$\begin{bmatrix} a_3 & b_3 & c_3 \end{bmatrix} = \begin{bmatrix} -0.099 & -0.137 & -9.0 \end{bmatrix} \qquad (4\text{-}7)$$

The R-squared value was 0.53 and the RMS residual error was 4.46 mm this time. Thus the SI component of T1's STA as a function of the adjacent joint angles for all six subjects can be expressed as:

$$V^1_{STA\_thigh\_3} = -0.099 \times \alpha_{hip} - 0.137 \times \alpha_{knee} - 9.0 \qquad (4\text{-}8)$$

For the example of Figure 4-25, by running the multilinear regression on all data points from six subjects for the SI component of S4 marker's STA, we obtained for marker S4:

$$\begin{bmatrix} a_3 & b_3 & c_3 \end{bmatrix} = \begin{bmatrix} 0.136 & -0.091 & -0.951 \end{bmatrix} \qquad (4\text{-}9)$$

The R-squared value was 0.72 and the RMS residual error was 2.10 mm this time. Thus the SI component of S4's STA as a function of the adjacent joint angles for all six subjects can be expressed as:

$$V^4_{STA\_shank\_3} = 0.136 \times \alpha_{ankle} - 0.091 \times \alpha_{knee} - 0.951 \qquad (4\text{-}10)$$

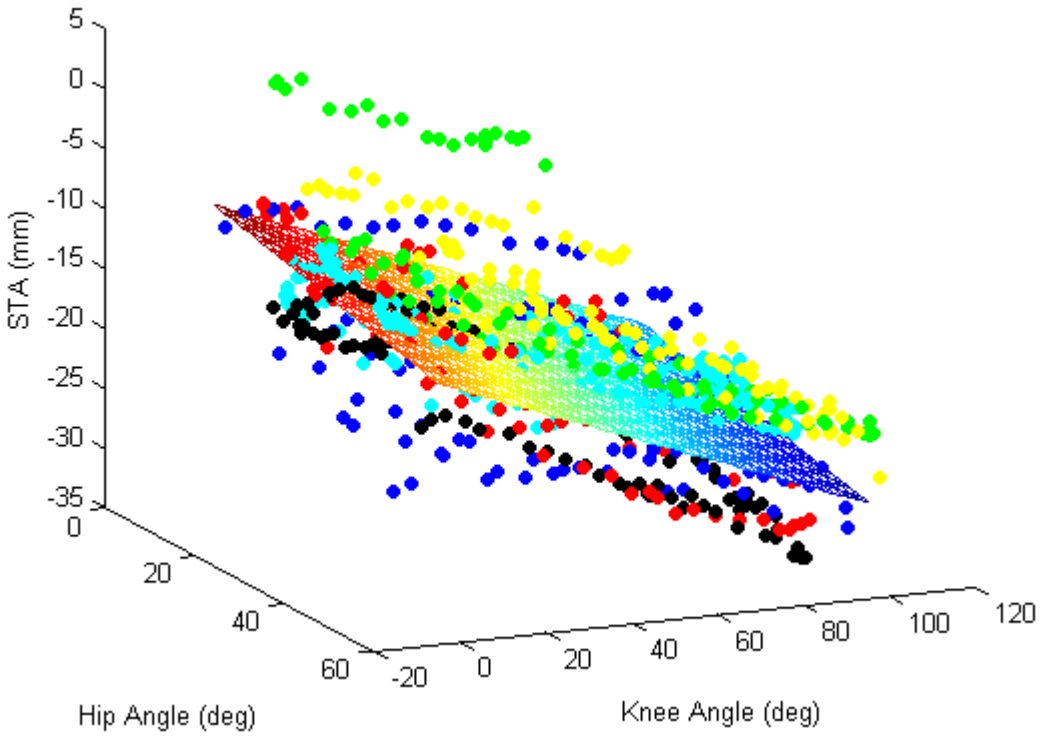

Figure 4-29. Multilinear regression on the data points of the SI component of T1's STA for all subjects.

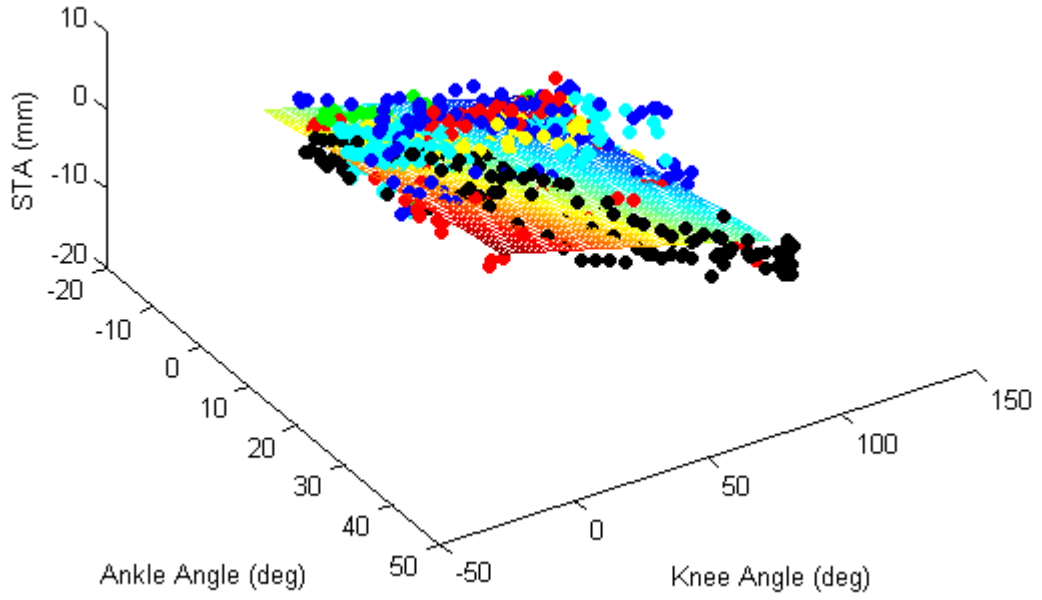

Figure 4-30. Multilinear regression on the data points of the SI component of S4's STA for all subjects.

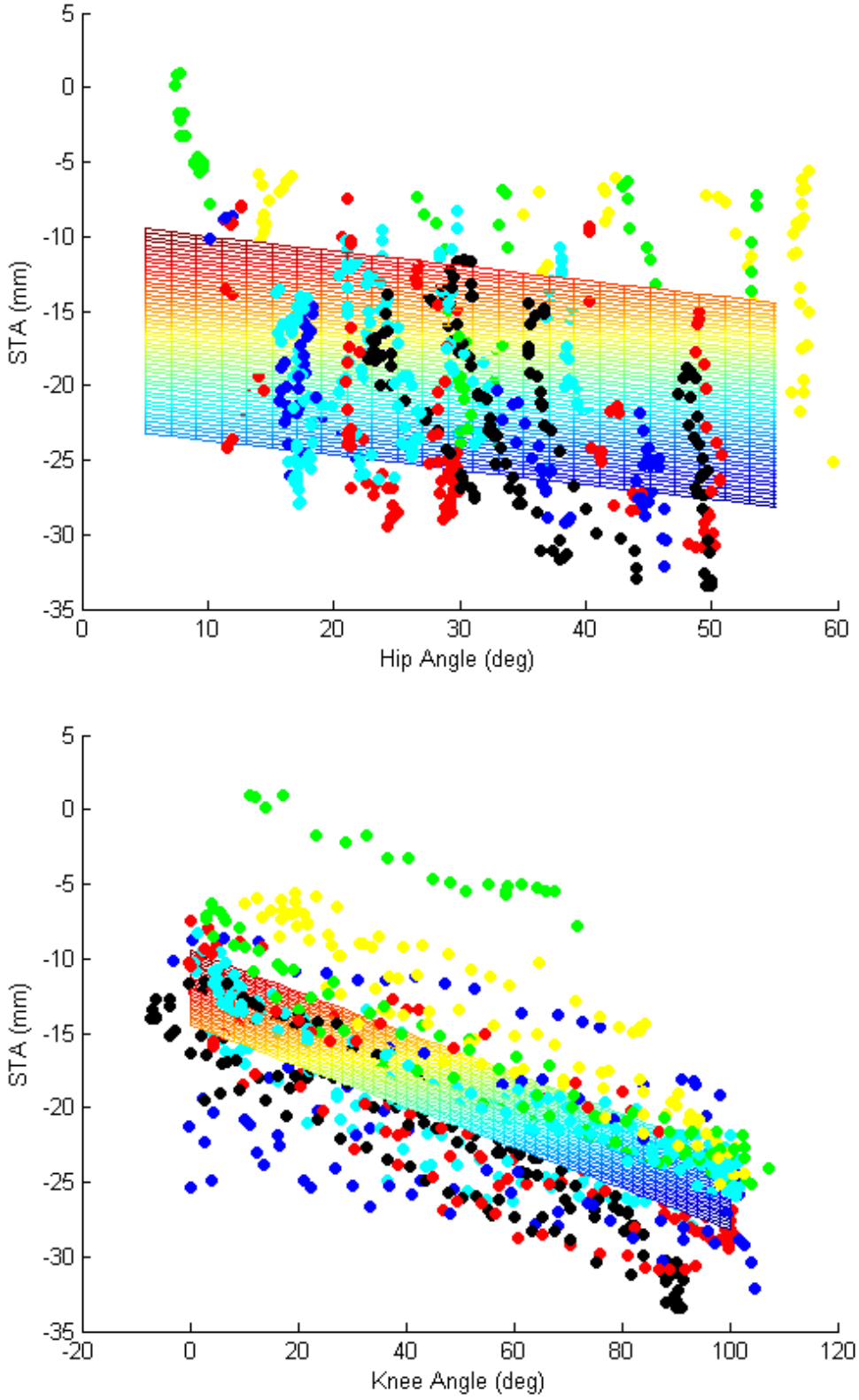

Figure 4-31. 2D projections of the regression model showing the dependency of the SI component of T1's STA to hip and knee joint angles for all subjects.

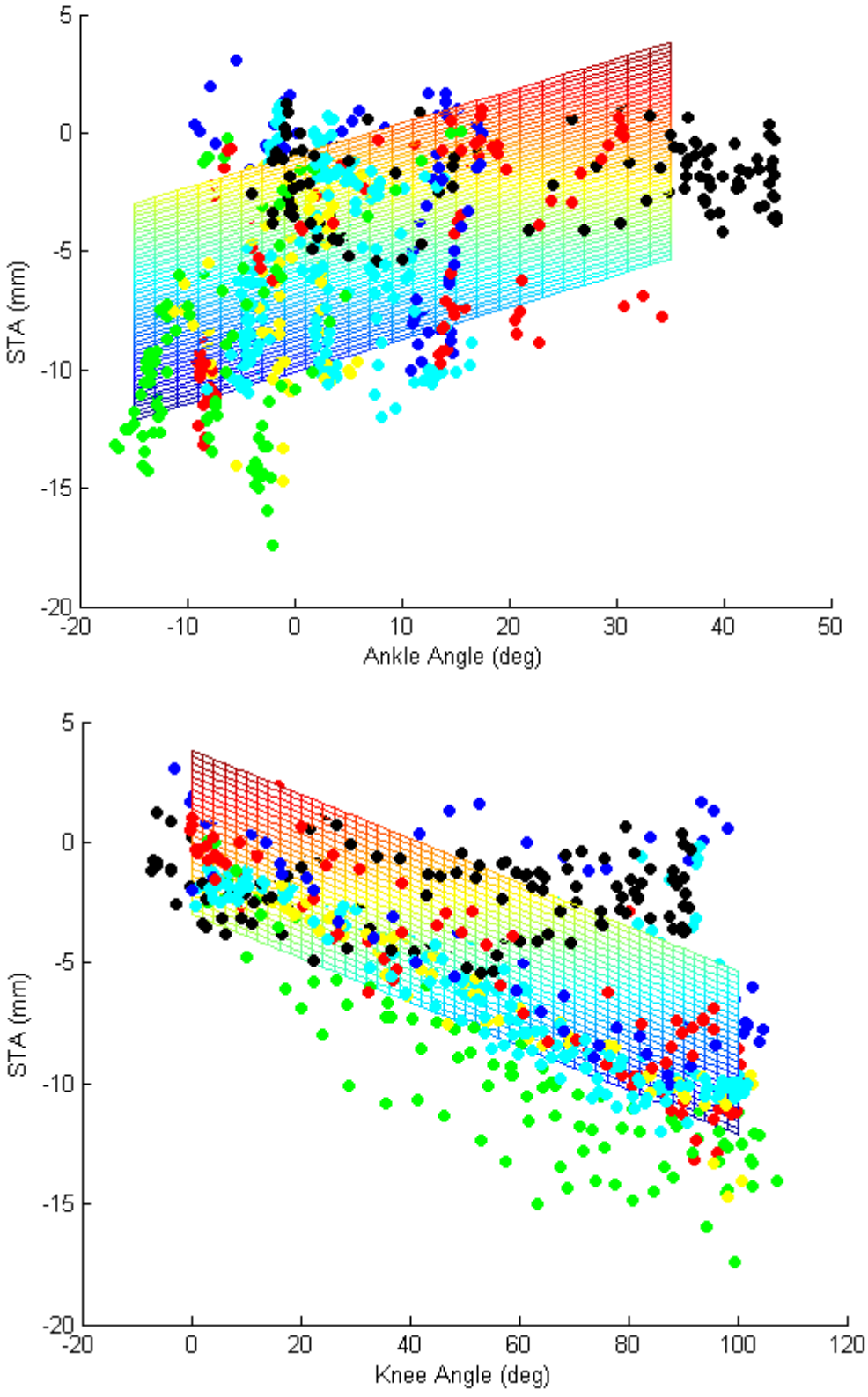

Figure 4-32. 2D projections of the regression model showing the dependency of the SI component of S4's STA to ankle and knee joint angles for all subjects.

After assembling all subjects together, the “universal” models were not as good representations as subject-specific models. This can be seen by the decreased R-squared values and the increased RMS residual errors. However, the “universal” models are still able to reflect major common patterns of STA on the group of subjects (Figures 4-29 to 4-32).

By repeating the multilinear regression procedure on every component of every marker on the thigh and shank, a series of 3-by-3 matrices that describe the relationship of the STA and adjacent joint angles for all the subjects could be obtained (Tables 4-1 and 4-2). These coefficient matrices mathematically represent the “universal” STA models of every marker for all the six subjects (Equations 4-1 and 4-2).

In Tables 4-1 and 4-2, indices 1, 2, and 3 represent AP, ML, and SI components respectively. From the matrices in the tables, it can be seen on the thigh the AP components of most markers’ STA are more sensitive to hip flexion angle, while the SI components of most markers’ STA are more sensitive to knee flexion angle. Most *c* values (offsets in the multilinear model) are smaller than 10 mm. A few markers’ ML components resulted in large *c* values (greater than 10 mm), which could be caused to large errors in ML STA measurements. On the shank, *a* and *b* values are generally smaller than those on the thigh, reflecting the smaller magnitudes of shank STA. All the *c* values for shank markers are generally small (less than 7 mm).

Table 4-1. Coefficient matrices of thigh markers for all subjects.

Marker	Component	a (mm/deg)	b (mm/deg)	c (mm)	R-Squared	RMS residual (mm)
	1	-0.136	-0.104	8.232	0.23	7.27
T1	2	0.608	0.023	-17.518	0.44	8.57
	3	-0.099	-0.137	-9.002	0.53	4.46
	1	0.222	-0.091	1.727	0.14	9.30
T2	2	0.360	-0.006	-13.984	0.21	8.44
	3	-0.018	-0.186	-5.697	0.69	4.09
	1	0.350	-0.111	-0.654	0.21	10.35
T3	2	0.092	-0.031	-3.723	0.04	7.40
	3	0.083	-0.134	-1.864	0.71	2.76
	1	-0.050	-0.057	2.571	0.08	6.99
T4	2	0.498	-0.005	-13.626	0.41	7.29
	3	0.012	-0.185	-6.954	0.66	4.30
	1	0.208	-0.072	-0.224	0.14	8.04
T5	2	0.309	-0.014	-11.297	0.21	7.42
	3	0.047	-0.202	-5.468	0.72	4.10
	1	0.279	-0.076	-2.626	0.17	8.88
T6	2	0.121	-0.069	-3.163	0.12	6.83
	3	0.086	-0.137	-1.923	0.68	3.02
	1	0.056	-0.058	-1.690	0.06	7.57
T7	2	0.298	-0.008	-8.509	0.25	6.29
	3	0.019	-0.248	-3.914	0.79	4.18
	1	0.202	-0.061	-3.243	0.14	7.52
T8	2	0.192	-0.012	-6.692	0.13	6.07
	3	0.074	-0.209	-6.040	0.69	4.47
	1	0.181	-0.057	-3.285	0.13	6.98
T9	2	0.119	-0.088	-2.427	0.19	6.35
	3	0.091	-0.104	-2.429	0.46	3.73
	1	0.181	-0.198	-10.880	0.28	10.44
T10	2	0.088	-0.043	-0.028	0.08	5.67
	3	0.095	0.105	-4.556	0.20	7.44
	1	-0.189	-0.280	5.251	0.76	5.57
T11	2	0.034	0.023	-0.787	0.02	5.66
	3	-0.032	0.251	-3.444	0.50	8.15

Table 4-2. Coefficient matrices of shank markers for all subjects.

Marker	Component	a (mm/deg)	b (mm/deg)	c (mm)	R-Squared	RMS residual (mm)
	1	0.046	-0.069	2.702	0.32	3.31
S1	2	0.148	-0.064	1.365	0.24	4.99
	3	0.077	-0.111	-0.265	0.53	3.46
	1	0.046	0.120	-0.911	0.44	4.36
S2	2	0.089	-0.077	1.034	0.23	4.63
	3	-0.138	-0.087	1.721	0.32	4.86
	1	-0.043	0.016	1.654	0.08	2.54
S3	2	0.175	-0.036	0.981	0.22	4.80
	3	0.066	-0.010	-0.601	0.20	1.86
	1	-0.008	0.003	0.596	0.00	3.37
S4	2	0.142	-0.046	0.781	0.16	5.26
	3	0.136	-0.091	-0.951	0.72	2.10
	1	-0.032	0.017	1.801	0.04	3.33
S5	2	0.123	-0.011	0.370	0.09	5.22
	3	0.069	-0.028	-0.453	0.37	1.67
	1	0.019	0.043	-0.029	0.13	3.78
S6	2	0.211	-0.024	1.400	0.20	5.76
	3	0.129	-0.060	-0.675	0.50	2.51
	1	-0.079	0.031	2.834	0.09	4.49
S7	2	0.110	0.005	-1.045	0.06	5.53
	3	0.032	-0.035	0.061	0.43	1.39
	1	-0.031	0.046	0.620	0.09	4.86
S8	2	0.125	-0.013	0.596	0.07	6.13
	3	0.128	-0.035	-0.529	0.39	2.47
	1	-0.243	0.047	2.270	0.21	6.75
S9	2	0.108	-0.005	-0.874	0.04	6.84
	3	0.149	-0.025	-2.986	0.37	2.72
	1	-0.108	0.023	5.337	0.07	5.80
S10	2	0.132	-0.009	-1.745	0.06	6.60
	3	0.016	-0.016	0.561	0.04	2.73
	1	0.000	0.012	1.428	0.02	2.36
S11	2	0.214	-0.078	1.656	0.39	4.70
	3	0.018	0.049	1.225	0.27	2.64

In addition to the multilinear coefficients, the R-squared value and the RMS residual error from each regression are also shown in Tables 4-1 and 4-2. For the thigh STA models, over 84% variables showed at least “small correlation” (R-squared > 0.1), about 40% showed at least “moderate correlation” (R-squared > 0.3), and about 30% showed “large correlation” (R-squared > 0.5). For the shank STA models, over 60% variables showed at least “small correlation” (R-squared > 0.1), about 33% showed at least “moderate correlation” (R-squared > 0.3), and about 10% showed “large correlation” (R-squared > 0.5). The average RMS residual error was 6.53 mm for thigh models, and 4.05 mm for shank models. These RMS residual errors were much smaller than the STA itself, indicating the effectiveness of using this “universal” STA model to compensate for STA effects.

Two New Methods for STA Compensation

With Tables 4-1 and 4-2 and Equations 4-1 and 4-2, the overall STA patterns of all the subjects under any given combinations of joint angles can be obtained. With this information, we developed two new “evidence-based’ methods for STA compensation: a “STA deduction” (STAD) method and a “directional weighted optimization” (DWO) method.

STA Deduction (STAD) Method

If a human body segment (thigh or shank) is a rigid body, a skin marker’s global position at a dynamic instant can be expressed as

$$\vec{p}_i^{\,g\_dynamic} = \vec{O}_{bone} + [R_{bone}]\vec{p}_i^{\,l\_static} \qquad (4\text{-}11)$$

where $\vec{O}_{bone}$ and $[R_{bone}]$ are the position and orientation of the bone; $\vec{p}_i^{\,l\_static}$ is the local position of the marker in the anatomical reference system at the static neutral posture.

$\vec{p}_i^{\,g\_dynanic}$ is the global position of the marker in the laboratory coordinate system at a dynamic instance. But if the body segment is not a rigid body, the equation will not hold:

$$\vec{p}_i^{\,g\_dynamic} \neq \vec{O}_{bone} + [R_{bone}]\vec{p}_i^{\,l\_static} \quad (4\text{-}12)$$

The cause of the inequity is marker's relative movement in the anatomical coordinate system, i.e. STA. It can be expressed as:

$$\vec{V}_i^{STA} = [R_{bone}]^{-1}(\vec{p}_i^{\,g\_dynamic} - \vec{O}_{bone}) - \vec{p}_i^{\,l\_static} \quad (4\text{-}13)$$

If $\vec{V}_i^{STA}$ is known, a new equation can be set up in a similar form of Equation 4-11:

$$\vec{p}_i^{\,g\_dynamic} = \vec{O}_{bone} + [R_{bone}](\vec{p}_i^{\,l\_static} + \vec{V}_i^{STA}) \quad (4\text{-}14)$$

Since $\vec{p}_i^{\,l\_static}$ and $\vec{p}_i^{\,g\_dynanic}$ are also known, $\vec{O}_{bone}$ and $[R_{bone}]$ can be solved using the same approach solving Equation 4-11. This is basic rationale of the STAD method.

To implement this method to solve joint kinematics, the STA vectors will be estimated using our "universal" STA model. First, hip, knee and ankle flexion angles will be computed at each instant. At this step, the flexion angles do not need to be highly accurate and can be determined using any conventional rigid body optimization method or simply using including angles between connections of specific markers. After determining joint angles at every instant of the trial, the STA models in Tables 4-1 and 4-2 will be used along with Equations 4-1 and 4-2 to compute the STA vector for every skin marker. Then the STA vectors will be applied into Equation 4-14 for multiple markers. If there are no less than 3 markers at that frame, $\vec{O}_{bone}$ and $[R_{bone}]$ can be solved.

Directional Weighted Optimization (DWO) Method

The concept of the DWO method can be explained as the following. In a conventional rigid-body optimization, each marker is considered having the same importance (weight). However, we have learned that different markers have different magnitudes of STA during an activity. In an equally-weighted optimization, a marker that has large STA generates larger contribution to analysis errors than a marker that has small STA does. It is logical to assign different weights to different markers in the optimization. Further, even for the same marker, the STA components along different directions are also not the same. One marker may have a large STA along AP direction but a small STA along SI direction, as demonstrated in the last chapter. Thus, it would be more effective to assign different weights to different directional components of each marker. The weights will be determined by STA magnitudes, and this approach represents a non-rigid body optimization.

The implementation of the DWO method can be expressed as the following:

Search for $\vec{O}_{bone}$ and $[R_{bone}]$ which minimize

$$\sum_{i=1}^{markers} \left| \begin{pmatrix} wx_i & wy_i & wz_i \end{pmatrix} . \times ([R_{bone}]^{-1} (\vec{p}_i^{\,g\_dynamic} - \vec{O}_{bone}) - \vec{p}_i^{\,l\_static}) \right|^2 \qquad (4\text{-}15)$$

where $\begin{pmatrix} wx_i & wy_i & wz_i \end{pmatrix}$ is the weight vector for marker *i*, and

$$\begin{pmatrix} wx_i & wy_i & wz_i \end{pmatrix} = \begin{pmatrix} 1 & 1 & 1 \end{pmatrix} ./ \vec{V}_i^{\,STA} \qquad (4\text{-}16)$$

where $\vec{V}_i^{\,STA}$ is the STA vector for the same marker at the specific frame, which is determined based on adjacent joint angles and the "universal" STA models.

Although the basic concept of this DWO method is similar to some other non-rigid optimization algorithms such as the "point cluster technique" (PCT) (Andriacchi

et al., 1998), a fundamental difference in our approach is that the weights are evidence-based instead of pure mathematical estimation. In addition, since the weights are determined based on continuous STA functions, the resultant kinematics would not have frequent discontinuities that are seen in using the PCT method.

Results and Discussions

Evaluation Approach

To evaluate the performance of STAD and DWO methods, the *in vivo* knee joint kinematic data collected in Chapter 3 were used. We collected data on six subjects. In order to fairly test the STA compensation methods, at this step we only used 5 of the 6 subjects' data to construct the "universal" STA models, and used the STA models to implement STAD and DWO methods and test their performance on the 6^{th} subject. This procedure was repeatedly applied to each of the six subjects. For example, the STA models established based on the data from subjects #2, #3, #4, #5, and #6 were used to analyzed the kinematics of subject #1; the STA models established based on the data of subjects #1, #3, #4, #5, and #6 were used to analyzed subject #2; and so on. Thus six sets of evaluation were performed.

The kinematic results obtained from a conventional rigid body optimization (RBO) method (Spoor and Veldpaus, 1980), the STAD method, and the DWO method were compared with the kinematics measured using the fluoroscopic technique. The RMS errors of each of the three skin marker-based methods were evaluated.

In addition to analyzing the errors in knee joint kinematics, the errors in femur and tibia kinematics were also evaluated. This was achieved by computing knee joint kinematics using one segment's motion determined using skin markers, and another segment's motion determined using fluoroscopy. For example, the comparison between

1) knee joint kinematics computed using the femur motion determined using skin markers and the tibia motion determined using fluoroscopy; and 2) knee joint kinematics computed using femur and tibia motion both determined using fluoroscopy; provides an evaluation of the errors caused by femur motion analysis. Similarly, the comparison between 1) knee joint kinematics computed using the femur motion determined using fluoroscopy and tibia motion determined using skin markers; and 2) knee joint kinematics computed using femur and tibia motion both determined using fluoroscopy; provides an evaluation of the errors caused by tibia motion analysis.

Kinematic Results

As examples, Figures 4-33 to 4-37 show the kinematic results of subject #3. The STA models were constructed based on the data from subjects #1, #2, #4, #5, and #6. In these figures, the solid black lines are knee joint kinematics measured from fluoroscopy, and each other color represents one skin marker-based method (red: RBO; blue: STAD; green: DWO). For each skin marker-based method (each color), thick solid lines are joint kinematics; thin solid lines are femur-based kinematics (femur motion determined using skin markers and tibia motion determined using fluoroscopy); thin dashed lines are tibia-based kinematics (tibia motion determined using skin markers and femur motion determined using fluoroscopy).

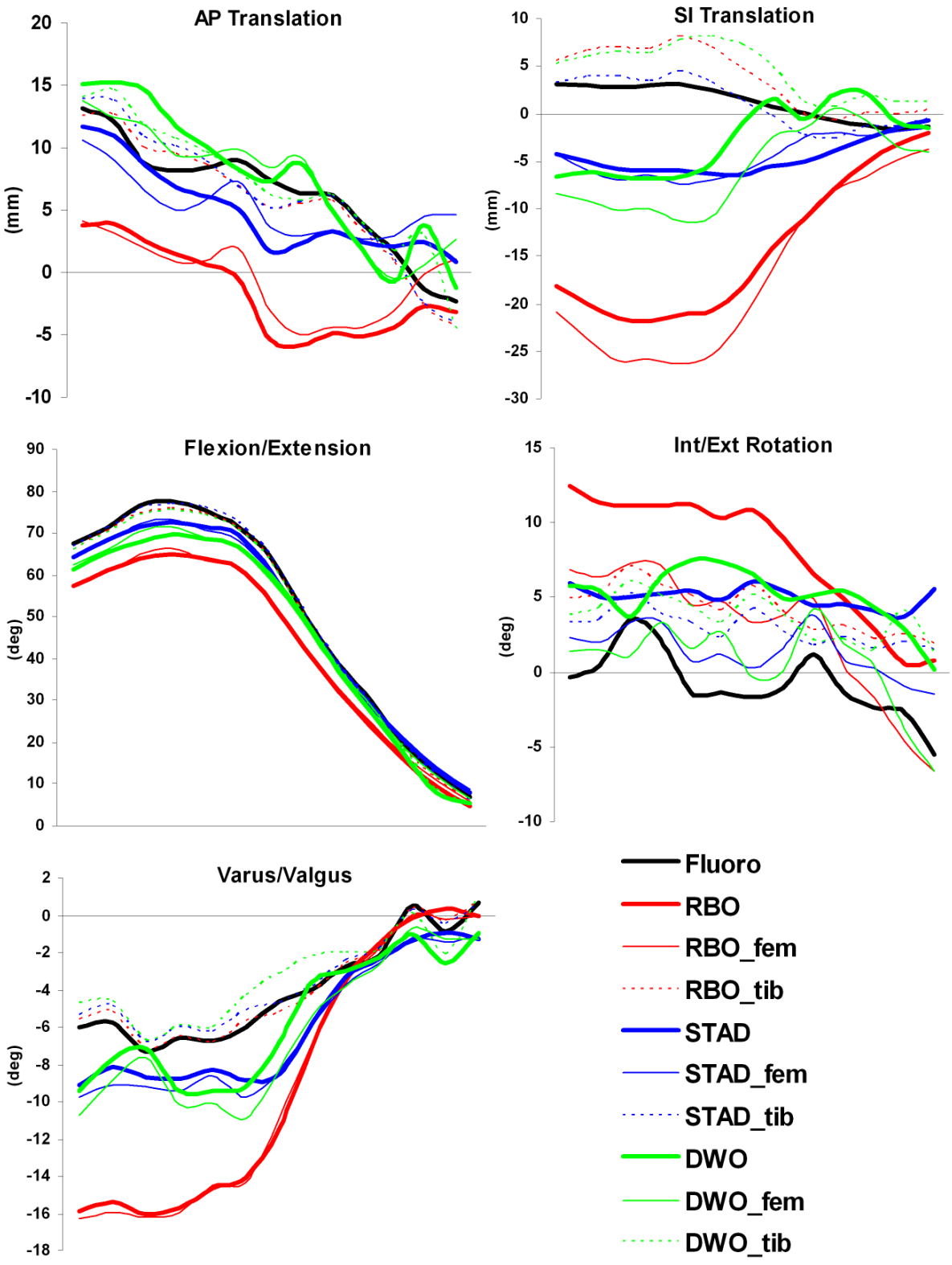

Figure 4-33. Kinematic results obtained using different methods for the stepping-up trial of a representative subject.

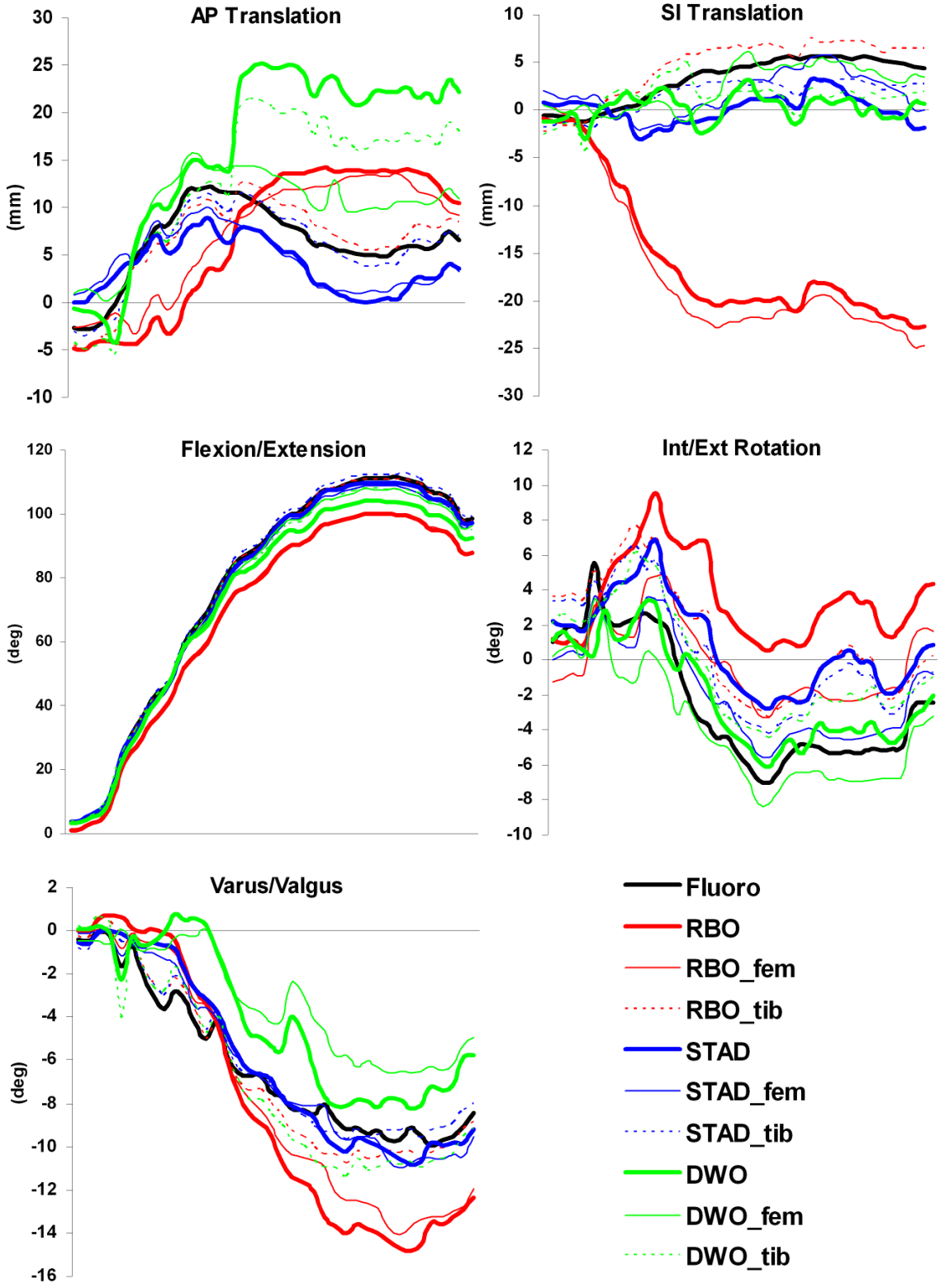

Figure 4-34. Kinematic results obtained using different methods for the knee flexion trial at 15° of hip flexion of a representative subject.

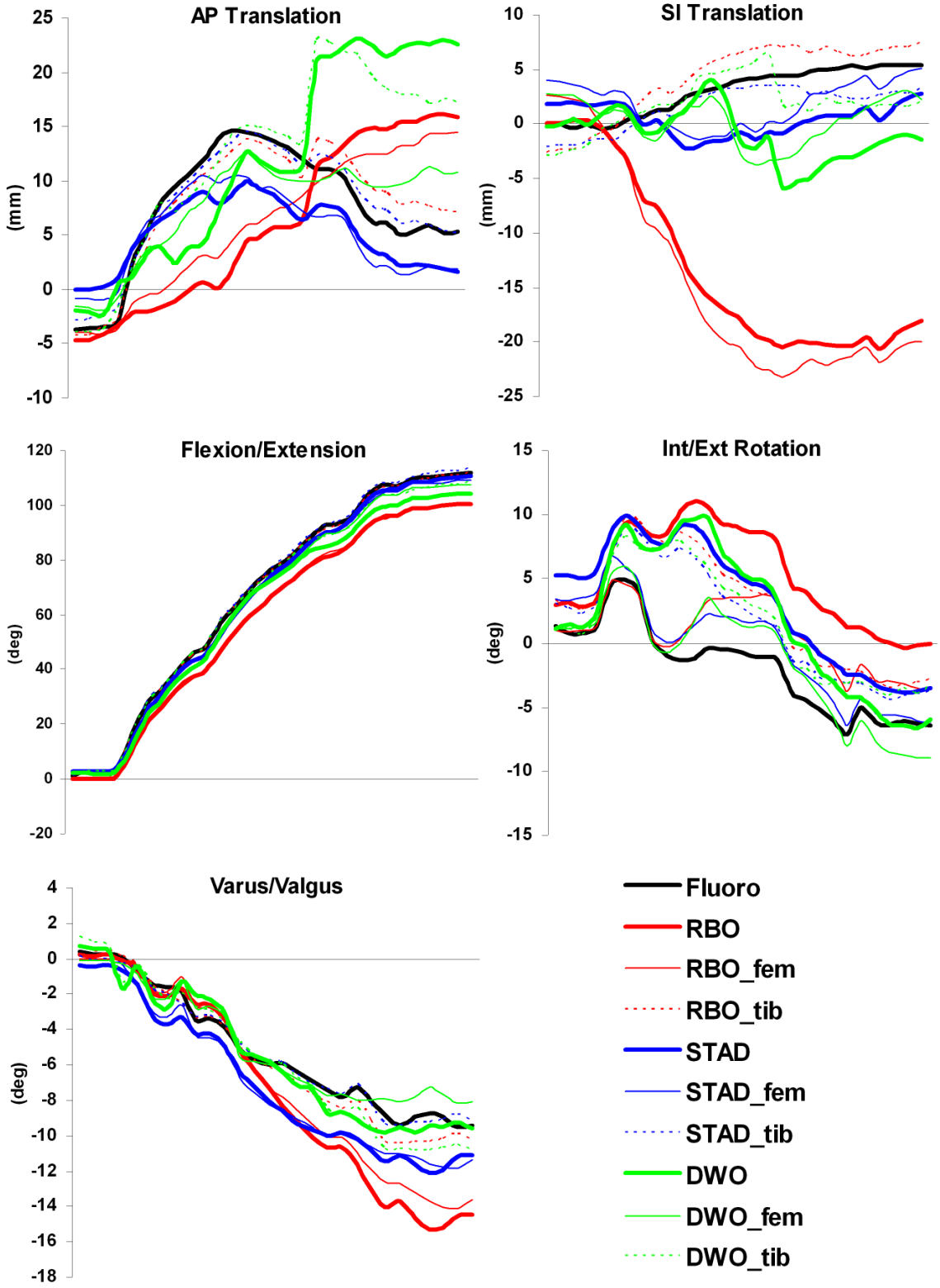

Figure 4-35. Kinematic results obtained using different methods for the knee flexion trial at 30° of hip flexion of a representative subject.

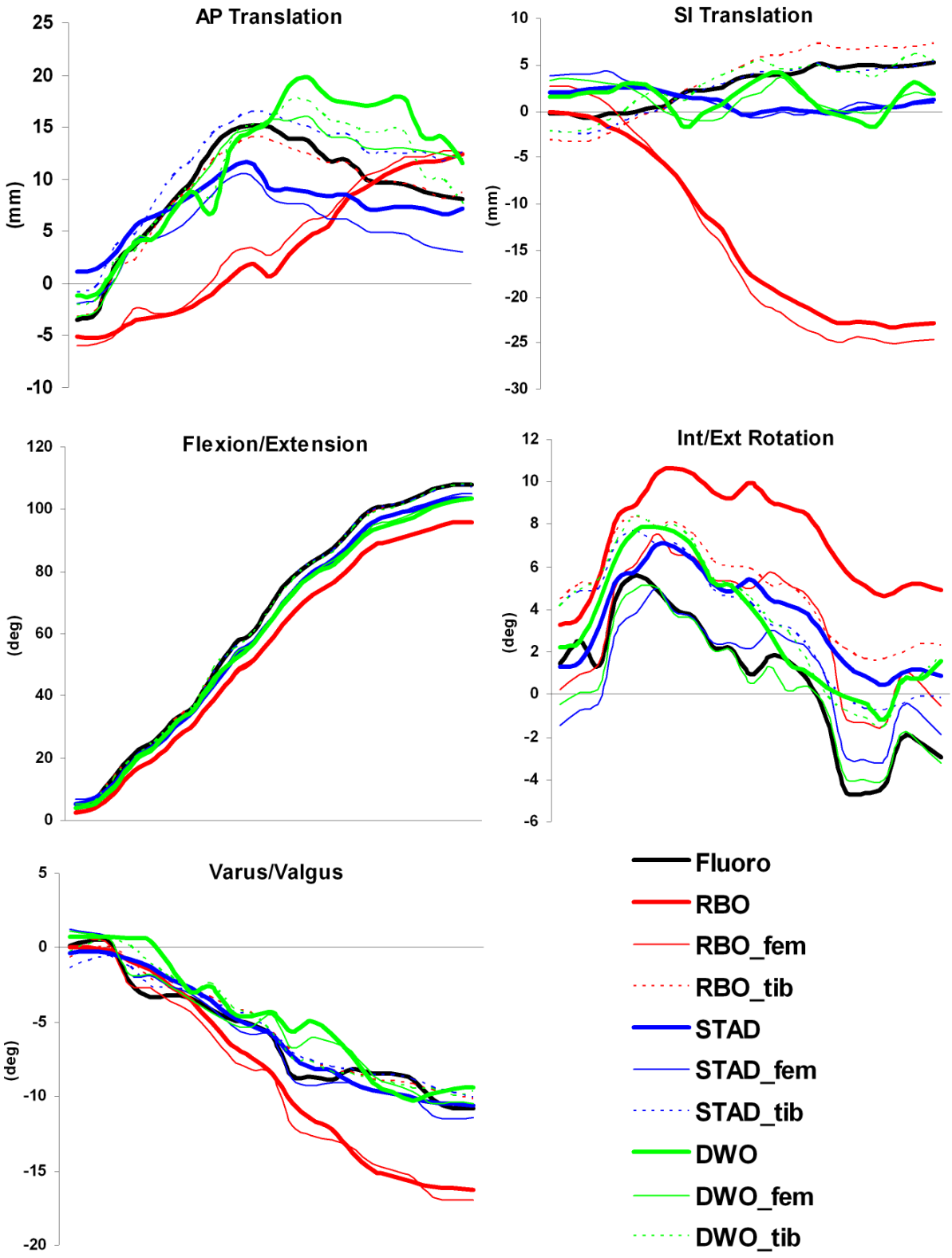

Figure 4-36. Kinematic results obtained using different methods for the knee flexion trial at 45° of hip flexion of a representative subject.

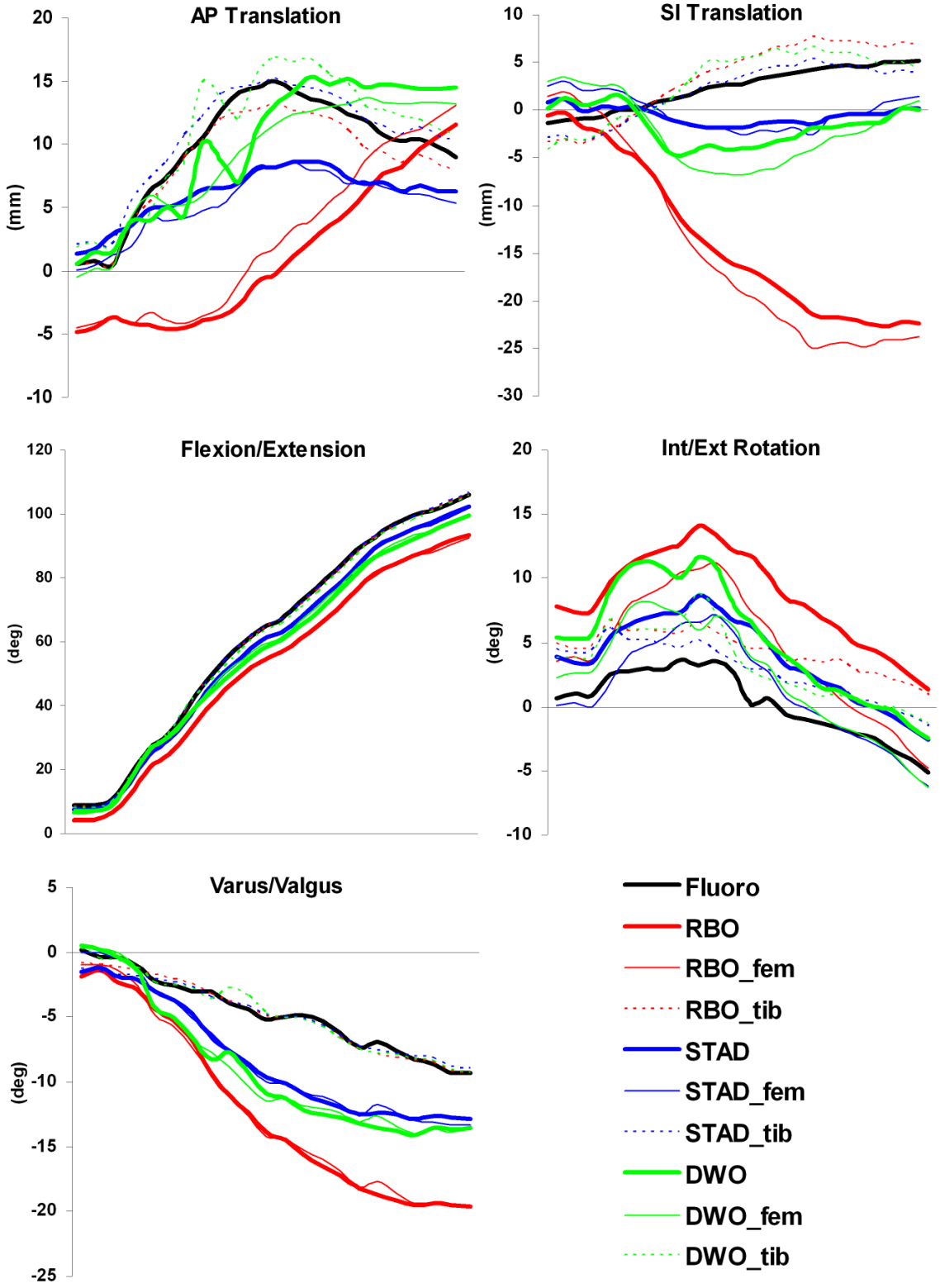

Figure 4-37. Kinematic results obtained using different methods for the knee flexion trial at 60° of hip flexion of a representative subject.

From these kinematic results, we can see the conventional RBO method has low errors when the joint is in a position that is close to the standing posture (joint angles are small). However, with the joint position deviated more and more from the standing posture, the RBO results also deviated more and more from the true skeletal motion (fluoroscopic results). When the knee joint highly flexed, the kinematic errors in RBO method were prominent. This phenomenon was especially apparent for SI translation, flexion/extension, and varus/valgus measurements. For SI translation, the RBO methods may have an error of over 20 mm when the knee was highly flexed. Based on the findings in Chapter 3, the underestimation of SI translation by the RBO method was mainly caused by the large inferior STA of thigh markers during knee flexion. The RBO method also underestimated knee flexion angle at high flexion, and the error could be as high as 8°. For the AP translation results of knee flexion movements (Figures 4-34 to 4-37), the RBO method failed to characterize the femoral “roll back” behavior during high flexion. By comparing the femur-based and tibia-based kinematics, it can be seen the tibia-based results were close to the skeletal motion while femur-based results were close to skin marker-derived joint kinematics. This observation once again emphasized that major portion of analysis error in knee joint kinematics comes from thigh STA effects.

Both STAD and DWO methods exhibited improvement over the RBO method. On Figures 4-33 to 4-37, the blue and green curves are much closer to the black curves than the red curves. Especially for SI translation and flexion/extension measurements, the STAD and DWO significantly reduced errors compared to the RBO method. The performance of STAD method was overall more consistent than the DWO method,

which sometimes produced larger error than the RBO method. In the AP translation results of knee flexion movements (Figures 4-34 to 4-37), the STAD method successfully characterize the femoral “roll back” behavior during high flexion. For all the three methods, tibia-based kinematics were much more accurate than femur-based kinematics.

Analysis Error Comparison

Figures 4-38 to 4-42 show the RMS kinematic errors for all the six subjects, during each specific motor task. In each subplot of these figures, the three bars of the STAD method and the three bars of the DWO method were compared accordingly to the three bars of the RBO method. The variables that resulted in statistical differences were marked using asterisks (* $P<0.05$; ** $P<0.01$).

Overall, the STAD method exhibited the best performance among the three, and it demonstrated significant improvement over the conventional RBO method. Compared to the RBO method, the STAD method on average reduced analysis errors by 49% for AP translation ($P<0.01$), 68% for SI translation ($P<0.01$), 75% for flexion/extension ($P<0.01$), 37% for internal/external rotation ($P<0.05$), and 45% for varus/valgus measurements ($P<0.05$).

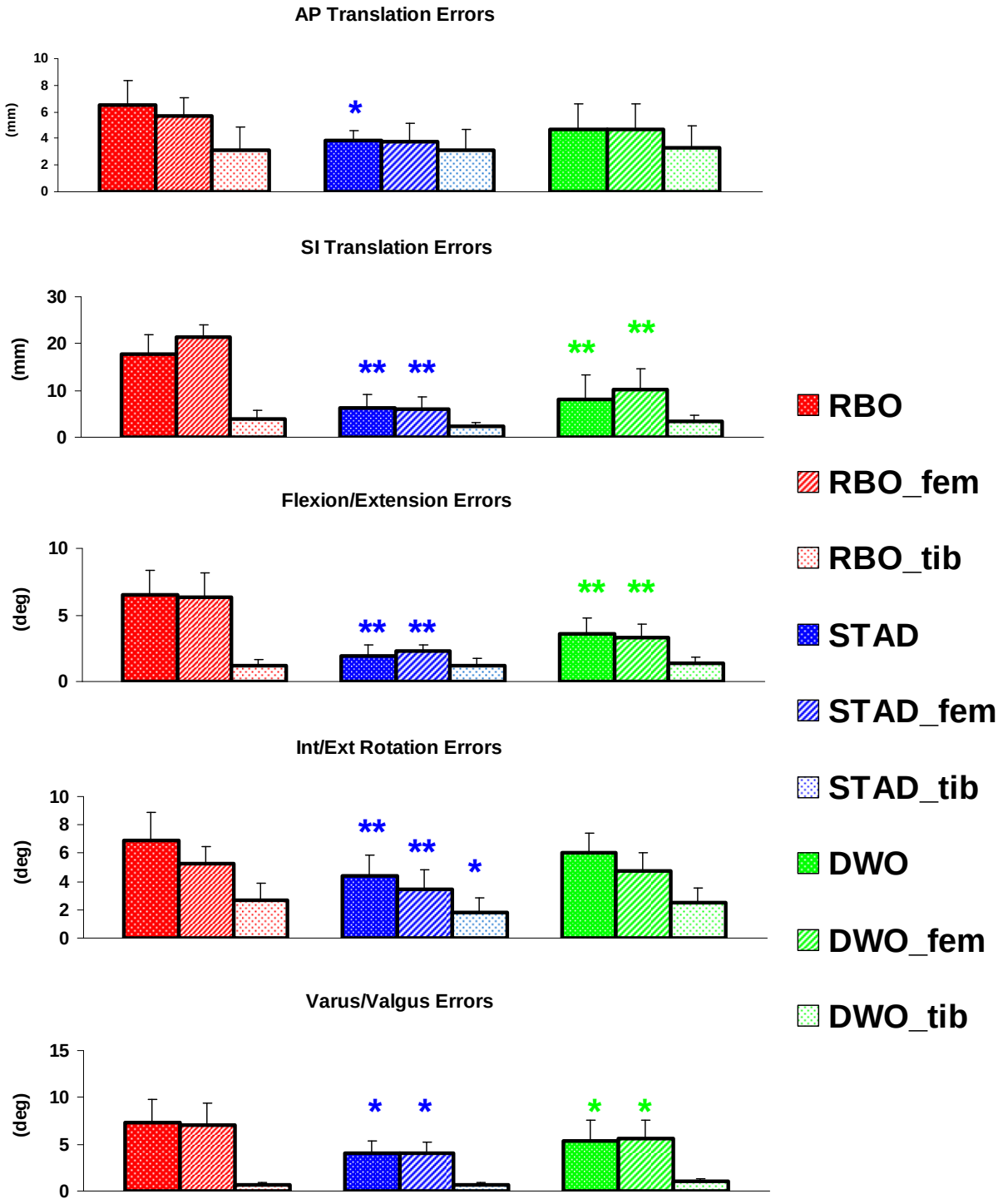

Figure 4-38. RMS kinematic errors of all subjects during stepping-up. The results of the STAD method and the DWO method were compared to the RBO method accordingly. Variables that had statistical differences were marked using asterisks (* $P<0.05$; ** $P<0.01$).

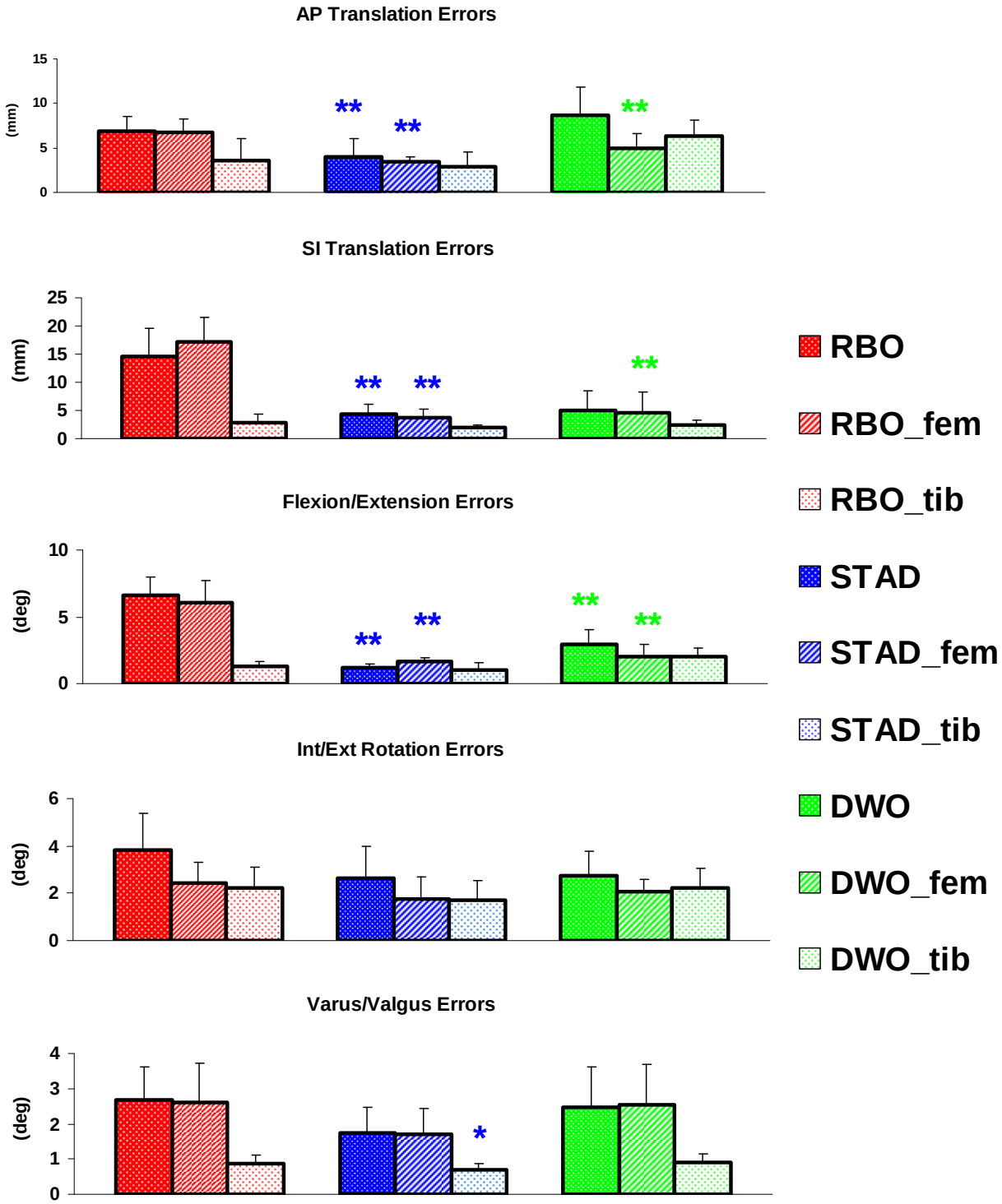

Figure 4-39. RMS kinematic errors of all subjects during knee flexion at 15° of hip flexion. The results of the STAD method and the DWO method were compared to the RBO method accordingly. Variables that had statistical differences were marked using asterisks (* $P<0.05$; ** $P<0.01$).

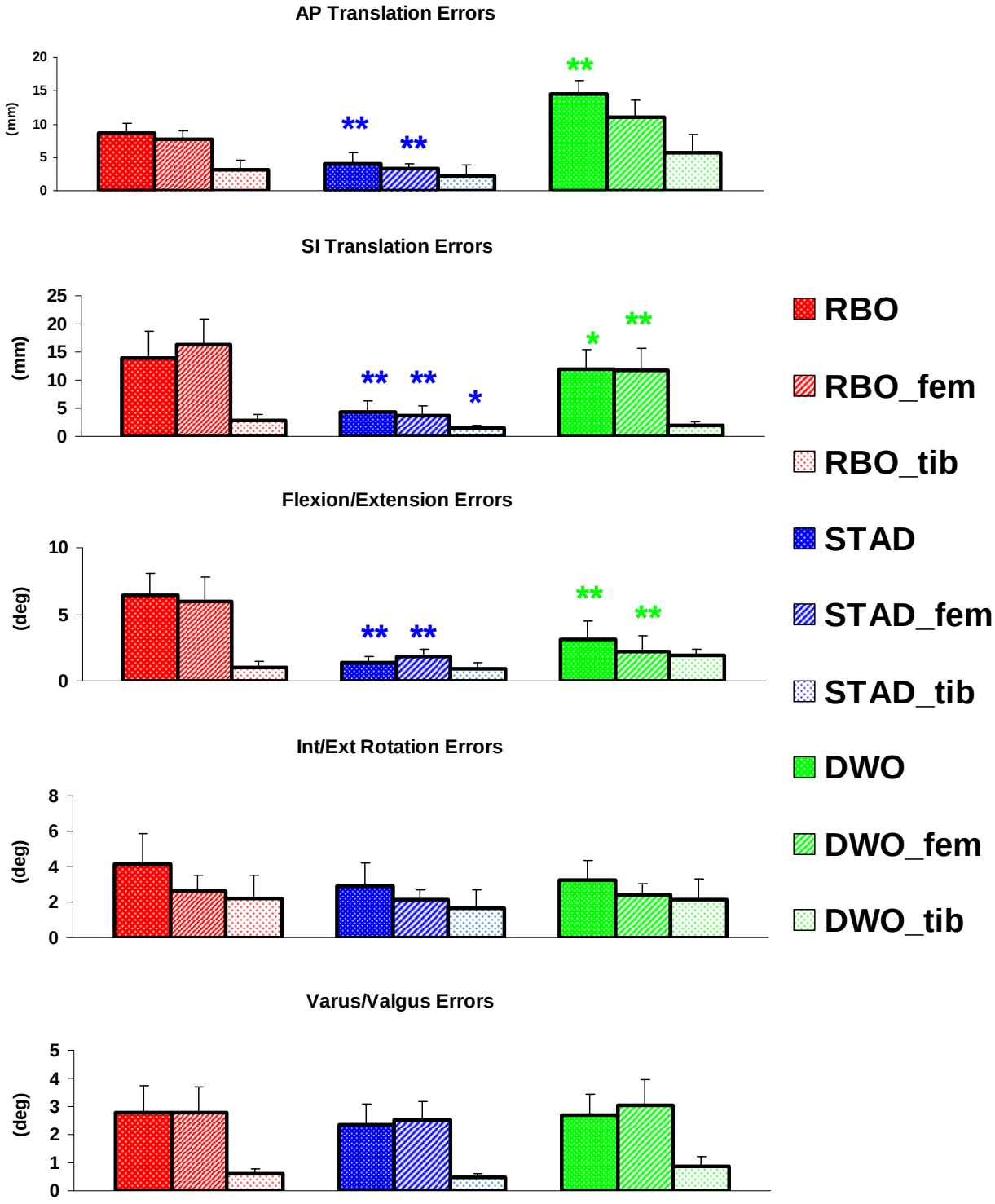

Figure 4-40. RMS kinematic errors of all subjects during knee flexion at 30° of hip flexion. The results of the STAD method and the DWO method were compared to the RBO method accordingly. Variables that had statistical differences were marked using asterisks (* $P<0.05$; ** $P<0.01$).

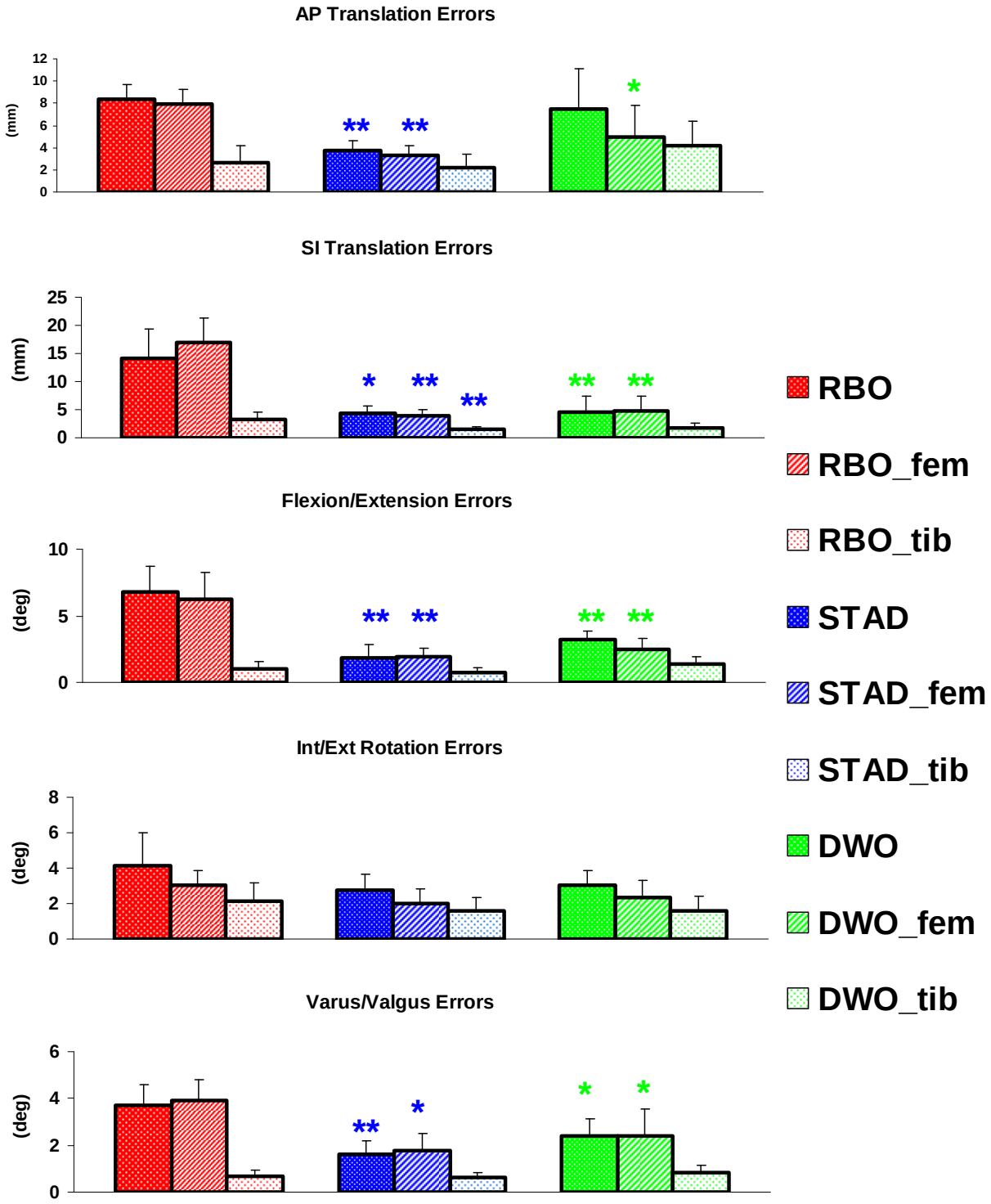

Figure 4-41. RMS kinematic errors of all subjects during knee flexion at 45° of hip flexion. The results of the STAD method and the DWO method were compared to the RBO method accordingly. Variables that had statistical differences were marked using asterisks (* $P<0.05$; ** $P<0.01$).

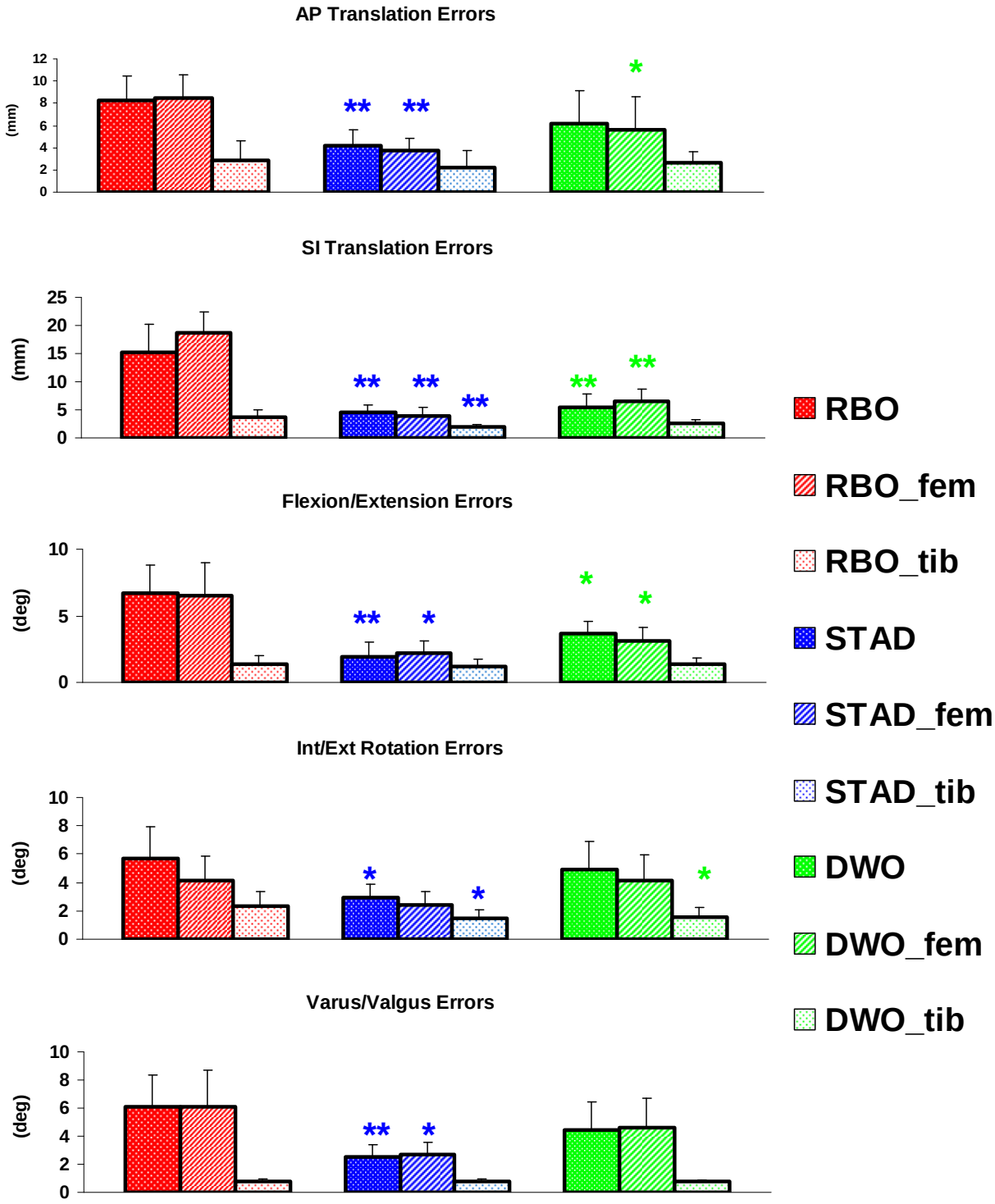

Figure 4-42. RMS kinematic errors of all subjects during knee flexion at 60° of hip flexion. The results of the STAD method and the DWO method were compared to the RBO method accordingly. Variables that had statistical differences were marked using asterisks (* P<0.05; ** P<0.01).

On average, the RMS errors of STAD method were 3.9 mm for AP translation, 4.7 mm for SI translation, 1.6° for flexion/extension, 3.1° for internal/external rotation, and 2.4° for varus/valgus measurements. It should be noted these error magnitudes were obtained in motor tasks that involved large ranges of knee/hip flexion. As we observed, the kinematic errors of skin marker-derived measurements are highly related to joint position. Thus the actual errors occurring in some other motor tasks that involved smaller ranges of knee/hip flexion, such as level walking, are very likely to be lower than the errors observed in this study. As evidence to this opinion, the kinematic errors from RBO method shown in this study were about 2 to 3 times higher than those identified in a previous study performed on cadaveric knee specimens (Gao et al., 2007). In that previous study, knee flexion angles of the specimens were usually less than 60°. This could be a main reason for the lower error magnitudes identified in the previous study, in addition to stiffer soft tissues in cadaveric specimens. In addition, the BMI of the TKA patients tested in this study (about 28 in average) was higher than that of many other sports injury patients, such as anterior cruciate ligament injury patients. Thus the STA magnitude found in this study is expected to be an upper bound representation of general patient population.

The STAD method exhibited its best error reduction capability in SI translation and flexion/extension measurements. These error reductions resulted mainly from the compensation of major patterns of AP and SI components of thigh STA in the STAD method. The compensation also benefited more accurate measurements of other kinematic variables. The error reduction capability of the STAD method was relatively lower on internal/external rotation and varus/valgus measurements. A possible reason

was that we were not able to obtain reliable ML STA patterns in the current STA models, because of the limitation of single view fluoroscopic technique. In addition to ML translation measurement, the ML STA could also affect axial rotation and varus/valgus measurements. Future work aiming to obtain more reliable ML STA assessment (for example, using a bi-plane fluoroscopic study design) could benefit further accuracy improvement on these secondary kinematic measurements.

The relatively small sample size of subjects in our study could also limit the effectiveness of the “universal” STA model and the performance of the STAD method. Only 6 (5 in evaluation) subjects’ STA data were included to establish the “universal” STA model. The variability in the small sample could reduce the effectiveness of the STA model in representing the common patterns of a general population. With more subjects’ data being included in future studies, it is expected that the “universal” STA model would be more robust and more representative. As a result, the STAD method may be even more effective.

Also because of the small subject sample size, the anthropometric parameters of individual subject were not taken into account in the STA models. With a larger subject sample size, it might be possible to design the STA models which incorporate the anthropometric characteristics of different subject, such as BMI, limb circumference, skin-fold thickness, etc.

Since the primary aim of this study is to demonstrate the feasibility and effectiveness of the STA compensation concept, a simple multilinear model was used to construct the STA models. The simple mathematical model provided an intuitive expression of the STA-joint angle relationship, and worked well for many

components/markers. However, for some components/markers (such as the T10 and T11), it is apparent that a linear model might not be the best option (Figures 3-20 to 3-23). It is likely with more complex mathematical functions (higher-order or piecewise), the STA models will be more reliable. All these aspects leave the possibilities for future methodological improvement.

CHAPTER 5
THREE DIMENSIONAL KINEMATICS OF ACL-DEFICIENT AND ACL-RECONSTRUCTED KNEES

Introduction

The human anterior cruciate ligament (ACL) plays an important role in controlling knee joint stability, not only by limiting tibia anterior translation but also by controlling knee axial rotation and varus movement (Andersen and Dyhre-Poulsen, 1997; Markolf et al., 1995). After ACL injury, knee joint stability and load-bearing patterns between joint surfaces can be altered, resulting in abnormal loadings on the cartilage during functional activities (Chaudhari et al., 2008; Li et al., 2006). This change in biomechanical environment has been associated with cartilage degeneration and progressive development of knee joint osteoarthritis (Andriacchi et al., 2006; Andriacchi and Mundermann, 2006; Stergiou et al., 2007; Wu et al., 2000). This model has been supported by both animal and human studies (Baliunas et al., 2002; Brandt et al., 1991; Neyret et al., 1993; Papaioannou et al., 2004; Pond and Nuki, 1973). For untreated ACL-deficient (ACL-D) knees, the risk of knee osteoarthritis development has been reported as high as 44% after 11 years (Noyes et al., 1983), and over 50% of cases have led to total knee arthroplasty before age 63 (Nebelung and Wuschech, 2005).

ACL reconstructive surgery is typically recommended to restore the knee joint stability and function after ACL injury. However, the effectiveness of ACL reconstruction in preventing cartilage degeneration and osteoarthritis development remains controversial (Jones et al., 2003; Lohmander and Roos, 1994). Studies have shown that even after constructive surgery, early cartilage degeneration cannot be successfully prevented and premature knee osteoarthritis can still develop (Asano et al., 2004; Daniel et al., 1994; Lohmander et al., 2004; Seon et al., 2006). These studies evaluated

the articular cartilage of ACL-reconstructed (ACL-R) knees with sample sizes from 41 to 105 knees, and the results showed a high prevalence of knee osteoarthritis 5 to 12 years post surgery. A significant degeneration of cartilage was observed as early as 15 months after surgery (Asano et al., 2004). These findings indicated that current reconstructive surgeries may not effectively reduce the risk of early cartilage degeneration and osteoarthritis development in ACL-R knees. Researchers have suggested this could be a consequence of the knee joint kinematics that have not been fully restored by the reconstructive surgery and the rehabilitation that follows (Brandsson et al., 2002; Papannagari et al., 2006). The residual abnormalities of joint motion and the resultant contact pattern change between articular surfaces could lead to progressive cartilage degeneration under millions of cycles of joint loading during daily activities. If the articular cartilage or menisci had suffered traumatic damage at the time of the ACL injury, the situation could deteriorate and have negative impact on the mechanical-biological dynamics more than would have resulted from the ACL injury alone.

Although ACL injury usually occurs during more intensive joint maneuvers, the cartilage degeneration and osteoarthritis development after the injury is considered a progressive process which happens under cyclic loading from less intensive but more frequent activities of daily living (Chaudhari et al., 2008; Miyazaki et al., 2002). In order to identify the risk factors that contribute to the biomechanical environment change after ACL injury, it is critical to understand the three-dimensional (3-D) joint kinematics of ACL-D and ACL-R knees during daily activities. Ground walking is the most common and frequently performed ambulatory activity. Quite a few studies have been performed

to evaluate joint kinematics of ACL-D/ACL-R knees during walking (Alkjaer et al., 2003; Andriacchi and Dyrby, 2005; Bush-Joseph et al., 2001; Georgoulis et al., 2003; Gokeler et al., 2003; Hurd and Snyder-Mackler, 2007; Knoll et al., 2004b; Kvist, 2004; von Porat et al., 2006). Most of these studies focused on joint movement in the sagittal plane. However, the knee joint has secondary movement other than that in the sagittal plane, and the secondary movement is considered to be clinically significant (Mundermann et al., 2005). In the handful studies that examined knee kinematics during walking in a full 3-D and 6 degree of freedom, reduced anterior translation and tibial external rotation before heel strike were observed in ACL-D knees (Andriacchi and Dyrby, 2005). In addition, more internal tibial rotation during the initial swing phase was reported in ACL-D knees compared to healthy knees (Georgoulis et al., 2003). So far little has been reported about kinematic alterations of frontal plane movement in ACL-D knees or about secondary movement in ACL-R knees during level walking. The purpose of this chapter was to examine in 3-D the effects of ACL deficiency and reconstruction on the knee joint kinematics during walking.

We hypothesized that ACL-D knees would exhibit altered joint kinematics in 3-D, and the kinematics of ACL-R knees that received reconstructive surgery would not been fully restored to a normal level. In order to test the hypothesis, we examined 3-D knee joint kinematics during walking in three subject groups: ACL-D, ACL-R and healthy controls with bilateral ACL-intact (ACL-I) knees. Kinematic variables of the three rotations and three translations of the knee joint were obtained using the STA compensation method developed in the previous chapter, and compared between the ACL-D and the ACL-I groups, as well as between the ACL-R and the ACL-I groups.

Design and Methods

Subjects

Three groups of subjects (ACL-D, ACL-R, and ACL-I) were recruited and tested in this study (Table 5-1).

Fourteen subjects who had sustained a unilateral ACL injury were tested as the ACL-D group, including 11 males and 3 females. All ACL-D subjects were tested within one year after ACL injury (average 3 months) and the ACL ruptures were confirmed with MRI examination. Fourteen subjects who had undergone a unilateral, primary ACL reconstruction were tested as the ACL-R group. This group was composed of 12 males and 2 females. Three types of grafts had been used in these ACL-R knees (7 hamstrings tendon autografts, 5 bone-patellar tendon-bone allografts, and 2 Achilles tendon allografts). All ACL-R subjects were tested at least 3 months post reconstruction (typically within 12 months), and had completed the postoperative rehabilitation programs before participating in this study. The ACL-D and ACL-R subjects included had no accompanying damage to the posterior cruciate and collateral ligaments, no more than 30% of the meniscus removed, no injuries on the contralateral limb, and no difficulty or pain in performing activities of daily living including walking. As the control group, 15 healthy subjects who had bilateral ACL-I knees and no history of musculoskeletal diseases on the lower extremities were included. The ACL-I group consisted of 12 males and 3 females. The age, height, and weight distributions of the ACL -I group were not significantly different from those of the ACL-D and ACL-R groups ($P > 0.05$). The protocol was approved by the institutional review board for human subject research and each subject gave informed consent.

Table 5-1. Subject information.

Group	Number	Age (year)	Height (m)	Weight (kg)	Body mass index (kg/m^2)
ACL-I	15 (12m & 3 f)	22.8 (SD 2.6)	1.81 (SD 0.10)	76.8 (SD 16.4)	23.3 (SD 3.2)
ACL-D	14 (11m & 3 f)	26.7 (SD 8.6)	1.78 (SD 0.12)	82.7 (SD 22.0)	25.3 (SD 3.6)
ACL-R	12 (12m & 2 f)	25.1 (SD 5.9)	1.80 (SD 0.07)	82.5 (SD 15.0)	25.8 (SD 4.8)

Experimental Setup

Motion data were collected using an 11-camera stereophotogrammetric system (Motion Analysis Corp., Santa Rosa, CA, USA) at 60 Hz. The measurement space was about 5.0 m × 2.0 m × 2.5 m and the 3-D residue of marker position tracking was lower than 1 mm after system calibration. Sphere-shaped reflective markers 10 mm in diameter were attached to bone landmarks and body segments of the subject to track body movements (Figure 5-1).

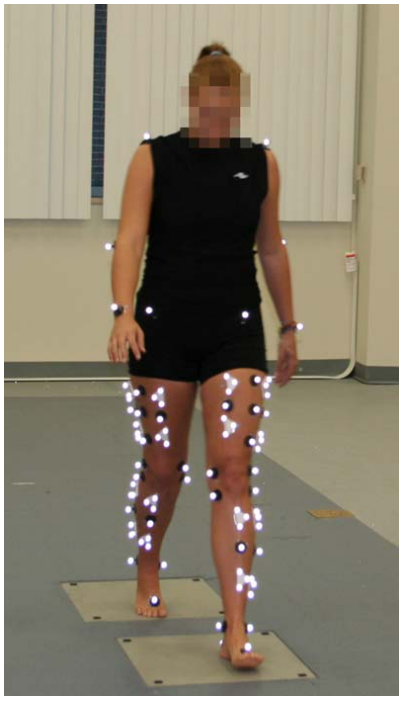

Figure 5-1. An ACL-D subject in test.

Marker Placement

Five markers were placed on the left and right anterior superior iliac spines, the left and right posterior superior iliac spines, and the sacrum. On each leg, eight markers were placed on the medial and lateral femoral epicondyles, the medial and lateral ridges of the tibial plateau, the medial and lateral malleoli, the second metatarsal head and the heel. Another 17 and 14 markers were placed on the anterolateral side of the thigh and the shank, respectively. The marker set used in this study was more complete than configurations commonly used in gait analyses such as the Helen Hayes marker set. The purpose of employing more markers to cover a larger region of body segments was to reduce errors caused by soft tissue artifact (Leardini et al., 2005).

Test Procedure

The test started with a static trial while the subject stood with feet shoulder width apart and toes facing forwards. This static trial was used for initial anatomical frame definition. After adequate practice, the subject was commanded to walk through the measurement space at his/her self-selected speed while the motion capture system recorded at least one gait cycle for each leg. Two force platforms (AMTI, MA, USA) embedded in the floor were used to record ground reaction force to facilitate gait event detection. At least five good walking trials were recorded for each subject.

Analysis Methods

From the static standing trial, anatomical frames on the femur and tibia were defined based on bone landmarks (Figure 5-2.a). Tibial origin was defined as the midpoint of the medial and lateral ridges of the tibial plateau. The midpoint of the transepicondylar line was considered the femoral origin. The midpoint of the medial and lateral malleoli was identified as the ankle joint center. Hip joint center was defined

using a predictive method (Bell et al., 1990). The axes of the femoral and tibial coordinate systems were then described (Figure 5-2.a): Z_f points from the femoral origin O_f to the hip joint center O_h; Y_f parallels to the cross product of Z_f and the vector from the heel to the second metatarsal head; $X_f = Y_f \times Z_f$. Z_t points from the ankle joint center O_a to the tibial origin O_t; Y_t parallels the cross product of Z_t and the vector from the heel to the second metatarsal head; $X_t = Y_t \times Z_t$. b) Calculation of the 3-D knee joint angles (Figure 5-2b). α is the flexion/extension angle, β is the varus/valgus angle, γ is the axial rotation angle, X_{f-xz} is the projected vector of X_f on the sagittal plane, Y_{f-xy} is the projected vector of Y_f on the transverse plane, and Y_{f-yz} is the projected vector of Y_f on the frontal plane.

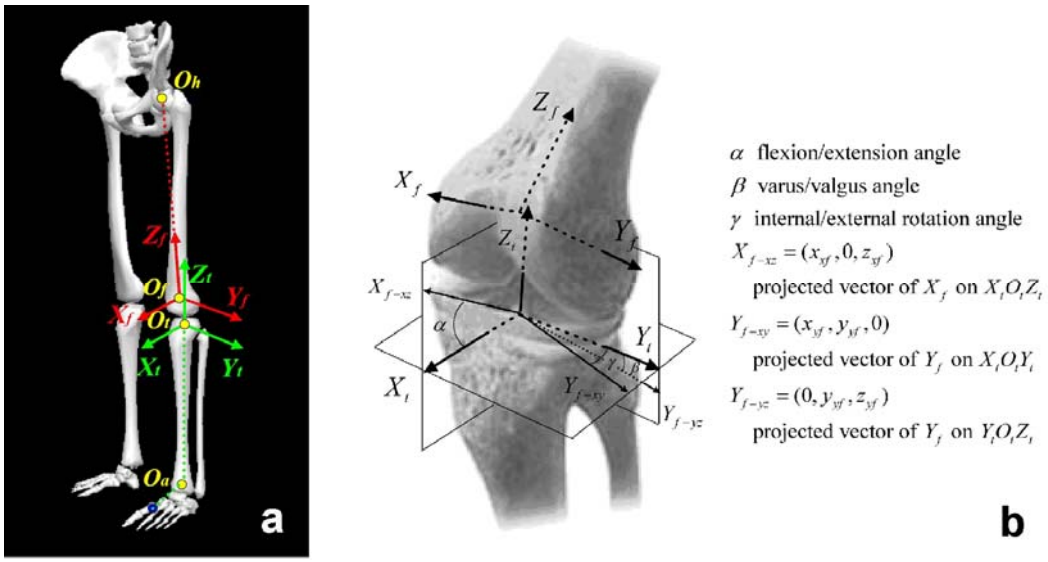

Figure 5-2. Definition of anatomical coordinate systems on the femur and the tibia.

A fourth order Butterworth low-pass filter (cut-off frequency 6 Hz) with zero lag was applied to smooth original marker position data. The 3-D dynamic poses of the thigh

and shank during walking were determined using the STA deduction (STAD) method developed in Chapter 4. Joint kinematics were then computed and described as the positional and orientational change of the femur relative to the tibia (Figure 5-2.b). The translations were derived from the movement of the femoral origin in the tibial coordinate system. In order to avoid rotational sequence dependency, the projection method was used to describe the joint rotations. A custom-developed MATLAB (MathWorks Inc., Natick, MA, USA) program was used to perform the kinematic analysis. As a comparison, another set of kinematics solved using conventional rigid body optimization (RBO) method were also presented.

The 3-D knee joint motion data during walking was normalized into each gait cycle (from heel strike 0% to heel strike 100%). Each of the six kinematic curves (three rotations and three translations) for five trials was ensemble averaged for each subject across the whole gait cycle. Spatiotemporal variables including step/stride length and speed, durations of double and single support phases, and timing of key events inside the gait cycle were examined. Six key events between two sequential heel strikes were selected, including contralateral toe off (CTO), maximum knee flexion during the stance phase (1^{st} FE peak), minimum knee flexion during midstance (FE valley), contralateral heel strike (CHS), toe off (TO), and maximum knee flexion during the swing phase (2^{nd} FE peak). For each of the three rotational and three translational components of knee joint kinematics, 101 discrete points corresponding to 0~100% gait cycle at 1% interval were extracted using one-dimensional interpolation for statistical analysis. Measures of each spatiotemporal variable as well as each discrete kinematic point were compared between ACL-D, ACL-R and ACL-I knees using a one-way analysis of variance (SPSS

Inc., IL, USA). A significance level of $\alpha = 0.05$ was used in the statistical analysis. For tests that resulted in a significant omnibus F result, *post hoc* analysis was performed using the Tukey's honestly significant difference (HSD) procedure.

Results

Spatiotemporal Parameters

At static standing posture, the initial knee joint angles were small for all the subjects and no statistical differences were detected between the patient and control groups (Table 5-2).

Table 5-2. Initial knee joint angles at the static standing posture and spatiotemporal variables during gait. For ACL-D and ACL-R subjects, the step length/speed was unilateral measurement on the injured or involved limb, while the stride length/speed was bilateral measurement on a complete gait cycle. For ACL-D/ACL-R subjects, the 1st double support phase started from the heel strike of the injured/involved limb, while the 2nd double support phase was from the heel strike of the non-injured/non-involved limb; the 1st single support phase was from the toe off of the non-injured/non-involved limb, while the 2nd single support phase started from the toe off of the injured/involved limb.

	ACL-I mean (SD)	ACL-D mean (SD)	ACL-R mean (SD)	Statistical Difference ($P < 0.05$)
Flexion @ static (deg)	0.5 (4.4)	2.4 (5.1)	2.7 (5.0)	None
Tibial Internal Rot @ static (deg)	-0.2 (0.4)	-0.1 (0.4)	0.2 (0.6)	None
Varus @ static (deg)	-1.8 (2.6)	-0.7 (2.9)	-0.5 (3.7)	None
Step Speed (m/sec)	1.23 (0.09)	1.12 (0.13)	1.15 (0.16)	ACL-I vs ACL-D
Stride Speed (m/sec)	1.23 (0.08)	1.14 (0.14)	1.15 (0.17)	None
Step Length (m)	0.69 (0.04)	0.65 (0.04)	0.67 (0.05)	ACL-I vs ACL-D
Stride Length (m)	1.38 (0.08)	1.31 (0.09)	1.34 (0.11)	None
1st Double Support phase (% gait cycle)	7.9 (1.5)	9.1 (1.7)	8.7 (2.1)	None
1st Single Support phase (% gait cycle)	42.0 (1.5)	40.7 (1.7)	41.8 (2.1)	ACL-I vs ACL-D
2nd Double Support phase (% gait cycle)	7.4 (1.7)	8.5 (1.4)	8.6 (2.2)	None
2nd Single Support phase (% gait cycle)	42.7 (1.8)	41.7 (1.7)	40.9 (1.8)	ACL-I vs ACL-R

The ACL-D knees showed a slower step speed and a shorter step length compared to the ACL-I knees ($P < 0.05$). The difference was about 0.1 m/sec in speed and 3 to 4 cm in each step. The speed and step length reduction trends were also visible in the ACL-R knees, but not statistically significant. The ACL-D and ACL-R knees exhibited shortened single support phases and prolonged double support phases compared to the ACL-I knees. The timing offset was about 1% gait cycle and it reached statistical significance on the 1st single support phase between the ACL-D and ACL-I groups, and on the 2nd single support phase between the ACL-R and ACL-I groups (Table 5-2).

Key Events during a Gait Cycle

In the gait cycle from the 1st heel strike (HS) to the 2nd HS, key events CTO, 1st FE peak, FE valley, CHS, TO, and 2nd FE peak occurred in sequence at about 8%, 12%, 38%, 50%, 58% and 72% of the gait cycle for the ACL-I subjects (Figure 5-3). Significant timing abnormalities were detected on the ACL-D and ACL-R groups. The occurrences of the 1st FE peak and FE valley of the ACL-D group was delayed by about 2% gait cycle compared to the ACL-I group ($P < 0.05$). The occurrences of TO and 2nd FE peak of the ACL-R group was delayed by about 2% compared to the ACL-I group ($P < 0.01$) (Figure 5-3).

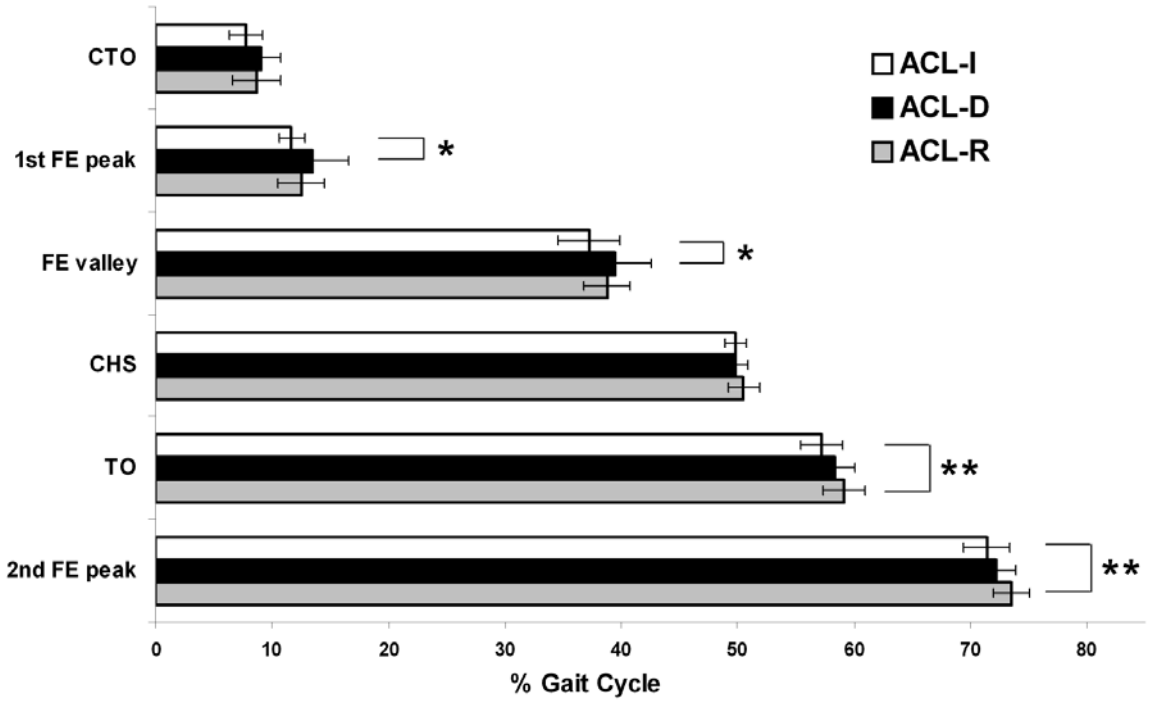

Figure 5-3. Timings of key events in the gait cycle for ACL-I, ACL-D and ACL-R groups. The gait cycle was normalized from one heel strike (0%) to the next heel strike (100%). The key events examined in this study included contralateral toe off (CTO), maximum knee flexion during the stance phase (1st FE peak), minimum knee flexion during midstance (FE valley), contralateral heel strike (CHS), toe off (TO), and maximum knee flexion during the swing phase (2nd FE peak). Significant statistical differences were marked with asterisks (*P < 0.05, **P < 0.01).

Joint Kinematics

Kinematic differences during walking were observed in 3-D rotations between ACL-D, ACL-R and ACL-I knees (Figure 5-4). In the sagittal plane, the ACL-D knees were significantly less extended than the ACL-I knees during a large portion of midstance (32% to 46% of gait cycle). The average FE valley during stance phase of the ACL-D knees was 15.3° (SD 6.3°), which was significantly higher than the value of the ACL-I knees (9.0° (SD 3.3°)) (P < 0.01). The ACL-R knees exhibited improvement on this phenomenon and the ensemble curve did not differ significantly to the curve of

ACL-I knees (Figure 5-4), but the average FE valley during stance phase (12.2° (SD 4.7°)) was still higher than that of the ACL-I knees. The ACL-R knees also showed a flexion offset during the second half of swing phase compared to the ACL-I knees ($P < 0.05$). In the frontal plane, there was a consistent offset between the curves of the ACL-D knees and ACL-I knees. The ACL-D knees were about 2° to 3° more varus than the ACL-I knees during the entire gait cycle, and this difference reached statistical significance during stance phase. A similar offset was also visible between the ACL-R and ACL-I knees although the difference was not statistically significant. A rotational offset was identified in the transverse plane. The ACL-D knees exhibited less tibial external rotation compared to the ACL-I knees during most part of the gait cycle, and the difference reached statistical significance during a large portion of swing phase. This axial rotation offset was about 2° to 4° throughout the gait cycle and had not been eliminated in the ACL-R knees. The offset reached statistical significance at late stance phase and before TO on the ACL-R knees.

No significant differences were observed on 3-D translations between ACL-D, ACL-R and ACL-I knees (Figure 5-5). Knee joint translations of the three subject groups exhibited similar patterns and the differences between groups were comparable to intra-group variability.

Comparison between STAD method and RBO method

Differences were observed in the kinematics obtained using the new STAD method and using the conventional RBO method. For rotations, the RBO method under-estimated knee flexion angle by about 3° compared to the STAD method (Figure 5-6). The RBO method also resulted in larger range of motion (ROM) for axial rotation measurement compared to the STAD method (Figure 5-6). For translations, the RBO

method under-estimated anterior translation and the femoral roll-back behavior during the swing phase (Figure 5-7). After STA compensation (the STAD results), AP translation was closer to zero during stance phase and femoral roll-back was better characterized during swing phase. ML translation was also closer to zero in the STAD results. The RBO method under-estimated superior translation measurement by 5 to 10 mm (Figure 5-7). Although the kinematic results obtained using the two methods differed quantitatively, the qualitative comparisons between different subject groups (ACL-D and ACL-I, ACL-R and ACL-I) were similar.

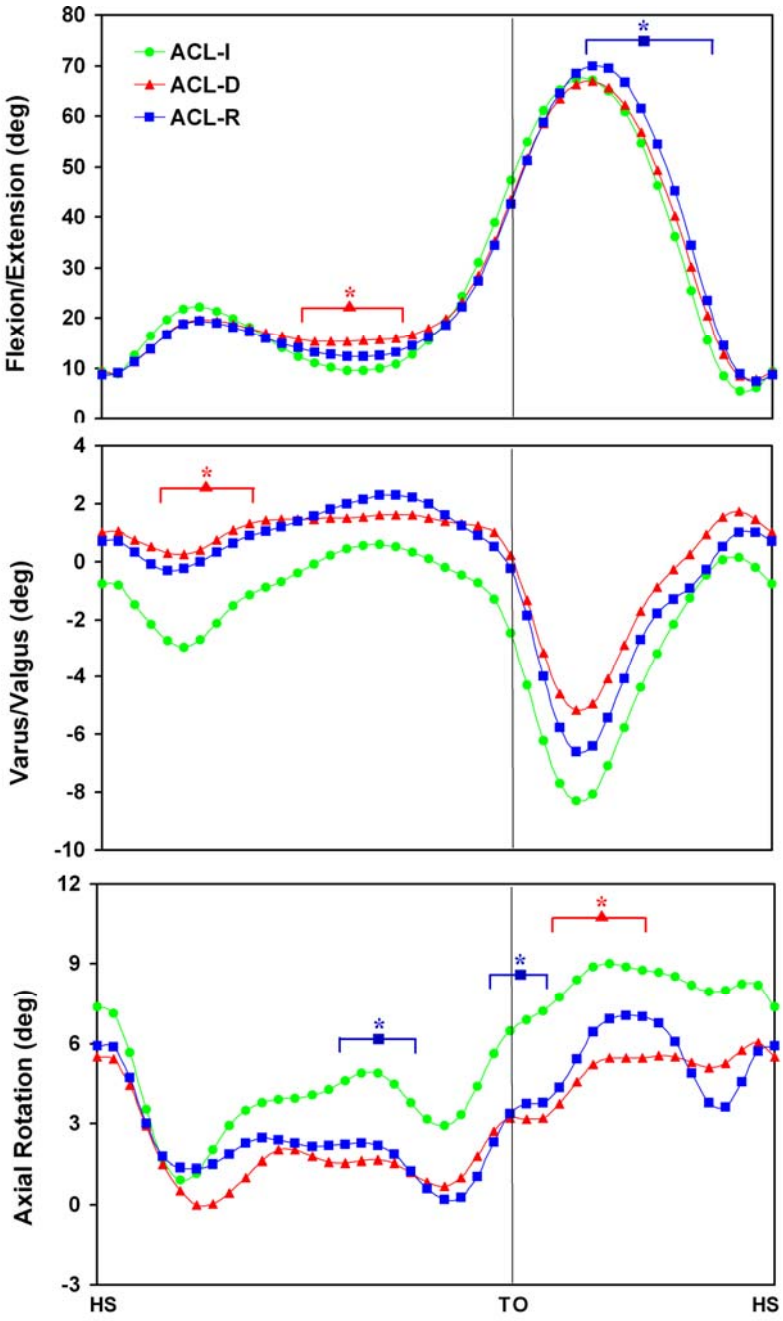

Figure 5-4. The 3-D joint rotations during walking of ACL-I, ACL-D and ACL-R knees. Ensemble curves of each subject group were normalized from heel strike to heel strike in a gait cycle. Segments with significant statistical differences ($P < 0.05$) between the patients and the control groups were marked with asterisks. Flexion, varus, and external tibial rotation were illustrated as positive in the graphs.

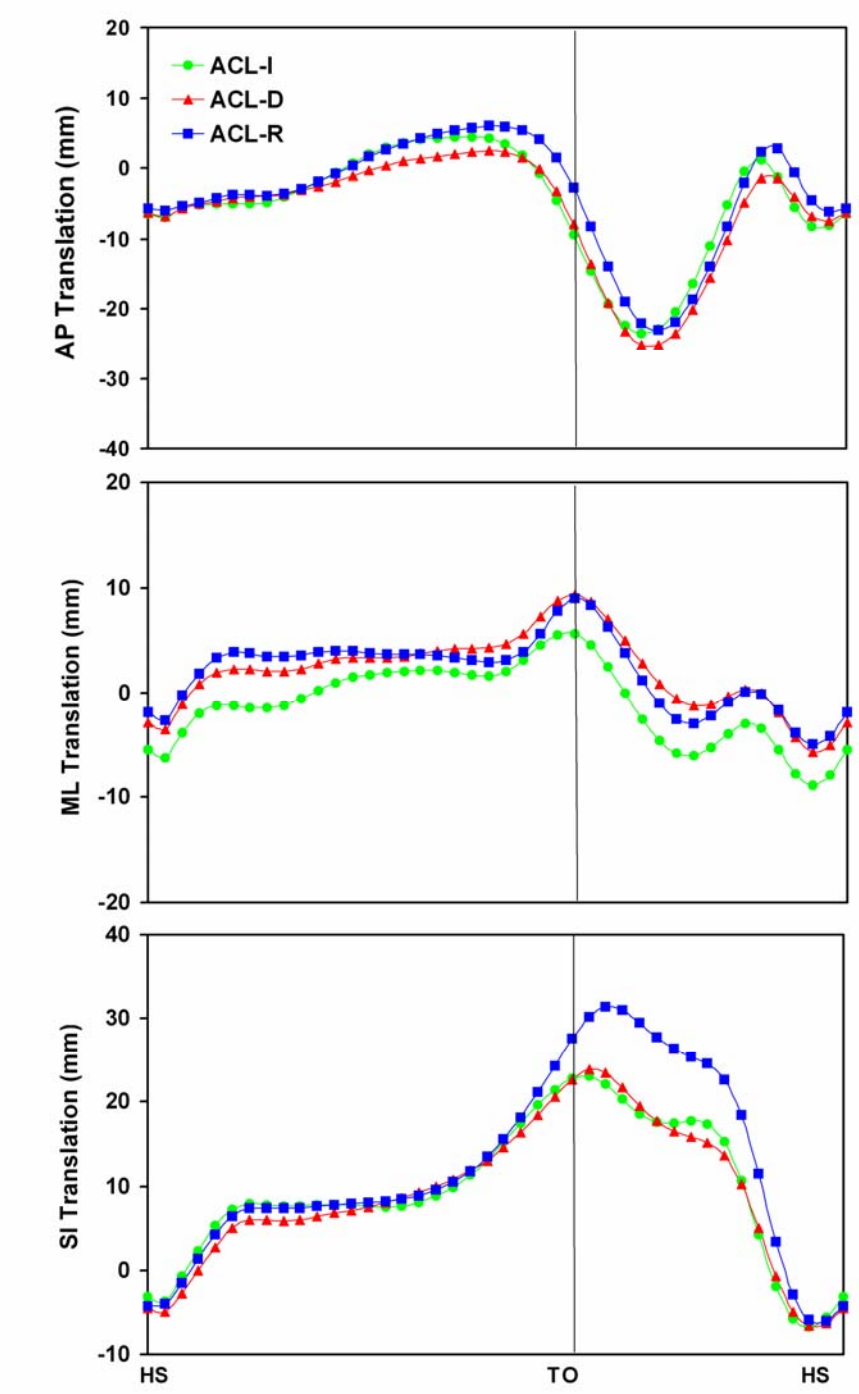

Figure 5-5. The 3-D joint translations during walking of ACL-I, ACL-D and ACL-R knees: anterior/posterior (AP), medial/lateral (ML), and superior/inferior (SI) translations. Ensemble curves of each subject group were normalized from heel strike to heel strike in a gait cycle. No significant statistical differences were observed between different subject groups. Anterior, medial, and superior translations (femur relative to tibia) were illustrated as positive in the graphs.

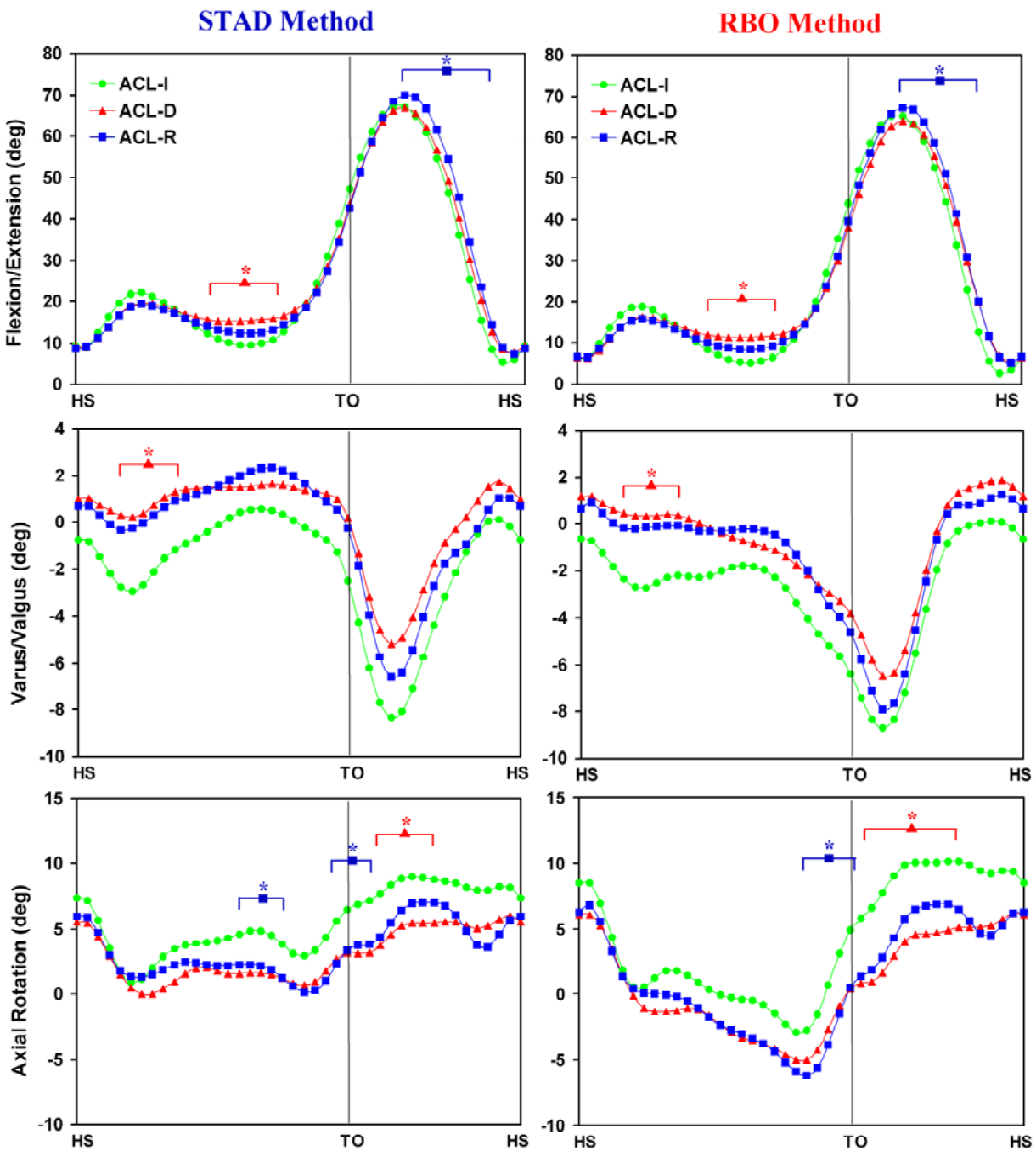

Figure 5-6. Comparison of 3-D knee joint rotations obtained using STAD method (left) and RBO method (right).

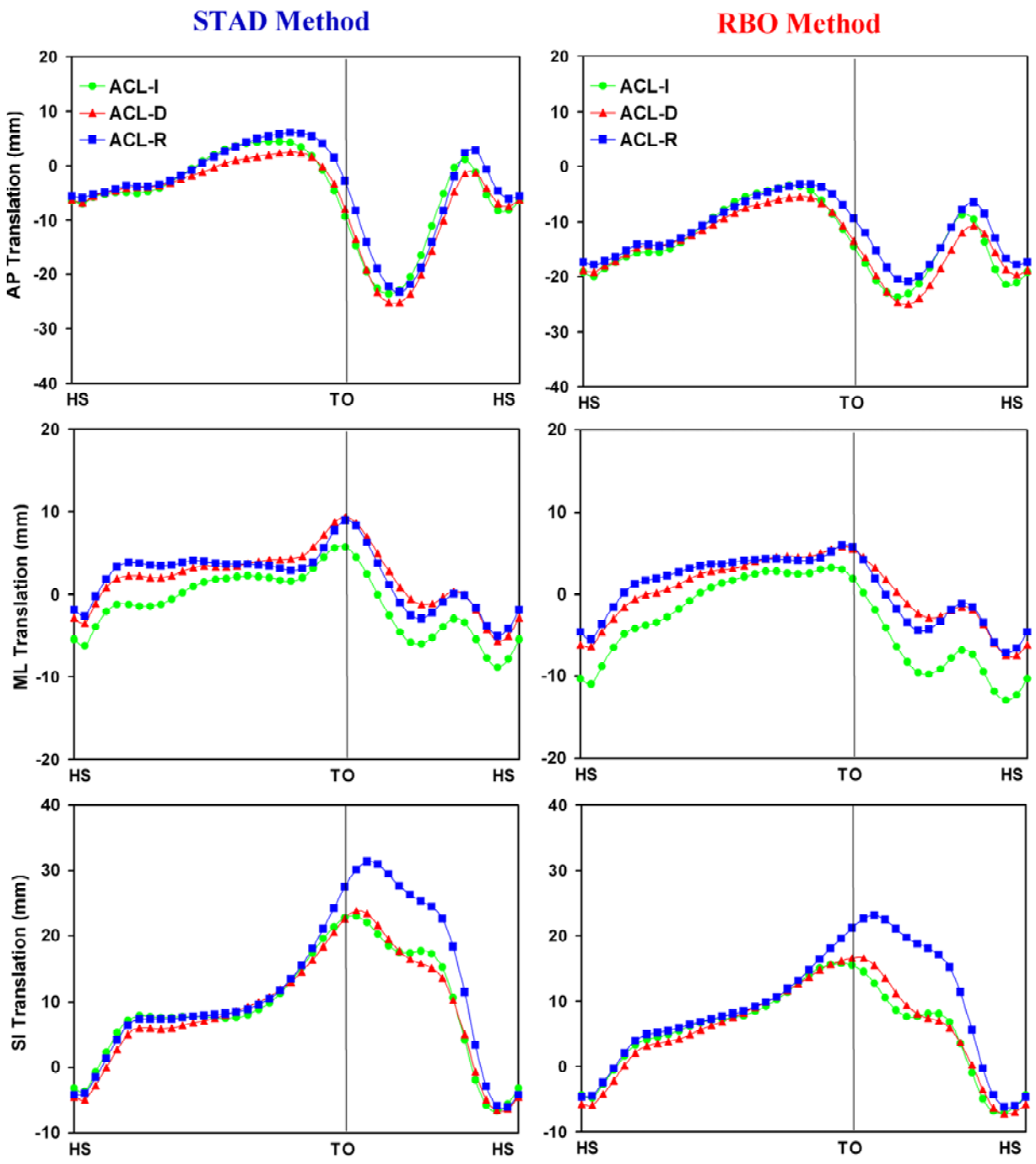

Figure 5-7. Comparison of 3-D knee joint translations obtained using STAD method (left) and RBO method (right).

Discussions

The purpose of this study was to examine the effects of ACL deficiency and reconstruction on the 3-D knee joint kinematics during walking. Findings of this study demonstrated significant alterations between the kinematics of the ACL-D knees and that of the ACL-I knees during walking. After reconstructive surgery, some of the alterations had been improved, but normal joint kinematics and function had not been fully restored in the ACL-R knees. These observations supported the hypotheses that motivated this study.

As spatiotemporal appearance, the ACL-D knees exhibited shorter step length and slower walking speed compared to the healthy knees. Similar phenomena have also been observed in another study (Knoll et al., 2004a). The reduction in step length and speed was also visible in the ACL-R knees, although not as significant as in the ACL-D knees. The shorter step length of the ACL-D and ACL-R subjects could result from the knee not being fully extended during the stance phase and at the end of the swing phase (Figure 5-4). Given the fact that the stride length was almost twice the step length and the stride speed was almost equal to the step speed in these subjects, it can be concluded that the contralateral non-injured/non-involved limb of the ACL-D/ACL-R subjects had developed compensatory motion patterns in order to adapt to the injured/involved limb. A decreased duration of single support phase was visible on ACL-D knees, as well as altered timing of key events in a gait cycle. The 1st FE peak and FE valley were postponed in ACL-D knees compared to the ACL-I knees. This reflects the increased time that the ACL-D knees tended to stay in flexion before the knee reached maximum extension in order to accomplish a less abrupt weight shift. This adaptation mechanism was also demonstrated by an electromyographic study showing that ACL-D

patients had extended firing of biceps femoris and vastus medialis during the stance phase compared to healthy controls (Knoll et al., 2004a). The ACL-R knees showed an improved timing during stance phase, but a prolonged flexion period was observed during the swing phase. These phenomenological observations indicate the ACL-R knees have not been restored to a normal spatiotemporal pattern.

Significant kinematic alterations were observed in the sagittal plane, not only in the ACL-D knees but also in the ACL-R knees. The most striking abnormality was that the injured knees did not reach full extension at midstance. As a comparison, at the static standing posture, the average knee flexion angles of all three subject groups were small and there was no statistical difference between them (Table 5-1). At midstance, the average FE valley of the ACL-I knees was close to the static standing posture, while the average FE valley of the ACL-D knees was significantly higher than the angle at the static posture. Thus, the lack of full knee extension of the ACL-D subjects was not caused by anatomical differences compared to the control subjects but by functional deficit of the joint. Because one major function of the ACL is to limit anterior tibial translation when the knee is in extension, the ACL-D patients appeared to use the adaptation strategy of limiting knee extension during movement to degrade the functional need for ACL. The kinematics had not returned to normal in the ACL-R knees. The average FE valley of the ACL-R knees was still significantly higher than that of the ACL-I knees. The findings of the extension deficit were consistent with one study on ACL-D knees (Gokeler et al., 2003) and another on ACL-R knees during walking (Hurd and Snyder-Mackler, 2007).

As one of the most important findings in this study, kinematic alterations were also identified in secondary movement of both the ACL-D and ACL-R knees. In the frontal plane, the injured knees were more varus than the healthy knees. Similar observations have been previously reported in ACL-R knees during downhill running (Tashman et al., 2004; Tashman et al., 2007), but little has been reported concerning level walking which is a much less intensive but more frequent ambulatory activity. In the transverse plane, an offset of internal tibial rotation was observed on both the ACL-D and ACL-R knees. This finding is consistent with the observations of two other studies on ACL-D knees during walking (Andriacchi and Dyrby, 2005; Georgoulis et al., 2003). From anatomical point of view, the ACL has an oblique medial orientation from femur to tibia, thus a less functional ACL could result in a more internally rotated tibial position. The offsets of varus and internal tibial rotation observed in the ACL-D and ACL-R knees in this study were small in magnitude (about 2° ~ 4°), but they were consistent throughout the whole gait cycle. With a more varus position, the lateral compartment of the knee joint tends to be more separated while the medial compartment of the knee contact tends to be more compressed. This could alter the normal load distribution on the joint surface and generate much higher stresses on the medial compartment of cartilage and menisci. With a more internally rotated tibia position, the contact location on the medial compartment of tibia plateau could shift to the anterior while the contact on the lateral compartment could shift to the posterior. This axial position alters both the contact location and contact stress on the cartilage, and could result in a more rapid cartilage thinning throughout the knee, especially in the medial compartment (Andriacchi et al., 2006). Clinical studies have shown that in ACL-D and ACL-R knees, the medial

compartment of the joint is more vulnerable to cartilage degeneration and osteoarthritis development (Seon et al., 2006). This is consistent with the kinematic abnormalities and risk factors we observed in the present study. Overall, the kinematics profiles of the ACL-R knees were closer to the ACL-D knees than to the ACL-I knees (Figure 5-4). This finding reflected that the reconstructive surgery had not restored the joint kinematics of the ACL-D knees to a normal level. This could potentially explain the outcomes observed in clinic that early cartilage degeneration and progressive development of knee osteoarthritis were not effectively prevented even after ACL reconstruction (Asano et al., 2004; Daniel et al., 1994; Seon et al., 2006). The position of the ACL-R profiles in Figure 5-4 also indicated that reconstructed ligaments in the ACL-R knees examined in this study were more likely to be under-functional rather than over-functional (e.g. over-tensioning).

Some “crosstalk” like appearance was observed between varus/valgus and flexion/extension curves. It should be note that our varus/valgus angle was defined as the frontal projection of including angle between femoral and tibial axis (Figure 5-2b). This angle is not the same thing as the angle between the contacting joint surfaces of the femur and tibia. Because the medial condyle of femur is larger in radius than the lateral condyle of femur, a valgus angle will always be observed from frontal projection during knee flexion even the joint surfaces keep contact. The magnitude of this valgus angle during swing phase (about 10°) was consistent to the results measured in the previous chapter using fluoroscopic technique (Figures 4-34 to 4-37). This indicated that the observed large valgus angle was not caused by analysis errors but mainly by the

anatomical asymmetry of medial and lateral condyles of the femur. To further examine the joint surface angle, image-based bone models have to be included.

No significant differences of knee joint translations were observed during walking between ACL-D, ACL-R and ACL-I knees in this study, although it is well known that the primary function of the ACL is to control tibial anterior translation and ACL deficiency could lead to excessive anterior tibial movement during the passive knee laxity test (Bendjaballah et al., 1998). The observation could be possibly explained by active muscle functioning which is absent in a passive laxity test. During dynamic movement, antagonist and agonist muscles of ACL-D knees function and coordinate together to compensate for the deficiency of the ACL, which is the dominant stabilizer during the passive laxity test. Studies have revealed that static knee laxity evaluation does not correlate with dynamic knee joint function after ACL injury (Gokeler et al., 2003; Kvist et al., 2007; Patel et al., 2003), indicating that muscle compensation plays a significant role in dynamic knee joint stability. The compensation strategy could either be a stronger contraction of the hamstrings to pull the tibia posteriorly (Kvist et al., 2007; Shelburne et al., 2005) or be a weaker contraction of the quadriceps to avoid pulling the tibia anteriorly (Andriacchi and Birac, 1993).

In the comparison between using STAD method and the conventional RBO method, we found that the kinematic results differed quantitatively. The RBO method under-estimated flexion angles, over-estimated axial rotation ROM, under-estimated superior translation, and under-estimated anterior translation during the swing phase. These findings were consistent to the observations in the previous chapter (e.g. Figure 4-35), which indicated that the STA compensation used in the STAD method modified

the kinematics obtained from RBO method to a correct direction. On the other hand, the qualitative comparisons between different subject groups were similar for the results obtained using STAD and RBO methods. This suggested that STA error is more systematic rather than random. Its effect on individual subject was generally similar and might not alter the overall comparisons between subject groups. Even though the conventional RBO method was not able to produce quantitatively accurate results, it might still be able to provide an effective qualitative comparison between different subject groups.

Several limitations need to be acknowledged. First, the ACL-D and ACL-R subjects included in this study were not the same group of patients tested pre- and postoperatively. The current design was adequate to provide meaningful comparison between each of the two patient groups and the healthy subject group, which was the aim of this study. But a pre- and postoperative matching design would be more useful to directly assess the functional improvement after ACL reconstructive surgery. Second, the subject population in this step of study (ACL-D, ACL-R and ACL-I subjects) differed to the subject population in the last chapter (total knee arthroplasty patients) from which the STA model was constructed for the STAD method, in age and BMI. Thus there might be some errors when using the STA model developed from last chapter in the subject population examined in this chapter. Third, the subjects in all three groups included in this study were generally young, averaging 25 years of age. This sample was in general agreement with the epidemiological population of ACL injury patients (Griffin et al., 2006), but would not be representative of all patient groups. Therefore the findings obtained from this study may not simply apply to populations with older ages.

Fourth, the ACL-D patients tested in this study were generally acutely injured (with one year), thus the findings in this study may not be the same for chronically ACL injured patients. Another limitation in this study was that we did not investigate the performance of different graft types separately. Three types of grafts (bone-patella tendon-bone allograft, Achilles allograft and hamstring tendon autograft) were used in the ACL-R group, and there might be a functional difference associated with the graft type although a systematic literature tends to support graft type may not play a primary role in the outcomes after ACL-R surgery (Spindler et al., 2004). Further research with larger subject sample size may be necessary to investigate these questions.

This study used a 3-D motion analysis and identified significant abnormalities of spatiotemporal performance and joint kinematics during walking in the ACL-D knees. After reconstructive surgery and rehabilitation, the ACL-R knees exhibited improvement, but were not fully restored to a normal level. In addition to an extension deficit in the sagittal plane, both ACL-D and ACL-R knees exhibited a varus offset in the frontal plane and a tibial internal rotation offset in the transverse plane, which were maintained throughout the whole gait cycle. The position change of varus and axial rotation of the knee joint could significantly alter the normal cartilage contact pattern and load distribution, causing different areas of cartilage to be newly loaded or unloaded, or subjected to a change in magnitude of compression or tension. Given the relatively low adaptation ability of mature cartilage, millions of repeated abnormal loading cycles during daily activity could exaggerate the risky biomechanical factors and gradually lead to cartilage degeneration and premature osteoarthritis in ACL-D and ACL-R knees. Identification of biomechanical environment alterations that occur during daily activities

in ACL-D and ACL-R knees could help us better understand clinical outcomes, as well as provide guidance for improvement in surgical technique and rehabilitative regimens for ACL injury treatment.

CHAPTER 6
SUMMARY AND CONCLUSIONS

Novelties and Key Points

In the framework of this dissertation, we focused on a long existing and challenging problem faced by the biomechanical research community. By investigating soft tissue artifact (STA) on the thigh and shank, this study provided better understanding and some new knowledge about the behavior of STA. This new information allowed us to develop a novel and evidence-based STA compensation technique for skin maker-based motion analysis. The new STA compensation technique demonstrated significant improvement in error reduction compared to the conventional best-performance method. The reduction of the major source of errors could make skin marker-based motion analysis a more powerful tool, and benefit biomechanical and clinical applications.

Methodological Novelties of this Study

The new findings of this study are directly related to new experimental and analysis methods.

First, we used non-invasive motion tracking methods through the study to ensure a measurement of free skin marker motion and STA. Majority of previous studies on STA utilized invasive devices to measure skeletal movement. The invasive devices (especially external fixators) could largely constrain free skin motion and alter the natural behavior of STA.

Second, we used a large subject sample size in Chapter 2 and a relatively large sample size in Chapters 3 and 4, compared to previous studies of similar types. Only if more subjects are included, the assessment of inter-subject similarity of STA behavior is

possible. Using too small subject sample size could be one reason for that no previous studies reported inter-subject evaluation of STA.

Third, most previous studies focused on assessment of analysis errors caused by STA by comparing skin marker derived kinematics and other gold standard method (invasive devices or medical imaging techniques) derived kinematics, but did not focus on STA itself, which is individual skin markers' movement relative to the bone. The "kinematic errors caused by STA" is not the same concept as "STA itself". Kinematic errors can be influenced by many factors in addition to STA. One can get different kinematic errors by using a different marker set or a different analysis method, even though the intrinsic STA is the same. Although our final goal is to reduce the "kinematic errors caused by STA", we need to study STA itself in order to find the solution. This was the rationale of our study design.

Fourth, no previous studies examined the relationship between STA and joint positions. Although a few studies examined individual markers' movement relative to the bone and measured STA magnitude of each marker, none further looked into the joint position dependence or time dependency (such as at different percentage of a gait cycle) of STA. Thus, the information obtained can only provide a "diagnosis" but not a "treatment". In Chapter 2, we examined soft tissue movement along a normalized time scope (gait cycles). And in Chapters 3 and 4, we further examined the relationship between STA and adjacent joint angles. These methodological improvements allowed us to reveal some new findings about STA behavior.

Fifth, we performed inter-subject similarity assessment on soft tissue movement (Chapter 2) and STA (Chapter 3), which had not been conducted before. This approach

finally led to a new insight about STA behavior and a non-subject-specific scheme for STA compensation (Chapter 4).

Table 6-1 summarizes a comparison between previous studies and the present study on the above aspects.

Table 6-1. Summary of studies about soft tissue movement on human lower extremity and the analysis scopes.

Reference	Non-invasive measurement of free skin motion?	More than 3 Subjects?	Examined individual marker movement?	Examined marker's movement with time or joint angles?	Performed inter-subject evaluation of marker movement?
(Cappozzo et al., 1996)	No	Yes	Yes	Yes	No
(Sati et al., 1996)	Yes	No	Yes	No	No
(Fuller et al., 1997)	No	No	Yes	Yes	No
(Holden et al., 1997)	No	No	No	No	No
(Reinschmidt et al., 1997a)	No	Yes	No	No	No
(Reinschmidt et al., 1997b)	No	No	No	No	No
(Manal et al., 2000)	No	Yes	No	No	No
(Stagni et al., 2005)	Yes	No	Yes	No	No
(Benoit et al., 2006)	No	Yes	No	No	No
(Garling et al., 2007)	Yes/No	Yes	Yes	No	No
(Akbarshahi et al., 2009)	Yes	Yes	Yes	No	No
The present study	Yes	Yes	Yes	Yes	Yes

Key Points Learned from this Study

STA is a systematic and natural movement, not random noise. "Soft tissue artifact" is not really an "artifact" but more a natural motion produced by muscles and skin movement. Any compensation methods that treat STA as random noise will have limited effectiveness.

STA has inter-subject similarity. Due to the fact that most people have similar muscular structure and coordination during activities, soft tissue movement has intrinsic similarities between different people.

A large portion of STA is related to the joint position, thus STA also has some inter-motor task similarity. Although muscle contraction and skin stretch (in addition to other types of STA causes, like inertial effects) are not exactly the same during different motor tasks, a large portion of the soft tissue movement is similar if the joint is at a same position. Thus, an STA model based on adjacent joint angles is effective across different motor tasks.

STA generally increases with increasing joint angles. Since the marker's anatomical positions are usually defined at a neutral standing posture (where STA is zero), the magnitudes of STA (markers' location deviation from the initial position) increase if the body posture deviates further from the neutral standing posture.

STA on the thigh plays a dominant role in determining knee kinematic errors. If the STA effects on the thigh can be successfully compensated, knee joint kinematics will have much lower errors even without compensating for the STA effects on the shank.

The largest STA on the thigh occurs along the superior/inferior (SI) direction. The STA magnitudes along SI direction are generally higher than those along

anterior/posterior (AP) and medial/lateral (ML) directions, and can be over 25 mm for some markers.

Most markers on the anterolateral side of the thigh tend to move posteriorly and inferiorly when the knee flexes. Exceptions: the markers on the medial and lateral femoral epicondyles tend to move anteriorly and superiorly. The markers on the lateral side exhibited the smallest SI displacement, while the markers on the anterior side exhibited the smallest AP displacement.

Most markers on the anterolateral side of the shank tend to move anteriorly and inferiorly when the knee flexes. Exceptions: the marker on the lateral ridge of tibial plateau along AP direction, and the marker on the tibial tubercle along SI direction. The markers on the anterior side of tibia exhibited small displacement along both SI and AP directions.

STA exhibited similar patterns for markers that are on a same vertical line. This was very prominent on the thigh, but also visible on the shank. The reason behind is that lower extremity muscles generally contract along SI direction.

The markers placed on commonly used “bone landmarks” did not show smaller STA than other markers. The markers on femoral epicondyles, ridges of tibial plateau, and malleoli exhibited larger STA than many other markers due to the large skin stretch near the joints.

The AP component of thigh STA is more sensitive to hip flexion angles, while the SI component of thigh STA is more sensitive to knee flexion angles. This is generally true for most thigh markers, while the markers on the femoral epicondyles behave differently.

Among existing STA compensation algorithms, the conventional rigid body optimization (RBO) method provides overall the best result. Other non-rigid body optimization methods (including the point cluster technique) have not convincingly demonstrated their superior performance over the RBO method.

The kinematic analysis errors derived from skin markers are not in a constant magnitude but are related to joint position. Skin marker derived kinematics (using the conventional method) could be fairly accurate if the joint angles are not too far away from the standing posture. But the errors can be significantly larger at large joint angles. This is similar to the behavior of STA, which is the cause of kinematic errors.

Both the STA deduction (STAD) method and the directional weighted optimization (DWO) method exhibited improved analysis accuracy compared to the conventional RBO method. The STAD method demonstrated the best performance in general.

ACL-deficient (ACL-D) knees exhibited altered spatiotemporal parameters and 3D kinematics compared to ACL-intact (ACL-I) knees in gait, and these alterations had not been completely restored to a normal level in the ACL-reconstructed (ACL-R) knees. Both ACL-D and ACL-R knees exhibited reduced extension, a more varus and internally rotated position compared to the ACL-I knees.

Limitations and Future Direction

Limitations of this Study

As being discussed in each previous chapter, there were some limitations with this study.

The ML component of STA was not reliably measured. This was mainly caused by the limitation of single view fluoroscopy technique. This limitation would reduce the reliability of the "universal" STA model in its ML direction, and further reduce the effectiveness of STAD method in accuracy improvement on ML translation, axial rotation, and varus/valgus measurements.

The subject sample size in the fluoroscopic study was still relatively small. Although 6 is already a relatively large sample size comparing to many other studies with a similar type, more subjects will definitely enhance the robustness of the "universal" STA models and enhance the effectiveness of the STAD method.

Only total knee arthroplasty (TKA) patients were included as subjects for *in vivo* STA measurement. Although we used special inclusive criteria in subject recruitment aiming to include only TKA subjects who had a physical condition closer to healthy population, there could be some differences between these TKA patients to other healthy/patient populations in terms of STA behavior.

Only one functional motor task was included in this study. Due to the purpose and scope of this study, only a stepping up activity was included as an example of functional motor task to evaluate the new STA compensation method.

Partially due to the limited subject sample size, the anthropometric information of the subjects was not included in the STA model. It is expected that

STA behavior is more or less related to a subject's anthropometric condition. Taking this information into account could possibly make the STA model more realistic.

The multilinear model used in this study to construct the STA models was relatively simple. This simple model does have its advantages, such as being intuitively meaningful, and easy to implement and transfer. It is likely with more complex functions, the STA model could be more realistic.

Future Study Suggestions

Based on the limitations discussed above, there are options for future study advancement.

To measure the ML component of STA more reliably. This can be achieved by either using a bi-plane fluoroscopy setup, or using a single-plane fluoroscopy in an AP view. Both approaches have extra challenges. By using a bi-plane fluoroscopy, the stereophotogrammetric cameras will have more obstructions and the skin marker tracking will be more difficult. Using a single-plane fluoroscopy in an AP view is also more difficult than using it in an ML view, considering the testing space and configuration.

To include more subjects and healthy controls if possible. This will increase the scope of the research project and also need to get IRB approval.

To study more ambulatory motor tasks and evaluate the STAD method performance. Level walking will be a good option for the next step, although it will require a fast shutter of the fluoroscopy to guarantee the image quality.

To include subjects' anthropometric information into the STA model, and to explore more complex mathematical expression of the STA model. To move into

this step, it is the author's opinion that larger quantity of more reliable STA data has to be obtained first.

LIST OF REFERENCES

Adam, F., Pape, D., Schiel, K., Steimer, O., Kohn, D., and Rupp, S., 2004, Biomechanical properties of patellar and hamstring graft tibial fixation techniques in anterior cruciate ligament reconstruction - Experimental study with roentgen stereometric analysis: American Journal of Sports Medicine, v. 32, no. 1, p. 71-78.

Akbarshahi, M., Fernandez, J. W., Schache, A., Baker, R., Banks, S., and Pandy, M. G., 2009, Quantifying the spatial variation of lower-limb soft tissue artefact during functional activity using MR imaging and X-ray fluoroscopy, *in* ASME 2009 Summer Bioengineering Conference, Lake Tahoe, CA, USA.

Alexander, E. J., and Andriacchi, T. P., 2001, Correcting for deformation in skin-based marker systems: J Biomech, v. 34, no. 3, p. 355-61.

Alkjaer, T., Simonsen, E. B., Jorgensen, U., and Dyhre-Poulsen, P., 2003, Evaluation of the walking pattern in two types of patients with anterior cruciate ligament deficiency: copers and non-copers: European Journal of Applied Physiology, v. 89, no. 3-4, p. 301-308.

Andersen, H. N., and Dyhre-Poulsen, P., 1997, The anterior cruciate ligament does play a role in controlling axial rotation in the knee: Knee Surg, Sports Traumatol, Arthrosc, no. 5, p. 145-149.

Andriacchi, T. P., and Alexander, E. J., 2000, Studies of human locomotion: past, present and future: J Biomech, v. 33, no. 10, p. 1217-24.

Andriacchi, T. P., Alexander, E. J., Toney, M. K., Dyrby, C., and Sum, J., 1998, A point cluster method for in vivo motion analysis: applied to a study of knee kinematics: J Biomech Eng, v. 120, no. 6, p. 743-9.

Andriacchi, T. P., and Birac, D., 1993, Functional Testing in the Anterior Cruciate Ligament-Deficient Knee: Clinical Orthopaedics and Related Research, no. 288, p. 40-47.

Andriacchi, T. P., Briant, P. L., Bevill, S. L., and Koo, S., 2006, Rotational changes at the knee after ACL injury cause cartilage thinning: Clin Orthop Relat Res, v. 442, p. 39-44.

Andriacchi, T. P., and Dyrby, C. O., 2005, Interactions between kinematics and loading during walking for the normal and ACL deficient knee: Journal of Biomechanics, v. 38, no. 2, p. 293-298.

Andriacchi, T. P., and Mundermann, A., 2006, The role of ambulatory mechanics in the initiation and progression of knee osteoarthritis: Curr Opin Rheumatol, v. 18, no. 5, p. 514-8.

Arendt, E., and Dick, R., 1995, Knee Injury Patterns among Men and Women in Collegiate Basketball and Soccer - Ncaa Data and Review of Literature: American Journal of Sports Medicine, v. 23, no. 6, p. 694-701.

Asano, H., Muneta, T., Ikeda, H., Yagishita, K., Kurihara, Y., and Sekiya, I., 2004, Arthroscopic evaluation of the articular cartilage after anterior cruciate ligament reconstruction: A short-term prospective study of 105 patients: Arthroscopy-the Journal of Arthroscopic and Related Surgery, v. 20, no. 5, p. 474-481.

Baliunas, A. J., Hurwitz, D. E., Ryals, A. B., Karrar, A., Case, J. P., Block, J. A., and Andriacchi, T. P., 2002, Increased knee joint loads during walking are present in subjects with knee osteoarthritis: Osteoarthritis Cartilage, v. 10, no. 7, p. 573-9.

Banks, S., Bellemans, J., Nozaki, H., Whiteside, L. A., Harman, M., and Hodge, W. A., 2003, Knee motions during maximum flexion in fixed and mobile-bearing arthroplasties: Clinical Orthopaedics and Related Research, no. 410, p. 131-138.

Banks, S. A., Banks, A. Z., Klos, T. V. S., and Cook, F. F., 1997, A simple fluoroscopy based technique for assessing 3D knee kinematics before, during, and after surgery: Cvrmed-Mrcas'97, v. 1205, p. 639-643.

Banks, S. A., and Hodge, W. A., 1996, Accurate measurement of three-dimensional knee replacement kinematics using single-plane fluoroscopy: Ieee Transactions on Biomedical Engineering, v. 43, no. 6, p. 638-649.

-, 2004, Implant design affects knee arthroplasty kinematics during stair-stepping: Clinical Orthopaedics and Related Research, no. 426, p. 187-193.

Bell, A. L., Pedersen, D. R., and Brand, R. A., 1990, A Comparison of the Accuracy of Several Hip Center Location Prediction Methods: Journal of Biomechanics, v. 23, no. 6, p. 617-621.

Bendjaballah, M. Z., Shirazi-Adl, A., and Zukor, D. J., 1998, Biomechanical response of the passive human knee joint under anterior-posterior forces: Clinical Biomechanics, v. 13, no. 8, p. 625-633.

Benoit, D. L., Ramsey, D. K., Lamontagne, M., Xu, L. Y., Wretenberg, P., and Renstrom, P., 2006, Effect of skin movement artifact on knee kinematics during gait and cutting motions measured in vivo: Gait & Posture, v. 24, no. 2, p. 152-164.

Bingham, J., and Li, G., 2006, An optimized image matching method for determining in-vivo TKA kinematics with a dual-orthogonal fluoroscopic imaging system: Journal of Biomechanical Engineering-Transactions of the Asme, v. 128, no. 4, p. 588-595.

Brandsson, S., Karlsson, J., Sward, L., Kartus, J., Eriksson, B. I., and Karrholm, J., 2002, Kinematics and laxity of the knee joint after anterior cruciate ligament reconstruction - Pre- and postoperative radiostereometric studies: American Journal of Sports Medicine, v. 30, no. 3, p. 361-367.

Brandt, K. D., Myers, S. L., Burr, D., and Albrecht, M., 1991, Osteoarthritic changes in canine articular cartilage, subchondral bone, and synovium fifty-four months after transection of the anterior cruciate ligament: Arthritis Rheum, v. 34, no. 12, p. 1560-70.

Bush-Joseph, C. A., Hurwitz, D. E., Patel, R. R., Bahrani, Y., Garretson, R., Bach, B. R., Jr., and Andriacchi, T. P., 2001, Dynamic function after anterior cruciate ligament reconstruction with autologous patellar tendon: Am J Sports Med, v. 29, no. 1, p. 36-41.

Cappello, A., Cappozzo, A., LaPalombara, P. F., Lucchetti, L., and Leardini, A., 1997, Multiple anatomical landmark calibration for optimal bone pose estimation: Human Movement Science, v. 16, no. 2-3, p. 259-274.

Cappello, A., Stagni, R., Fantozzi, S., and Leardini, A., 2005, Soft tissue artifact compensation in knee kinematics by double anatomical landmark calibration: performance of a novel method during selected motor tasks: IEEE Trans Biomed Eng, v. 52, no. 6, p. 992-8.

Cappozzo, A., Catani, F., Leardini, A., Benedetti, M. G., and Croce, U. D., 1996, Position and orientation in space of bones during movement: experimental artefacts: Clin Biomech (Bristol, Avon), v. 11, no. 2, p. 90-100.

Cappozzo, A., Della Croce, U., Leardini, A., and Chiari, L., 2005, Human movement analysis using stereophotogrammetry - Part 1: theoretical background: Gait & Posture, v. 21, no. 2, p. 186-196.

Cereatti, A., Della Croce, U., and Cappozzo, A., 2006, Reconstruction of skeletal movement using skin markers: comparative assessment of bone pose estimators: J Neuroengineering Rehabil, v. 3, p. 7.

Chaudhari, A. M. W., Briant, P. L., Bevill, S. L., Koo, S., and Andriacchi, T. P., 2008, Knee kinematics, cartilage morphology, and osteoarthritis after ACL injury: Medicine and Science in Sports and Exercise, v. 40, no. 2, p. 215-222.

Cheze, L., Fregly, B. J., and Dimnet, J., 1995, A Solidification Procedure to Facilitate Kinematic Analyses Based on Video System Data: Journal of Biomechanics, v. 28, no. 7, p. 879-884.

Chiari, L., Della Croce, U., Leardini, A., and Cappozzo, A., 2005, Human movement analysis using stereophotogrammetry - Part 2: Instrumental errors: Gait & Posture, v. 21, no. 2, p. 197-211.

Croce, U. D., 2006, Soft tissue artifacts in human movement analysis, *in* Ninth international symposium on the 3D analysis of human movement, Valenciennes, France.

Daniel, D. M., Stone, M. L., Dobson, B. E., Fithian, D. C., Rossman, D. J., and Kaufman, K. R., 1994, Fate of the Acl-Injured Patient - a Prospective Outcome Study: American Journal of Sports Medicine, v. 22, no. 5, p. 632-644.

Della Croce, U., Leardini, A., Chiari, L., and Cappozzo, A., 2005, Human movement analysis using stereophotogrammetry - Part 4: assessment of anatomical landmark misplacement and its effects on joint kinematics: Gait & Posture, v. 21, no. 2, p. 226-237.

Dennis, D. A., Mahfouz, M. R., Komistek, R. D., and Hoff, W., 2005, In vivo determination of normal and anterior cruciate ligament-deficient knee kinematics: Journal of Biomechanics, v. 38, no. 2, p. 241-253.

Elble, R. J., 2005, Gravitational artifact in accelerometric measurements of tremor: Clinical Neurophysiology, v. 116, no. 7, p. 1638-1643.

Feipel, V., and Rooze, M., 1999, Three-dimensional motion patterns of the carpel bones: an in vivo study using three-dimensional computed tomography and clinical applications: Surgical and Radiologic Anatomy, v. 21, no. 2, p. 125-131.

Ferber, R., Osternig, L. R., Woollacott, M. H., Wasielewski, N. J., and Lee, J. H., 2002, Gait mechanics in chronic ACL deficiency and subsequent repair: Clinical Biomechanics, v. 17, no. 4, p. 274-285.

Fleming, B. C., Peura, G. D., Abate, J. A., and Beynnon, B. D., 2001, Accuracy and repeatability of Roentgen stereophotogrammetric analysis (RSA) for measuring knee laxity in longitudinal studies: Journal of Biomechanics, v. 34, no. 10, p. 1355-1359.

Fuller, J., Liu, L. J., Murphy, M. C., and Mann, R. W., 1997, A comparison of lower-extremity skeletal kinematics measured using skin- and pin-mounted markers: Human Movement Science, v. 16, no. 2-3, p. 219-242.

Gao, B., Conrad, B., and Zheng, N., 2007, Accuracies of Skin Marker Based Knee Motion Analysis Using Different Techniques, *in* 31st American Society of Biomechanics Annual Conference, Stanford, CA.

Gao, B., and Zheng, N., 2006, Soft tissue artifact error can be reduced by using multiple reference positions: Annual meeting of American Society of Biomechanics.

Garling, E. H., Kaptein, B. L., Mertens, B., Barendregt, W., Veeger, H. E. J., Nelissen, R. G. H. H., and Valstar, E. R., 2007, Soft-tissue artefact assessment during step-up using fluoroscopy and skin-mounted markers: Journal of Biomechanics, v. 40, p. S18-S24.

Georgoulis, A. D., Papadonikolakis, A., Papageorgiou, C. D., Mitsou, A., and Stergiou, N., 2003, Three-dimensional tibiofemoral kinematics of the anterior cruciate ligament-deficient and reconstructed knee during walking: American Journal of Sports Medicine, v. 31, no. 1, p. 75-79.

Gokeler, A., Schmalz, T., Knopf, E., Freiwald, J., and Blumentritt, S., 2003, The relationship between isokinetic quadriceps strength and laxity on gait analysis parameters in anterior cruciate ligament reconstructed knees: Knee Surgery Sports Traumatology Arthroscopy, v. 11, no. 6, p. 372-378.

Griffin, L. Y., Agel, J., Albohm, M. J., Arendt, E. A., Dick, R. W., Garrett, W. E., Garrick, J. G., Hewett, T. E., Huston, L., Ireland, M. L., Johnson, R. J., Kibler, W. B., Lephart, S., Lewis, J. L., Lindenfeld, T. N., Mandelbaum, B. R., Marchak, P., Teitz, C. C., and Wojtys, E. M., 2000, Noncontact anterior cruciate ligament injuries: risk factors and prevention strategies: J Am Acad Orthop Surg, v. 8, no. 3, p. 141-50.

Griffin, L. Y., Albohm, M. J., Arendt, E. A., Bahr, R., Beynnon, B. D., DeMaio, M., Dick, R. W., Engebretsen, L., Garrett, W. E., Hannafin, J. A., Hewett, T. E., Huston, L. J., Ireland, M. L., Johnson, R. J., Lephart, S., Mandelbaum, B. R., Mann, B. J., Marks, P. H., Marshall, S. W., Myklebust, G., Noyes, F. R., Powers, C., Shields, C., Shultz, S. J., Silvers, H., Slauterbeck, J., Taylor, D. C., Teitz, C. C., Wojtys, E. M., and Yu, B., 2006, Understanding and preventing noncontact anterior cruciate ligament injuries - A review of the Hunt Valley II Meeting, January 2005: American Journal of Sports Medicine, v. 34, no. 9, p. 1512-1532.

Holden, J. P., Orsini, J. A., Siegel, K. L., Kepple, T. M., Gerber, L. H., and Stanhope, S. J., 1997, Surface movement errors in shank kinematics and knee kinetics during gait: Gait & Posture, v. 5, no. 3, p. 217-227.

Hurd, W. I., and Snyder-Mackler, L., 2007, Knee instability after acute ACL rupture affects movement patterns during the mid-stance phase of gait: Journal of Orthopaedic Research, v. 25, no. 10, p. 1369-1377.

Jones, H. P., Appleyard, R. C., Mahajan, S., and Murrell, G. A., 2003, Meniscal and chondral loss in the anterior cruciate ligament injured knee: Sports Med, v. 33, no. 14, p. 1075-89.

Knoll, Z., Kiss, R. M., and Kocsis, L., 2004a, Gait adaptation in ACL deficient patients before and after anterior cruciate ligament reconstruction surgery: Journal of Electromyography and Kinesiology, v. 14, no. 3, p. 287-294.

Knoll, Z., Kocsis, L., and Kiss, R. M., 2004b, Gait patterns before and after anterior cruciate ligament reconstruction: Knee Surgery Sports Traumatology Arthroscopy, v. 12, no. 1, p. 7-14.

Komistek, R. D., Dennis, D. A., and Mahfouz, M., 2003, In vivo fluoroscopic analysis of the normal human knee: Clinical Orthopaedics and Related Research, no. 410, p. 69-81.

Kozanek, M., Hosseini, A., Liu, F., Van de Velde, S. K., Gill, T. J., Rubash, H. E., and Li, G. A., 2009, Tibiofemoral kinematics and condylar motion during the stance phase of gait: Journal of Biomechanics, v. 42, no. 12, p. 1877-1884.

Kvist, J., 2004, Sagittal plane translation during level walking in poor-functioning and well-functioning patients with anterior cruciate ligament deficiency: American Journal of Sports Medicine, v. 32, no. 5, p. 1250-1255.

Kvist, J., Good, L., and Tagesson, S., 2007, Changes in knee motion pattern after anterior cruciate ligament injury - A case report: Clinical Biomechanics, v. 22, no. 5, p. 551-556.

Lafortune, M. A., Cavanagh, P. R., Sommer, H. J., and Kalenak, A., 1992, 3-Dimensional Kinematics of the Human Knee during Walking: Journal of Biomechanics, v. 25, no. 4, p. 347-357.

Leardini, A., Chiari, L., Della Croce, U., and Cappozzo, A., 2005, Human movement analysis using stereophotogrammetry. Part 3. Soft tissue artifact assessment and compensation: Gait Posture, v. 21, no. 2, p. 212-25.

Li, G., DeFrate, L. E., Rubash, H. E., and Gill, T. J., 2005, In vivo kinematics of the ACL during weight-bearing knee flexion: Journal of Orthopaedic Research, v. 23, no. 2, p. 340-344.

Li, G. A., Moses, J. M., Papannagari, R., Pathare, N. P., DeFrate, L. E., and Gill, T. J., 2006, Anterior cruciate ligament deficiency alters the in vivo motion of the tibiofemoral cartilage contact points in both the anteroposterior and mediolateral directions: Journal of Bone and Joint Surgery-American Volume, v. 88A, no. 8, p. 1826-1834.

Lohmander, L. S., Ostenberg, A., Englund, M., and Roos, H., 2004, High prevalence of knee osteoarthritis, pain, and functional limitations in female soccer players twelve years after anterior cruciate ligament injury: Arthritis Rheum, v. 50, no. 10, p. 3145-52.

Lohmander, L. S., and Roos, H., 1994, Knee ligament injury, surgery and osteoarthrosis. Truth or consequences?: Acta Orthop Scand, v. 65, no. 6, p. 605-609.

Lu, T. W., and O'Connor, J. J., 1999, Bone position estimation from skin marker co-ordinates using global optimisation with joint constraints: Journal of Biomechanics, v. 32, no. 2, p. 129-134.

Lucchetti, L., Cappozzo, A., Cappello, A., and Della Croce, U., 1998, Skin movement artefact assessment and compensation in the estimation of knee-joint kinematics: J Biomech, v. 31, no. 11, p. 977-84.

Manal, K., McClay, I., Stanhope, S., Richards, J., and Galinat, B., 2000, Comparison of surface mounted markers and attachment methods in estimating tibial rotations during walking: an in vivo study: Gait & Posture, v. 11, no. 1, p. 38-45.

Markolf, K. L., Burchfield, D. I., Shapiro, M. M., Shepard, M. E., Finerman, G. A. M., and Slauterbeck, J. L., 1995, Combined knee loading states that generate high anterior cruciate ligament forces: Journal of Orthopaedic Research, v. 13, no. 6, p. 930-935.

Martelli, S., 2003, New method for simultaneous anatomical and functional studies of articular joints and its application to the human knee: Computer Methods and Programs in Biomedicine, v. 70, no. 3, p. 223-240.

Meyer, K. E., Saether, E. E., Soiney, E. K., Shebeck, M. S., Paddock, K. L., and Ludewig, P. M., 2008, Three-dimensional scapular kinematics during the throwing motion: Journal of Applied Biomechanics, v. 24, no. 1, p. 24-34.

Miyazaki, T., Wada, M., Kawahara, H., Sato, M., Baba, H., and Shimada, S., 2002, Dynamic load at baseline can predict radiographic disease progression in medial compartment knee osteoarthritis: Annals of the Rheumatic Diseases, v. 61, no. 7, p. 617-622.

Mundermann, A., Dyrby, C. O., and Andriacchi, T. P., 2005, Secondary gait changes in patients with medial compartment knee osteoarthritis - Increased load at the ankle, knee, and hip during walking: Arthritis and Rheumatism, v. 52, no. 9, p. 2835-2844.

Nebelung, W., and Wuschech, H., 2005, Thirty-five years of follow-up of anterior cruciate ligament-deficient knees in high-level athletes: Arthroscopy, v. 21, no. 6, p. 696-702.

Neyret, P., Donell, S. T., DeJour, D., and DeJour, H., 1993, Partial meniscectomy and anterior cruciate ligament rupture in soccer players. A study with a minimum 20-year followup: Am J Sports Med, v. 21, no. 3, p. 455-60.

Noyes, F. R., Dunworth, L. A., Andriacchi, T. P., Andrews, M., and Hewett, T. E., 1996, Knee hyperextension gait abnormalities in unstable knees. Recognition and preoperative gait retraining: Am J Sports Med, v. 24, no. 1, p. 35-45.

Noyes, F. R., Mooar, P. A., Matthews, D. S., and Butler, D. L., 1983, The symptomatic anterior cruciate-deficient knee. Part I: the long-term functional disability in athletically active individuals: J Bone Joint Surg Am, v. 65, no. 2, p. 154-62.

Papaioannou, N., Krallis, N., Triantafillopoulos, I., Khaldi, L., Dontas, I., and Lyritis, G., 2004, Optimal timing of research after anterior cruciate ligament resection in rabbits: Contemp Top Lab Anim Sci, v. 43, no. 6, p. 22-7; quiz 58.

Papannagari, R., Gill, T. J., DeFrate, L. E., Moses, J. M., Petruska, A. J., and Li, G. A., 2006, In vivo kinematics of the knee after anterior cruciate ligament reconstruction - A clinical and functional evaluation: American Journal of Sports Medicine, v. 34, no. 12, p. 2006-2012.

Patel, R. R., Hurwitz, D. E., Bush-Joseph, C. A., Bach, B. R., Jr., and Andriacchi, T. P., 2003, Comparison of clinical and dynamic knee function in patients with anterior cruciate ligament deficiency: Am J Sports Med, v. 31, no. 1, p. 68-74.

Patel, V. V., Hall, K., Ries, M., Lotz, J., Ozhinsky, E., Lindsey, C., Lu, Y., and Majumdar, S., 2004, A three-dimensional MRI analysis of knee kinematics: Journal of Orthopaedic Research, v. 22, no. 2, p. 283-292.

Penney, G. P., Batchelor, P. G., Hill, D. L. G., Hawkes, D. J., and Weese, J., 2001, Validation of a two- to three-dimensional registration algorithm for aligning preoperative CT images and intraoperative fluoroscopy images: Medical Physics, v. 28, no. 6, p. 1024-1032.

Pond, M. J., and Nuki, G., 1973, Experimentally-induced osteoarthritis in the dog: Ann Rheum Dis, v. 32, no. 4, p. 387-8.

Reinschmidt, C., vandenBogert, A. J., Lundberg, A., Nigg, B. M., Murphy, N., Stacoff, A., and Stano, A., 1997a, Tibiofemoral and tibiocalcaneal motion during walking: external vs. skeletal markers: Gait & Posture, v. 6, no. 2, p. 98-109.

Reinschmidt, C., vandenBogert, A. J., Nigg, B. M., Lundberg, A., and Murphy, N., 1997b, Effect of skin movement on the analysis of skeletal knee joint motion during running: Journal of Biomechanics, v. 30, no. 7, p. 729-732.

Rowe, P. J., 1996, Development of a low-cost video vector for the display of ground reaction forces during gait: Medical Engineering & Physics, v. 18, no. 7, p. 591-595.

Sangeux, M., Marin, F., Charleux, F., Durselen, L., and Tho, M. C. H. B., 2006, Quantification of the 3D relative movement of external marker sets vs. bones based on magnetic resonance imaging: Clinical Biomechanics, v. 21, no. 9, p. 984-991.

Sati, M., Guise, K. A. d., Larouche, S., and Drouin, G., 1996, Quantitative assessment of skin-bone movement at the knee: The Knee, v. 3, p. 121-138.

Seon, J. K., Song, E. K., and Park, S. J., 2006, Osteoarthritis after anterior cruciate ligament reconstruction using a patellar tendon autograft: International Orthopaedics, v. 30, no. 2, p. 94-98.

Shelburne, K. B., Torry, M. R., and Pandy, M. G., 2005, Effect of muscle compensation on knee instability during ACL-Deficient gait: Medicine and Science in Sports and Exercise, v. 37, no. 4, p. 642-648.

Soderkvist, I., and Wedin, P. A., 1993, Determining the Movements of the Skeleton Using Well-Configured Markers: Journal of Biomechanics, v. 26, no. 12, p. 1473-1477.

Spindler, K. R., Kuhn, J. E., Freedman, K. B., Matthews, C. E., Dittus, R. S., and Harrell, F. E., 2004, Anterior cruciate ligament reconstruction autograft choice: Bone-tendon-bone versus hamstring - Does it really matter? A systematic review: American Journal of Sports Medicine, v. 32, no. 8, p. 1986-1995.

Spoor, C. W., and Veldpaus, F. E., 1980, Rigid Body Motion Calculated from Spatial Coordinates of Markers: Journal of Biomechanics, v. 13, no. 4, p. 391-393.

Stagni, R., Fantozzi, S., Cappello, A., and Leardini, A., 2005, Quantification of soft tissue artefact in motion analysis by combining 3D fluoroscopy and stereophotogrammetry: a study on two subjects: Clin Biomech (Bristol, Avon), v. 20, no. 3, p. 320-9.

Stergiou, N., Ristanis, S., Moraiti, C., and Georgoulis, A. D., 2007, Tibial rotation in anterior cruciate ligament (ACL)-deficient and ACL-reconstructed knees - A theoretical proposition for the development of osteoarthritis: Sports Medicine, v. 37, no. 7, p. 601-613.

Stiehl, J. B., Komistek, R. D., Dennis, D. A., Paxson, R. D., and Hoff, W. A., 1995, Fluoroscopic Analysis of Kinematics after Posterior-Cruciate-Retaining Knee Arthroplasty: Journal of Bone and Joint Surgery-British Volume, v. 77B, no. 6, p. 884-889.

Tashman, S., Collon, D., Anderson, K., Kolowich, P., and Anderst, W., 2004, Abnormal rotational knee motion during running after anterior cruciate ligament reconstruction: American Journal of Sports Medicine, v. 32, no. 4, p. 975-983.

Tashman, S., Kolowich, P., Collon, D., Anderson, K., and Anderst, W., 2007, Dynamic function of the ACL-reconstructed knee during running: Clinical Orthopaedics and Related Research, no. 454, p. 66-73.

Taylor, W. R., Ehrig, R. M., Duda, G. N., Schell, H., Seebeck, P., and Heller, M. O., 2005, On the influence of soft tissue coverage in the determination of bone kinematics using skin markers: Journal of Orthopaedic Research, v. 23, no. 4, p. 726-734.

von Porat, A., Henriksson, M., Holmstrom, E., Thorstensson, C. A., Mattsson, L., and Roos, E. M., 2006, Knee kinematics and kinetics during gait, step and hop in males with a 16 years old ACL injury compared with matched controls: Knee Surgery Sports Traumatology Arthroscopy, v. 14, no. 6, p. 546-554.

Wu, J. Z., Herzog, W., and Epstein, M., 2000, Joint contact mechanics in the early stages of osteoarthritis: Medical Engineering & Physics, v. 22, no. 1, p. 1-12.

You, B. M., Siy, P., Anderst, W., and Tashman, S., 2001, In vivo measurement of 3-D skeletal kinematics from sequences of biplane radiographs: Application to knee kinematics: Ieee Transactions on Medical Imaging, v. 20, no. 6, p. 514-525.

BIOGRAPHICAL SKETCH

Bo Gao was born in Baoji, China. He graduated from Baoji High School in 1998. He earned his B.S. degree in mechanical engineering from the University of Science and Technology of China (USTC, Hefei, China) and entered the Graduate School of Chinese Academy of Sciences (GSCAS, Beijing, China) in 2002. Since August 2003, he worked as a research assistant in the Nano-Bioengineering Laboratory, Institute of Mechanics of Chinese Academy of Sciences, and earned his M.S. degree in biomechanics in 2005. In August 2005, he entered the Ph.D program of biomedical engineering in the University of Florida (UF). Since then he started working as a research assistant in the Biomechanics and Motion Analysis Laboratory in the Orthopaedics and Sports Medicine Institute (OSMI), UF & Shands. He earned his second M.S. degree in biomedical engineering in 2007, and is completing his Ph.D in 2009.